行政院國家科學委員會補助專題研究計畫 ■ 成 果 報 告
□期中進度報告

崩積地層之調查與監測-電學方法
Subsurface Investigations and Monitoring in Colluvium - Electrical Methods

計畫類別：□ 個別型計畫 ■ 整合型計畫
計畫編號：NSC 95－2221－E－009－200－
執行期間： 94 年 8 月 1 日至 97 年 7 月 31 日

計畫主持人：林志平 國立交通大學土木工程系
共同主持人：
計畫參與人員： 湯士弘 國立交通大學土木工程系
鍾志忠 國立交通大學土木工程系
姚奕全 國立交通大學土木工程系
吳瑋晉 國立交通大學土木工程系
林哲毅 國立交通大學土木工程系

成果報告類型(依經費核定清單規定繳交)：□精簡報告 ■完整報告

本成果報告包括以下應繳交之附件：
□赴國外出差或研習心得報告一份
□赴大陸地區出差或研習心得報告一份
■出席國際學術會議心得報告及發表之論文各一份
□國際合作研究計畫國外研究報告書一份

處理方式：除產學合作研究計畫、提升產業技術及人才培育研究計畫、列管計畫及下列情形者外，得立即公開查詢
□涉及專利或其他智慧財產權，□一年□二年後可公開查詢

執行單位： 國立交通大學土木系

中 華 民 國 97 年 10 月 30 日

行政院國家科學委員會專題研究計畫成果報告

崩積地層之調查與監測-電學方法

Subsurface Investigations and Monitoring in Colluvium - Electrical Methods

計畫編號：NSC 95－2221－E－009－200－
執行期限：94 年 8 月 1 日至 97 年 7 月 31 日

主持人：林志平　國立交通大學土木工程系

一、中文摘要

崩積地層之鑽探調查非常困難，而其穩定性又常由降雨入滲與地下水位所控制，利用非侵入式的地電阻法輔助工址調查及以電學性質監測地層之含水特性應該是值得發展的方向。崩積地層及殘餘土內之含水量、飽和度、與地水位，影響崩積層邊坡之穩定性甚巨，而地層含水特性與電學性質（包括電阻率與介電度）具有密切的關連性，本計畫旨在發展以電學性質調查地層分佈及監測崩積地層之含水量、土壤吸力、地水位之技術。本計畫所採用之量測方法包括時域反射（TDR）量測技術與地電阻影像剖面技術（ERT），TDR 是以導波器探測頭量測土壤之電阻率與介電頻譜，而 ERT 則可以非侵入的方式量測電阻率之二維分佈。ERT 雖可以非破壞性的方法進行大範圍的 2-D 探測，但單一電阻率量測值受到許多物理性質所影響（如含水量、土壤種類及地下水特性等），TDR 介電頻譜較能直接反應土壤含水量與土壤種類。因此本研究首先建立並改良 TDR 與 ERT 量測系統，建立崩積土之電學性質資料庫，再推導崩積土層含水特性與電學性質間之關係，並討論判讀 ERT 影像剖面資料之原則，最終目的希望能發展適合崩積地層之 TDR 多功能邊坡監測系統包括降雨量、含水量、土壤吸力、地水位與變形，及可提供在空間上與時間上連續資料的自動化 ERT 監測系統。

本研究計畫為三年期整合型研究計畫『崩積地層工址特性評估與大地工程問題』其中子計畫之一，本報告簡述本計畫之執行成果。

關鍵詞：崩積層、時域反射法、地電阻影像探測

Abstract

Drilling in colluvium, and especially in talus, is difficult, relatively expensive, and often does not provide the geotechnical engineer with a complete profile of the deposit. Intense rainfall is cited as the most common triggering mechanism for landslides involving colluvium. Hence, electrical geophysical methods hold great promise to supplement drilling data and determine hydrogeological conditions in colluvium. The main objectives of this study is to develop electrical techniques for site investigation and monitoring soil water content, matrix suction, and groundwater level in colluvium. Methods utilized include time domain reflectometry and electrical resistivity tomography. ERT is a non-destructive method that can estimate 2-D distribution of ground resistivity. However, interpretation of the resistivity alone for soil properties is difficult because it is sensitive to many factors, such as water content, soil types and ground water characteristics. TDR uses a waveguide probe to measure soil dielectric spectrum and resistivity. The dielectric permittivity provides extra information for estimating soil water content and soil types. This study will first establish and improve the TDR and ERT measuring methodology. A database will be constructed for electrical properties of colluvial materials. The relationship between soil water retention characteristic and electrical properties will then be established. Guidelines for interpreting ERT resistivity tomograms will be subsequently illustrated. The final goal is to develop a multi-function TDR monitoring system for colluvial slopes including rainfall, water content, matrix suction, groundwater level, and slope deformation. An ERT monitoring system will also be developed to obtain information

which is continuous in both space and time. This report briefly describes the study result of this prject.

Keywords: Colluvium, Time Domain Reflectometry, Electrical Resistivity Tomography

二、計畫緣由與目的

崩積地層可能是最為普遍的地表覆蓋層，Costa and Baker (1981) 估計在潮濕氣候地區超過 95%的地表面為崩積層所覆蓋。台灣由於地震頻繁，整體地質環境脆弱，加上氣候潮濕、地形陡峻、河川溪流侵蝕旺盛，山區崩坍的岩石及土壤物質容易因滾落、滑動、崩塌等經過位移作用而在崖錐或邊坡下方原有的地層之上堆積，形成「崩積層」或「崩積土」，覆蓋於原出露之地盤上。崩積層邊坡常具有高度活動性，因此，當工程或土地利用位於或通過崩積層組成之邊坡，常引致重大災害以及可觀之經濟損失，如新店、外雙溪地區數處山坡地上之大型社區、中橫公路梨山地區、..等等邊坡問題，都屬於崩塌地之不穩定邊坡問題。

崩積地層因為受到原有邊坡材料、破壞型態、形成年代等的影響，具高度的不均質性、不易調查性、及實驗結果代表性不足等現象，因此，無論力學或水力特性均不易掌握。雖然國內外已有許多相關研究報告，但是仍有不少有關崩積層的問題仍有其進一步研討，譬如：地形地相與過去崩滑、位移、堆積歷史與崩積層型態與特性的因果關係與研判，地下水與逕流入滲的影響與分析，風化與侵蝕的角色與影響，含水量/飽和度的變化與穩定性之關連，崩積層材料具代表性之力學行為與力學性質及力學模式、崩積層破壞機制及模式、崩積層邊坡之復發性及漸進性破壞的分析方法、推估材料參數的合宜手段、合理考量材料性質高度不確定性的途徑、和最佳的工址調查計畫等。上述待釐清的問題非單一計畫所能完成，本研究團隊因此擬針對這些問題組成整合性研究計畫，推動不同的子計畫，分頭進行同時相互合作，期能在崩積層之調查、試驗、模擬、分析等問題上多方面加以研討，本計畫旨在發展以電學性質調查崩積地層分佈及監測崩積地層含水量、毛細張力、地水位之技術。

崩積地層之鑽探調查非常困難，而其穩定性又常由降雨入滲與地下水位所控制，利用非侵入式的地電阻法輔助工址調查及以電學性質監測地層之含水特性應該是值得發展的方向。崩積地層及殘餘土內之含水量、飽和度、與地水位，影響崩積層邊坡之穩定性甚巨，而地層含水特性與電學性質（包括電阻率與介電度）具有密切的關連性，本計畫旨在發展以電學性質調查崩積地層分佈及監測崩積地層之含水量、土壤張力、地水位之技術。本計畫所採用之量測方法包括時域反射（Time Domain Reflectometry, TDR）量測技術與地電阻影像剖面技術（Electrical Resistivity Tomography，ERT），TDR 是以導波器探測頭量測土壤之電阻率與介電頻譜，而 ERT 則可以非侵入的方式量測電阻率之二維分佈。ERT 雖可以非破壞性的方法進行大範圍的 2-D 探測，但單一電阻率量測值受到許多物理性質所影響（如含水量、土壤種類及地下水特性等），TDR 介電頻譜較能直接反應土壤含水量與土壤種類。因此本研究首先建立並改良 TDR 與 ERT 量測系統，建立崩積土之電學性質資料庫，再推導崩積土層含水特性與電學性質間之關係，並討論判讀 ERT 影像剖面資料之原則，最終目的希望能發展適合崩積地層之 TDR 多功能邊坡監測系統包括降雨量、含水量、土壤吸力、地水位與變形，及可提供在空間上與時間上連續資料的自動化 ERT 監測系統。

三、結果與討論

3.1 TDR 量測方法之建立與改良

本研究擬發展適用於崩積層邊坡監測之含水量、導電度、地層種類、毛細張力及地下水位等 TDR 量測技術。圖 1a 為 TDR 量測系統的示意圖，它包含階躍脈衝電壓產生器、訊號採樣器與示波器，脈衝產生器產生電壓脈衝傳至同軸纜線，訊號採樣器擷取並透過示波器顯示由同軸纜線傳回之反射訊號。感測導波器為同軸纜線之延伸使得電磁波傳進所要量測之材料或環境中。

3.1.1 TDR 全波形模擬

為能夠進一步改良 TDR 之各種量測方法，特別是在邊坡監測實務上需要不同延長纜線長度的影響，本研究建構考慮各項因子

的完整 TDR 波傳模型，以作為資料分析及方法研擬的工具。TDR 傳輸線之波傳控制方程式可以圖 1b 之電路模型推導得到，其中之單位長度電路參數（conductance g, capacitace c, inductance l, and resistance r）為介質電學性質與傳輸線幾何的參數，波動控制方程式通解中的主要參數為傳遞常數（propagation constant γ）與特徵阻抗（characteristic impedance Z_c），傳遞常數控制波傳的速度與衰減，特徵阻抗控制阻抗不連續面的反射量，在頻率域（f），傳遞常數與特徵阻抗經推導為

$$\gamma = \frac{j2\pi f}{c}\sqrt{\varepsilon_r^*} * A \qquad (1a)$$

$$Z_c = \frac{Z_p}{\sqrt{\varepsilon_r^*}} * A \qquad (1b)$$

$$A = \sqrt{1+(1-j)\left(\frac{\eta_0}{Z_p}\right)\frac{\alpha_R}{\sqrt{f}}} \qquad (1c)$$

其中 c 是光速, $\varepsilon_r^* = \varepsilon_r - j\sigma/(2\pi f\varepsilon_0)$ 是 complex dielectric permittivity（包含介電度 dielectric permittivity ε_r 及導電度 electrical conductivity σ之性質，其中ε_0 是真空的介電度）, Z_p 是幾何特徵阻抗(真空的特徵阻抗), A 是考慮纜線電阻之修正因子， j 是$\sqrt{-1}$，$\eta_0 = \sqrt{\mu_0/\varepsilon_0} \approx 120\pi$ （μ_0 為真空的磁導率)，α_R (sec$^{-0.5}$) 是電阻衰減因子（為纜線的特性）。TDR 量測系統之傳輸線至少包括延長線段及感應段，不同段之傳遞常數與特徵阻抗不同，可以多段模式模擬（如圖 2a），每一段可以參數化為傳輸線幾何特性（Z_p）介質電學性質（ε_r^*）、傳輸線電阻衰減因子（α_R）及段落長度（L），一旦各段落的這四個參數得知，即可完整模擬 TDR 訊號。波傳的模擬首先先將不同段落的整體效應以 TDR 起始端的輸入阻抗（input impedance Z_{in}）表示，起始端的輸入阻抗可由末端阻抗（Z_L）及各段落之特徵阻抗以下式之遞回方式求得：

$$\begin{aligned}
Z_{in}(z_n) &= Z_L \\
Z_{in}(z_{n-1}) &= Z_{c,n}\frac{Z_L + Z_{c,n}\tanh(\gamma_n l_n)}{Z_{c,n} + Z_L\tanh(\gamma_n l_n)} \\
Z_{in}(z_{n-2}) &= Z_{c,n-1}\frac{Z_{in}(z_{n-1}) + Z_{c,n-1}\tanh(\gamma_{n-1} l_{n-1})}{Z_{c,n-1} + Z_{in}(z_{n-1})\tanh(\gamma_{n-1} l_{n-1})} \\
&\vdots \\
Z_{in}(0) &= Z_{c,1}\frac{Z_{in}(z_1) + Z_{c,1}\tanh(\gamma_1 l_1)}{Z_{c,1} + Z_{in}(z_1)\tanh(\gamma_1 l_1)}
\end{aligned} \qquad (2)$$

其中下標 i 代表各段落。一般之 TDR 量測系統邊界條件為($Z_L = \infty$). TDR 波形在頻率域之反應可由輸入阻抗與起始端之邊界條件推導得到：

$$V(0) = \frac{Z_{in}(0)}{Z_{in}(0)+Z_S}V_S = HV_S \qquad (3)$$

其中 $V(0)$ 是 TDR 波形的富立葉轉換，V_s 是 TDR 輸入方波的富立葉轉換，Z_s 是源頭阻抗（source impedance），通常 TDR 儀器之 $Z_s = 50\ \Omega$， TDR 波形(v_t)之模擬可由 $V(0)$ 之富立葉反轉換得到，典型之 TDR 波形如圖 2c 所示。TDR 全波形之模擬與應用詳已發表之論文 Lin and Tang (2007)（附錄 A）.

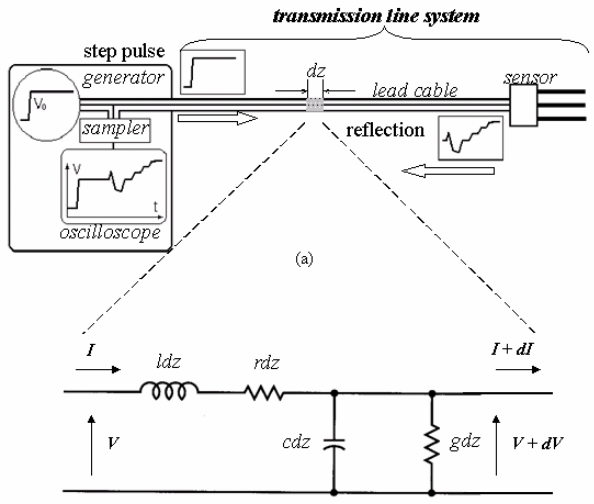

圖 1 (a) TDR 量測系統 (b) 傳輸線微小元素之電路模型.

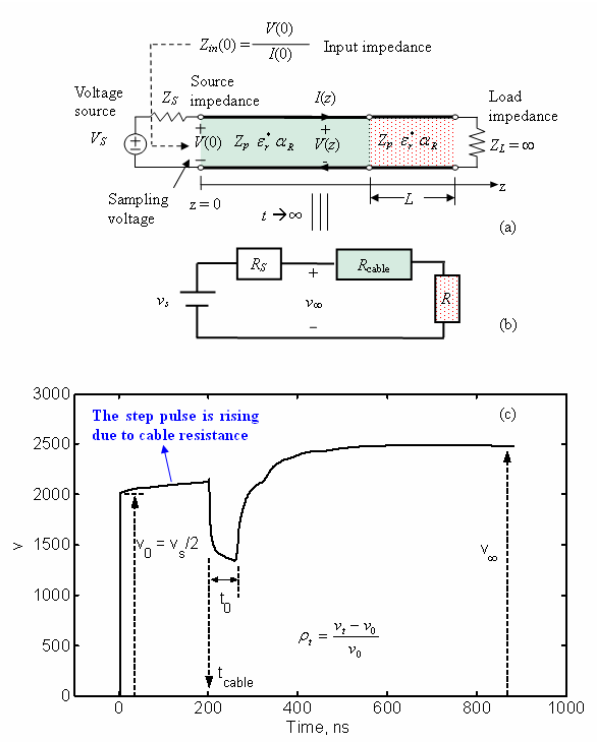

圖 2. (a) TDR 量測系統之傳輸線經點模型(b)直流電電路模型(c)典型 TDR 波形

3.1.2 TDR 含水量量測

材料之基本電學性質包括介電度（Dielectric Permittivity, ε_r） 與導電度（Conductivity, σ為電阻率 resistivity 的倒數）。其中，介電度為頻率之函數，在不同頻率之電場下，材料有如動態反應譜呈現不同之介電度。在頻率域，介電度可以表示為複數，實部（ε_r'）表示外部電場能量在材料中之儲存，虛部（ε_r''）表示阻尼效應之能量消散。波動方程式在頻率域之解析中，介電度與導電度兩項材料性質可合併為等值介電度（ε_r^*）如下式所示

$$\varepsilon_r^* = \varepsilon_r' - j\varepsilon_r^{ii} = \varepsilon_r' - j\left(\varepsilon_r'' + \frac{\sigma_{dc}}{2\pi f \varepsilon_0}\right) \qquad (4)$$

其中ε_0為真空之介電常數，電磁波在傳輸纜線中之傳遞常數可寫為

$$\gamma = \frac{j2\pi f}{c}\sqrt{\varepsilon_r^*} = \alpha + j\beta \qquad (5)$$

其中α 與 β 分別為傳遞係數之實部與虛部，實部α 反應電磁波之衰減，虛部β 為空間頻率，時間頻率（$2\pi f$）除以空間頻率（β）可得波傳之相位速度（Phase velocity）

$$v(f) = \frac{2\pi f}{\beta} = \frac{c}{\sqrt{\frac{\varepsilon_r'(f)}{2}\left(1+\sqrt{1+\left(\frac{\varepsilon_r^{ii}(f)}{\varepsilon_r'(f)}\right)^2}\right)}} \qquad (6)$$

由（6）式可知，因為材料介電性質隨頻率而異，電磁波之波速也成為頻率的函數，此種頻散現象(Dispersion) 使得方波於電纜中傳輸後之波形趨於圓滑，上升斜率趨緩。如圖 2c 所示，其 TDR 反射訊號之上升時間（rise time）較原入射方波上升時間長，且波形較為圓滑。

Topp et al. (1980)以 TDR 在時間域的視速度(apparent velocity，如圖 2a 中的 t_0 所示)定義了視介電常數 K_a(apparent dielectric constant)，v_a 與 K_a 的關係為(6)式之簡化：

$$v_a = \frac{c}{\sqrt{K_a}} \qquad (7)$$

其中視速度通常利用切線分析法決定電磁波在感測器中的來回走時 t_0：

$$v_a = 2L/t_0 \qquad (8)$$

因此，視介電常數可利用下式決定：

$$K_a = \left(\frac{ct_0}{2L}\right)^2 \qquad (9)$$

土壤之介電度與含水量具有高度相關性，Topp et al. (1980)提出 K_a 與土壤含水量的經驗公式，獲得良好的含水量量測結果並廣被引用，但有一些土壤需要經過個別標定方能得到合理的結果。事實上，視介電度不是一個真實的物理量，其值受到走時分析方法、介電度頻散現象、導電度、延長線長度及感測器末端邊界條件所影響。本研究以 TDR 全波形模擬進行參數研究，廣泛充分探討上述影響土壤含水量的因子，其中走時分析的方法包括雙切線法、單切線法及反曲點法，主要結論如下：

- K_a 的等效頻率視材料介電頻散的 relaxation 頻率，目前並無有效的方法

可以決定 K_a 的等效頻率。

- TDR 頻寬範圍內的頻散線現象主要來自於固相與液相的交互作用，頻散現象因土壤種類而異，其對於導電度與纜線長度如何影響 K_a 扮演關鍵的角色。
- 如果土壤介電度之頻散現象不明顯，則 K_a 不受導電度的影響，且纜線長度的影響可透過空氣與水之探頭時間點與探頭長度的標定修正。
- 若土壤介電度在 TDR 頻寬內展現明顯的頻散現象，則所量測到之 Ka 將受到導電度的影響及纜線長度的影響。
- 感測器末端斷路確實會有 fringing 效應，末端短路可以避免此一問題，末端短路之感測器可以 TDR 貫入是感測器（Lin et al. 2006a, 2006b）的形式實現。
- 雙切線法所得到 Ka 之等效頻率最高，且較導電度與纜線長度之影響較輕微，但雙切線法的自動化較困難。
- 單切線法除了受導電度的影響較大之外，其餘結果與雙切線法類似，但單切線法不適用於末端短路之感測器。
- 反曲點法之等效頻率最低，且對於導電度與纜線長度的影響較敏感，且當導電度很高或纜線長度很常時會出現不合理的結果（Ka 高於各頻率之介電度）

上述研究成果對於 TDR 土壤含水量量測的意義詳已發表之期刊論文（Chung and Lin 2008）（附錄 B）。

現有的 TDR 傳感器不太適合於崩積層邊坡之監測，在感測器之改良研究方面，建議利用 TDR 貫入式感測器(Lin et al. 2006a, 2006b）作為崩積地層監測的感測器形式，並提出末端短路的感測器設計，以降低走時分析受導電度之影響及末端的 fringing effect，提高後續資料解析的正確性。可量測土壤含水量剖面及 wetting front 亦是未來持續努力的目標。

3.1.3 TDR 介電頻譜分析

雖然利用 TDR 視介電度量測土壤含水量已是眾多電學方法較佳的，但視介電度因為缺乏明確的物理意義，可能受到土壤種類、導電度及纜線長度影響，因此本研究將持續進行 TDR 的介電頻譜分析。

等值介電頻譜（$\varepsilon_r^*(f)$）可經由量測訊號之系統分析求得，將反射訊號之富立葉轉換（$Y(f)$）除以脈衝產生器之入射訊號（$X(f)$）可得 TDR 量測系統之系統函數（System function, H）之量測值，此量測值必須等於量測系統之理論系統函數，如下式表示

$$H(\varepsilon_r^*, f) = \frac{Y(f)}{X(f)} \qquad (10)$$

理論系統函數為纜線阻抗、纜線傳遞常數、纜線長度、與邊界條件之函數，此函數可由波傳理論推得(Lin 2003a; Lin and Tang 2007)。經由解（10）式在不同頻率下之非線性函數可以得到不同頻率之等值介電度，如此可以得到介質之等值介電頻譜(Lin 2003a; Lin 2003b)，等值介電頻譜包含介電度與導電度之綜合影響。本研究利用新發展考慮纜線電阻的 TDR 波傳模型（詳 3.1.1）改善介電頻譜分析，圖 3 顯示未考慮纜線電阻及考慮纜線電阻水的介電頻譜量測結果，新的方法已克服實務上無可避免的纜線問題，相關期刊論文發表準備中（Tang et al., in preparation）。本研究雖已解決纜線電阻的問題，但高頻量測結果仍較為散亂，本研究將持續改善高頻量測可靠度及量測頻寬（低頻的量測），並利用介電頻譜分析改善含水量量測及應用於土壤種類的判別。

介電頻譜在低頻的頻散現象與土壤種類應該存在高度相關性，但有待實驗定量的探討。根據 Lin (2003a)的結果顯示，頻率範圍 500 MHz~1GHz 較不受土壤種類的影響，為量測土壤含水量的最佳頻率（如圖 4），除了完整的介電頻譜分析，本研究另嘗試利用訊號分析的方法研究出直接量測高頻（含水量最佳頻率範圍）介電度的量測方法，稱之為 TDR 頻率域相位速度分析法（TDR Frequency Domain Phase Velocity Method）所發之技術具有原創性與新穎性，量測專利技術申請中，該方法亦詳載於指導學生之博士論文（鍾志忠，2008）。

3.1.4 TDR 導電度量測

導電度可經由 DC 分析直接量測，經過許多學者多年研究，目前普遍認為早期 Giese and Tiemann (1975)所提的方法最佳，

$$\sigma_{GT} = \frac{K_p}{R_S}\left(\frac{1-\rho_\infty}{1+\rho_\infty}\right) \qquad (11)$$

其中反射係數 $\rho_\infty = (v_\infty - v_0)/v_0$，$v_0$ 為入射方波之電壓大小（理想狀態為電壓源的一半

$v_0 = v_{S0}/2$），v_∞為訊號最終之電壓大小，K_p為形狀因子，R為TDR的source impedance。但該方法未能考慮纜線電阻的影響，本研究以考慮纜線電阻的DC串聯電阻電路（圖 1b）重新推導導電度：

$$\sigma = \frac{K_p}{R_S}\left(\frac{1}{v_\infty / v_{S0}} - 1\right)\left[\frac{1}{1 - \frac{R_{cable}}{R_S}\left(\frac{1}{v_\infty / v_{S0}} - 1\right)}\right] \quad (12)$$

其中纜線電阻可由感測器短路之量測求得

$$R_{cable} = \frac{R_S}{\left(\frac{1}{v_{\infty,SC} / v_{S0}} - 1\right)} \quad (13)$$

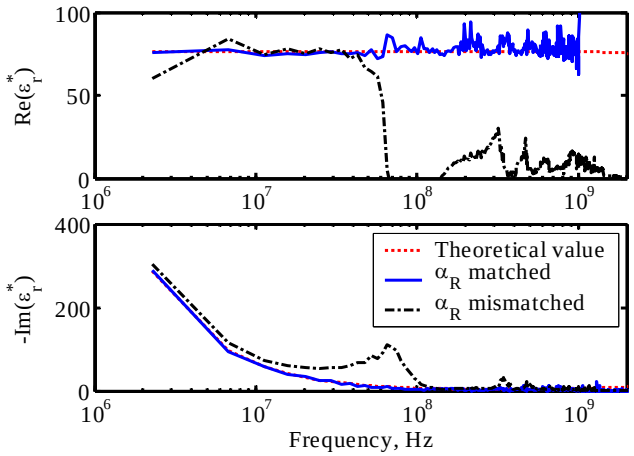

圖 3. 介電頻譜分析--考慮及為考慮纜線電阻對於水介電頻譜的量測結果

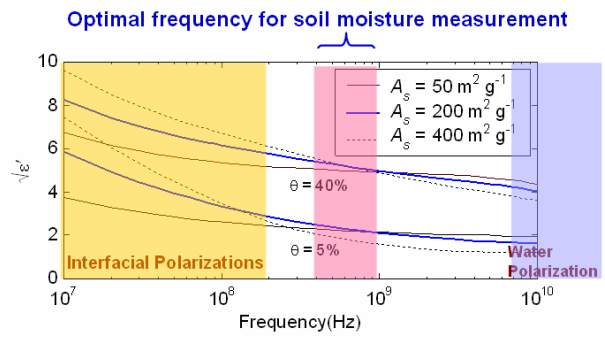

圖 4. 介電頻譜與土壤含水量及土壤種類的關係

藉由全波形模擬分析驗證串聯電阻電路的正確性及探討量測穩態值所需要的時間，結果發現，當纜線長度較長時，過去的研究低估獲得穩態電壓所需的時間，特別是處於低導電度及高導電度時。本研究提出明確可獲得穩態電壓值的時間，該時間必須在10次感測器段的多重反射及3次纜線段多重反射之後。此外本研究亦發現，除了纜線電阻的影響之外，TDR儀器在轉換電壓為反射係數時，無法準確反應電壓源的大小，該誤差可由感測器在空氣中的量測得知與標定，為了維持習用的Giese-Tiemann計算方式及簡化計算過程，本研究提出同時考慮儀器誤差及纜線電阻的反射係數標定方程式：

$$\rho_{\infty,Scale} = 2\frac{(\rho_{\infty,air} - \rho_{\infty,SC})(\rho - \rho_{\infty,air})}{(1+\rho_{\infty,SC})(\rho - \rho_{\infty,air}) + (\rho_{\infty,air} - \rho_{\infty,SC})(1+\rho_{\infty,air})} + 1 \quad (14)$$

本節所述之研究成果細節可參考已發表之期刊論文 Lin et al. (2007)（附錄 C）及 Lin et al. (2008)（附錄 D）。

3.1.5 TDR 毛細張力量測

毛細張力對於非飽和土壤邊坡之穩定性扮演極重要的角色，台灣的崩積層邊坡大部分屬於此類型淺層破壞。Or and Wraith (1999)提出利用TDR量測陶瓷材料的含水量，利用陶瓷含水量與毛細張力的關係量測毛細張力，許多後續的改良研究仍然在進行中，本研究經過研究探討，這類型的毛細張力感測器會有顯著的時間延遲，不適合應用在邊坡穩定監測。由於現階段毛細張力的現地即時監測技術仍有困難，因此建議以經過率定或經驗推估的水土保持特徵曲線，由土壤體積含水量之推估現地毛細張力。

3.1.6 TDR 地下水位

本研究團隊曾提出利用TDR偵測不同介質界面的能力量測地下水位及降雨量（林志平等人 2003），本研究利用全波形分析可考慮纜線電阻影響，準確量測水位面及水的電學性質（Lin and Tang 2007），並提出由TDR波形決定地下水位的自動化演算法。

3.2 ERT 量測方法之建立與資料詮釋

傳統的鑽探與監測方法並無法一窺崩積地層的全貌，本研究期望結合地球物理方法提供崩積層邊坡2D以上的調查與監測方法，主要選擇地電阻率影像探測（ERT），因其與影響崩積層邊坡穩定性的含水特性具有高度相關性。

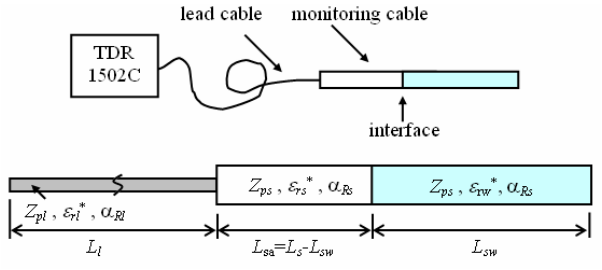

(a)

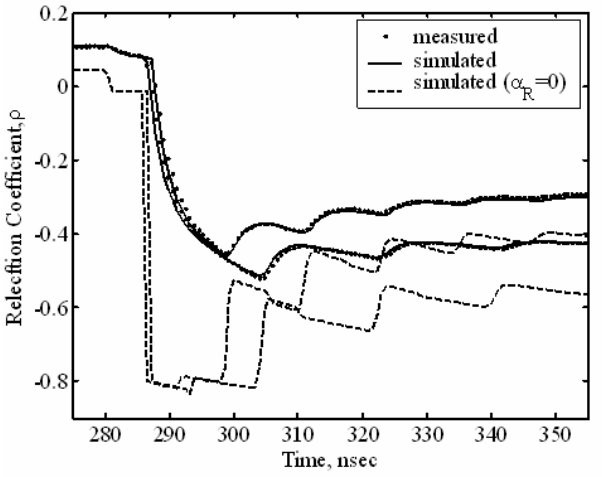

(b)

圖 5 (a)水位面量測之傳輸線模型與(b)實測結果

地電阻探測主要施測原理在於給予一探測物質外部的電流或是電壓（如圖 6 中 A、B 端），利用佈設的電極接收透過探測物質回傳的電勢能差值(如圖 6 中 M、N)，由量測之電流與電壓可根據靜電學理論計算出受測物體之視電阻率。量測之空間影響範圍視電極之間距而定，電極間距越大，影響深度越大。若改變量測之位置與電極間距，可得到許多不同空間影響範圍之視電阻率，可據以反算地層之真實電阻分佈（地電阻剖面影像），藉以瞭解地層構造（Loke 2003）。施測方法依電極之佈設方式可分為以下幾類：(1) Dipole-Dipole(2) Pole-Dipole (3) Pole-Pole(4) Wenner(5) Wenner-Schlumberger。

各種施測方法均能以平移及改變電極間距之方式進行地電阻剖面量測，可探測之深度視其電極佈設方式以及現地佈設展距而定，地電阻剖面影像之施測方法可依照當地地層狀況及施測目標選擇適當之方式，以 dipole-dipole 為例，改變電流極與電壓極之位置與間距，可得到不同影響深度的量測值，地電阻量測之結果以 pseudosection 展示，如圖 8 所示。地電阻量測之 psuedosection 表示每一施測幾何（電極配置）所得到之視電阻率，必須透過反算分析方能得到地層真正的電阻率分佈。反算分析之方法主要以正算模式為基礎，亦即，若假設一電阻率分佈，量測之視電阻率可依據靜電學理論與有限元素法或有線差分法(如圖 8)模擬預測，若設法改變電阻率分佈，使得預測值盡量逼近量測值，則可估計出地層之電阻率分佈。由於資料量大，反算分析通常以結合正算模式之最佳化方法進行，由實際量測資料（pseudosection）反算地層之電阻率分佈。

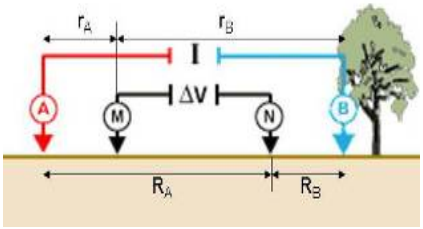

圖 6.電流極與電位極排列示意圖

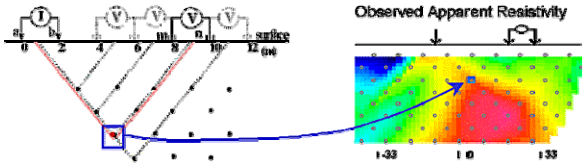

圖 7. 地電阻量測結果之 pseudosection

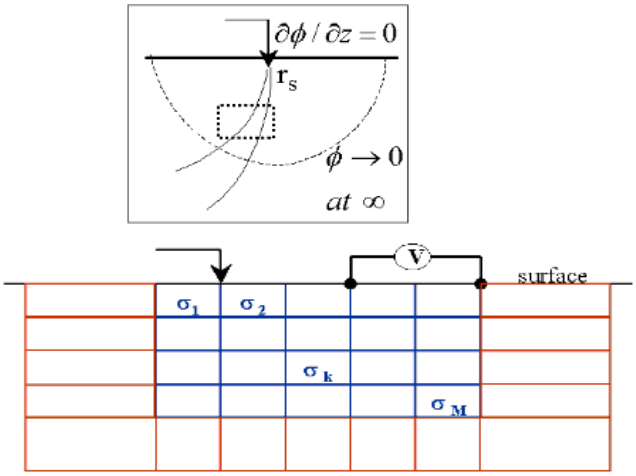

圖 8. 地電阻有限元素法正算模式示意圖

3.2.1 ERT 之重複性與空間解析度

ERT 資料解讀對於工程師而言常是一項很大的挑戰，主要原因是缺乏空間解析度與反算不確定性的資訊。為了解 ERT 在監測應用的可行性，本研究首先測試不同電極佈設方式的施測重複線，結果顯示淺層探測

以 Wenner 施測法重複性最佳，深層探測以 Pole-Pole 施測法較佳。

在空間解析度方面，本研究從幾個不同的角度探討，首先利用一些簡易的地電阻率模型（例如不同夾層厚度、夾層距地表深度、夾層與周圍材料電阻率比值），分析在不同地質狀況下主要地層參數的靈敏度；另一方面，利用正算模擬，探討真實模型與反算模型之間的差異（如圖 9），並探討靈敏度影像是否能反應反算結果的可靠度；此外，目前 ERT 的施測與分析主要以 2D 的方法進行，三維效應對於 ERT 空間解析的影響有必要做進一步的探討。目前已有許多相關參數研究，可作為研判 ERT 施測結果之空間解析度與可靠度的導引，相關的細節可參考姚奕全（2007）。

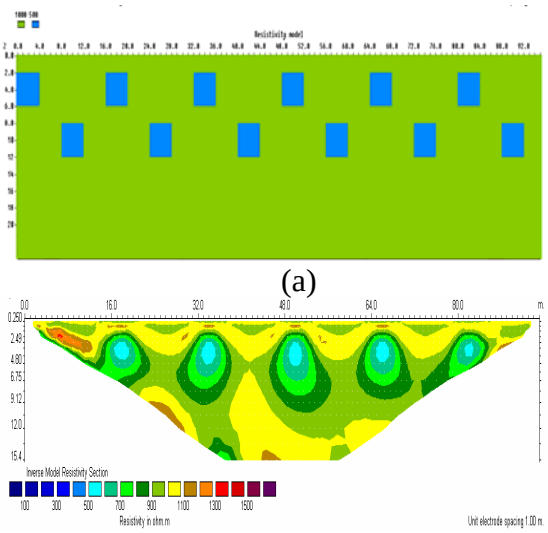

(a)

(b)

圖 9. (a)設定之真實地電阻率分佈及(b)反算之地電阻率剖面

3.2.1 ERT 之資料詮釋

ERT 雖然可以產生生動的地電阻率空間分佈，姑且不論其空間解析度與資料的準確度，如何利用地電阻率的資料亦是一項挑戰，由於地電阻率受到土壤種類、地下水特性、含水量等之影響，因此從單一的地電阻率剖面並無法直接解讀崩積地層的含水特性。地電阻率與土壤性質的關係可利用廣義的 Archi's law 表示(Shah and Singh, 2005)：

$$\sigma = c\sigma_w\theta^m = A\theta^m \qquad (15)$$

其中 c 與 m 與土壤種類有關。吳瑋晉(2008)亦探討其他替代公式(15)的模式，並以試體試驗率定相關參數及模式的適用性。

由於利用取樣率定與地層種類及地下水相關的參數相當困難且不經濟，本研究提出結合 TDR 監測技術於現地率定這些參數，如圖 10 所示。在現地可利用 TDR 於不同地層同時監測其電阻率、含水量及毛細張力，利用一段時間的觀測資料，可統計分析(15)式之與場址相關的參數。經過此一率定，可將 ERT 試驗所得到的 2D 地電阻率剖面影像轉換為 2D 的含水量剖面（由適當的土壤密度估計水土保持特徵可以轉換為飽和度剖面及毛細張力剖面，這些結果將有助於分析崩積層邊坡的潛在滑動區及其穩定性。圖 11 為某一土壤利用 TDR 同時量測含水量與電阻率所得到之結果，本研究進行砂箱模型試驗，監測模擬降雨過程中之 TDR 含水量、電阻率及 ERT 電阻率剖面，試驗設計及模型如圖 12 所示，其中砂箱試驗的 ERT 觀測為了克服邊界效應，採用 3D ERT 試驗方法，並適當調整電極間距與反算方法以達合適的空間解析度（吳瑋晉, 2008）。

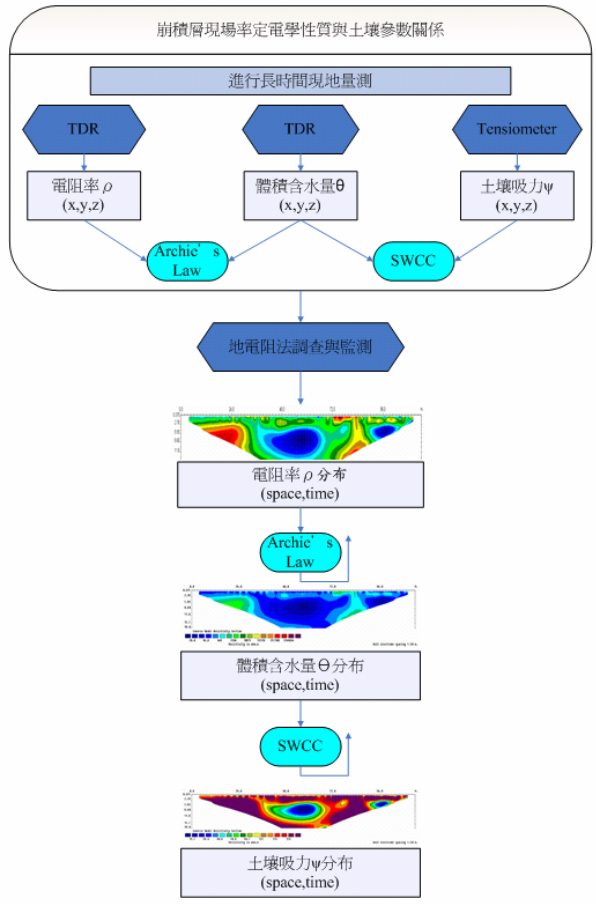

圖 10. 結合 TDR 與 ERT 進行地層 2D 的含水特性影像調查與監測方法的流程圖

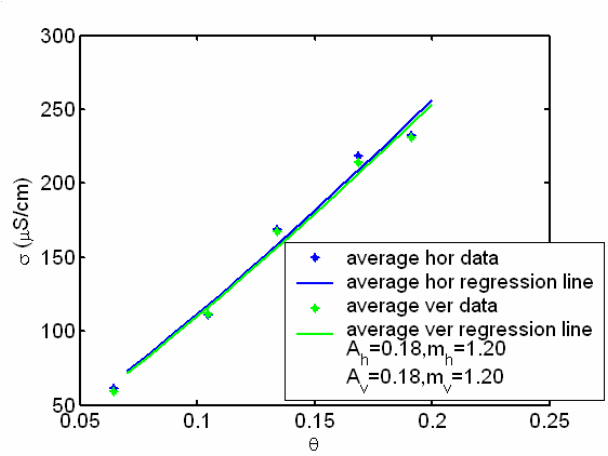

圖 11. 導電度與土壤含水量率定關係

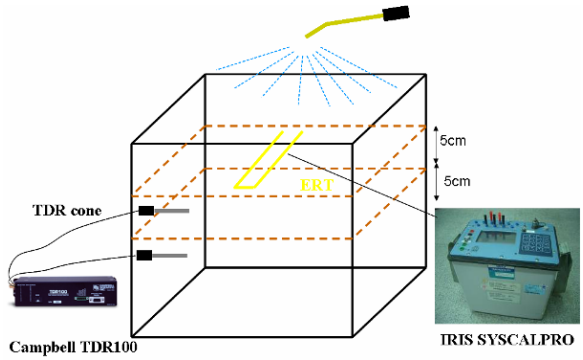

(a)

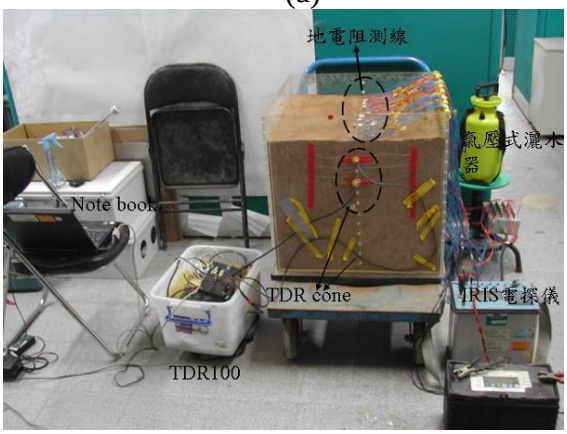

(b)

圖 12. 地電阻試驗砂箱模型試驗

圖 13 顯示降雨入滲過程與 3D 電探代表性二維剖面的結果，顯示電探影像可以定性的掌握地層含水分佈的變化。為進一步由電探詮釋土壤含水特性，需藉由同時進行 TDR 量測土壤含水量與導電度，圖 14 顯示降雨過程含水量與導電度的歷線，觀測結果顯示，淺層的感測器，含水量與導電度的反應有明顯的時間延遲，有不明因素造成導電度在降雨停止前即達到尖峰並迅速下降。利用 TDR 觀測資料進行含水量與導電度現地率定，結果如圖 15 所示，雖然與均質試體試驗所得到的含水量與導電度關係有相似性，但濕潤階段與乾燥階段有顯的遲滯線性，未來尚須進一步探討時間延遲與遲滯現象背後的原因與意義。

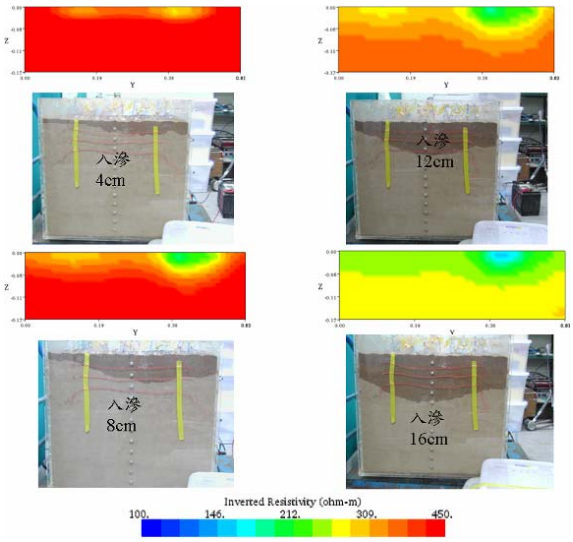

圖 13 不同入滲深度電阻率分布與入滲側照

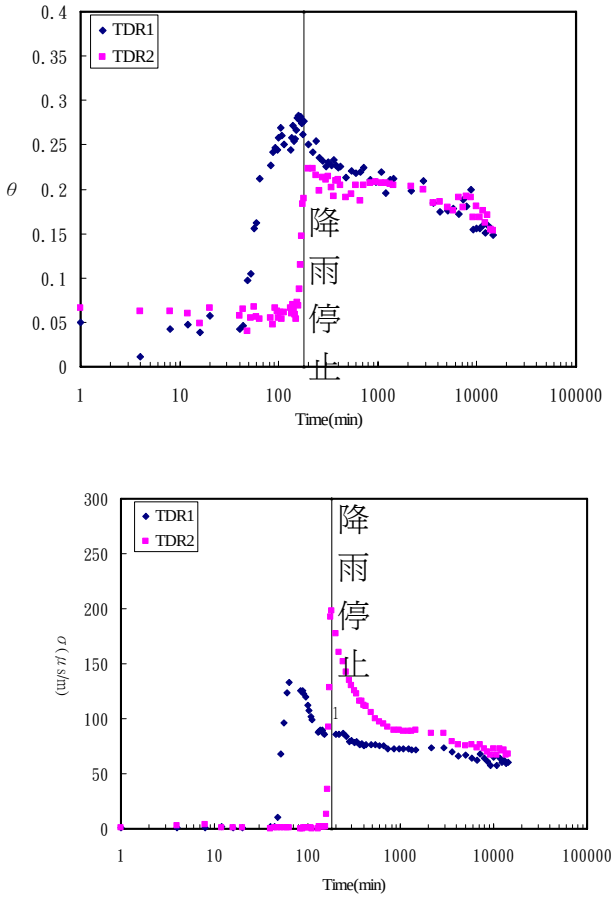

圖 14 砂箱試驗(a)體積含水量（θ）及(b)導電度（σ）監測資料

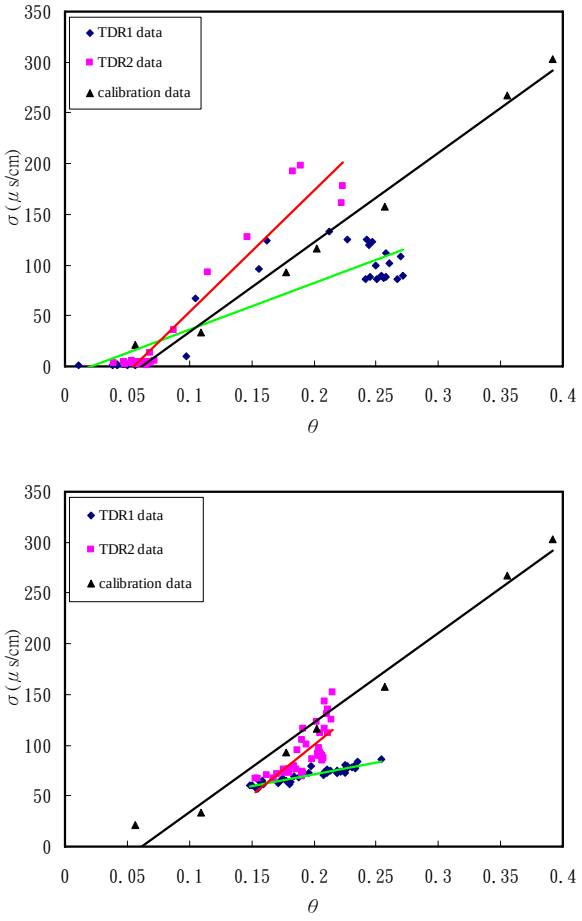

圖 15　砂箱(a)濕潤階段與(b)乾燥階段 σ v.s θ 率定結果

四、結果與討論

本研究提出新穎的整合式電學方法，作為崩積地層調查與監測的工具，其概念主要利用 TDR 可以同時量測土壤含水量與導電度，而地電阻法（ERT）可以量測導電度的空間變化，結合此兩種技術，可望可以發展出監測地層含水特性分佈的調查與監測技術。本研究計畫在初期投入許多改善 TDR 監測土壤含水量與導電度的研究，成果豐碩，已發表 4 篇期刊論文。在 ERT 的應用上，主要探討其空間解析能力與推估含水特性的資料詮釋方式，其中含水特性的推估，主要利用 TDR 與 ERT 的整合應用，由模擬降雨砂箱試驗的結果發現 TDR 含水量與導電度有不明因素造成時間延遲與遲滯現象，造成由 ERT 電探剖面詮釋含水特性剖面的不確定性，未來尚須進一步的釐清及現地試驗，以落實所提出的新方法。該計畫相關之學生畢業論文有博士論文一篇及碩士論文兩篇。

五、參考文獻

Chung, C.-C and Lin, C.-P. (2008), “Apparent Dielectric Constant and Effective Frequency of TDR Measurements: Influencing Factors and Comparison”, Vadose Zone Journal, (in press).

Costa, J.E. and Baker, V.R. (1981), Surficial Geology: Building with the Earth, John Wiley and Sons, New York, 498pp.

Giese, K. & Tiemann, R. (1975), “Determination of the complex permittivity from thin-sample time domain reflectometry: Improved analysis of the step response wave form,” Adv. Mol. Relax. Processes, Vol. 7, pp. 45-59.

Lin, C.-P. (2003a), “Analysis of a Non-uniform and Dispersive TDR Measurement System with Application to Dielectric Spectroscopy of Soils,” Water Resources Research, 39 (1): art. no. 1012.

Lin, C.-P. (2003b), "Frequency Domain versus Traveltime analyses of TDR Waveforms for Soil Moisture Measurements," Soil Sci. Soc. Am. J., 67: 720-729.

Lin, C.-P, Tang, S.-H., and Chung, C.-C., 2006a, "Development of TDR Penetrometer Through Theoretical and Laboratory Investigations: 1. Measurement of Soil Dielectric Permittivity," Geotechnical Testing Journal, GTJODJ, Vol. 29, No. 4.

Lin, C.-P, Chung, C.-C., and Tang, S.-H., 2006b, " Development of TDR Penetrometer through Theoretical and Laboratory Investigations: 2. Measurement of Soil Electrical Conductivity," Geotechnical Testing Journal, GTJODJ, Vol. 29, No. 4.

Lin, C.-P. and Tang, S.-H. (2007), “Comprehensive Wave Propagation Model to Improve TDR Interpretations for Geotechnical Applications,” Geotechnical Testing Journal, Vol. 30, No. 2, Paper ID GTJ 100012.

Lin, C.-P., Chung, C.-C., and Tang, S.-H. (2007), “Accurate TDR Measurement of Electrical Conductivity Accounting for Cable Resistance and Recording Time,” Soil Sci. Soc. Am. J., Soil Sci. Soc. Am. J., 71(4): 1278-1287.

Lin, C.-P., Chung, C.-C., Tang, S.-H., Huisman, J.A. (2008), “Clarification and Calibration of Reflection Coefficient for TDR Electrical Conductivity Measurement“, Soil Sci. Soc. Am. J, 72(4): 1033–1040.

Loke, M.H. (2003), Tutorial: 2-D and 3-D Electrical Imaging Survey, http://www.geoelectric.com.

Or, D., and Wraith, J.M. (1999), “A new soil matric-potential sensor based on time-domain-reflectometry,” Water Resources Research, 35: 3399-3407.

Shah, P. H. and Singh, D. N. (2005), “Generalized Archie’s Law for Estimation of Soil Electrical Conductivity”, Journal of ASTM International, Vol. 2, No. 5, pp. 145-164.

Tang, S.-H. Chung, C.-C. and Lin, C.-P., “Effect of Cable Resistance on Dielectric Spectroscopy using TDR,” Water Resources Research, (in preparation)

林志平、湯士弘、葉志翔、楊培熙、盧吉勇（2003），"TDR 山坡地監測系統之研發"，中華民國第十屆大地工程學術研討會，中華民國 92 年。

林志平、尤仁弘、洪瑛鈞、鄒和瀚（2006），"電阻剖面影像法於霸體滲漏調查之應用"，第十四屆非破壞性檢測技術研討會，中華民國非破壞性檢測協會年度會議。

姚奕全（2007），”應用地電阻法於崩積層含水特性調查與監測之初探”，國立交通大學土木系碩士論文。

吳瑋晉（2008），”結合地電阻法與 TDR 於土層含水特性之監測”， 國立交通大學土木系碩士論文。

鍾志忠（2008），”時域反射量測技術改良及於水土混和物之應用”， 國立交通大學土木系博士論文。

附錄A

Geotechnical Testing Journal, Vol. 30, No. 2
Paper ID GTJ100012
Available online at: www.astm.org

Chih-Ping Lin[1] *and Shr-Hong Tang*[1]

Comprehensive Wave Propagation Model to Improve TDR Interpretations for Geotechnical Applications

ABSTRACT: Time domain reflectometry (TDR) is becoming an important monitoring technique for various geotechnical problems. Better data interpretation and new developments rely on the ability to accurately model the TDR waveform, especially when long cables are used. This study developed an efficient, complete, and general-purpose TDR model that accounts for all wave phenomena including multiple reflection, dielectric dispersion, and cable resistance all together. Inverse analysis based on the TDR wave propagation model is proposed to calibrate the TDR system parameters and determine the TDR parameter that changes with the physical parameter to be monitored. Calibration of TDR cable and data interpretations for various geotechnical applications were demonstrated with laboratory experiments. The excellent match between the simulated and measured waveforms validates the TDR wave propagation model. The results show that the proposed numerical procedure is a relatively simple, efficient and high-resolution tool for probe design, parametric studies, data interpretation, and inverse analyses. This study should provide a sound theoretical foundation for further TDR developments in geotechnical monitoring.

KEYWORDS: time domain reflectometry (TDR), transmission line, cable resistance

Introduction

Time domain reflectometry (TDR) is an emerging technique for various geotechnical measurements by a cable radar and different sensing waveguides. It is based on transmitting an electromagnetic pulse through a coaxial cable connected to a sensing waveguide and watching for reflections of this transmission due to changes in characteristic impedance along the waveguide. Depending on the design of the wave guide and analysis method, the reflected signal can be used to monitor various engineering parameters. Unlike conventional electronic transducers, the TDR technique is a versatile uphole pulsing method in which the transducer (i.e., the inserted sensing waveguide) requires no electronic component.

In the past two decades, the TDR technique has being finding many innovative applications for geotechnical monitoring. A good overview of the TDR technique can be found in O'Connor and Dowding (1999), Benson and Bosscher (1999), and Robinson et al. (2004). The technique has been applied to measuring physical properties of a soil in which TDR probes are inserted into, such as water content and electrical conductivity (Topp et al. 1980; Dalton 1992; Siddiqui et al. 2000; Yu and Drnevich 2004). The spectral analysis of the TDR signal allows dielectric spectroscopy (i.e., measurement of dielectric permittivity at various frequencies) for studying soil-water interaction (Heimovaara 1994; Feng et al. 1999; Lin 2003a; Lin 2003b). Lin et al. (2006a; 2006b) developed a TDR penetrometer for simultaneously measuring dielectric permittivity and electrical conductivity during cone penetration testing. The TDR technique has also been employed in landslide monitoring to monitor localized shear deformation (Dowding et al. 1988; Dowding and Huang 1994), relative displacement (Lin and Tang 2005), and piezometric water pressure (Dowding et al. 1996). Monitoring scouring of bridge piers and detection of chemical leakage by the TDR technique have also been reported (Yankielun and Zabilansky 1999; PermAlert 1995).

Much work has been done on geotechnical applications of the TDR technique, yet to date only limited features in a TDR waveform are used for data interpretations. The features include the travel time (for measuring water content and locating cable crimp, relative displacement, groundwater level, and bridge scouring), reflection spike magnitude (for correlating with cable deformation), and steady-state reflection magnitude (for measuring electrical conductivity). These apparent features simplify the data analysis but are affected by several factors, such as the dielectric relaxation, multiple reflections, and cable resistance, aside from the parameter to be measured. The wave propagation in the transmission line is dispersive (that is, velocity is a function of frequency) due to cable resistance and dielectric relaxation. Clearly defining the arrival times of a dispersive waveform is difficult. Different methods were proposed to determine the reflection arrivals in a TDR waveform (Timlin and Pachepsky 1996; Klemunes et al. 1997), causing ambiguity in travel time analysis. The importance of cable resistance effect has also been recognized for steady-state reflection magnitude when making conductivity measurement (Reece 1998) and peak spike reflection when monitoring rock mass deformation (Pierce et al. 1994). Corrections for cable resistance effect were done by empirical calibration equations or charts. However, establishing the calibration equation is very tedious and it varies with the type of cable used.

Modeling the complete TDR waveform may lead to additional information and a more accurate data interpretation, especially for measurements with long cables. In the context of improving soil water content measurements, Feng et al. (1999) and Lin (2003a; 2003b) introduced a wave propagation model based on the spectral analysis in which multiple reflections and dielectric dispersion are taken into account. Neglecting the cable resistance in their model was justified by the short lead cable used. However, as the cable length increases, the cable resistance "smears" the reflected wave-

Manuscript received October 24, 2005; accepted for publication July 6, 2006.
[1]Associate Professor and Graduate Student, respectively, of Civil Engineering,National Chiao Tung University, Hsinchu, Taiwan, corresponding author e-mail: cplin@mail.nctu.edu.tw

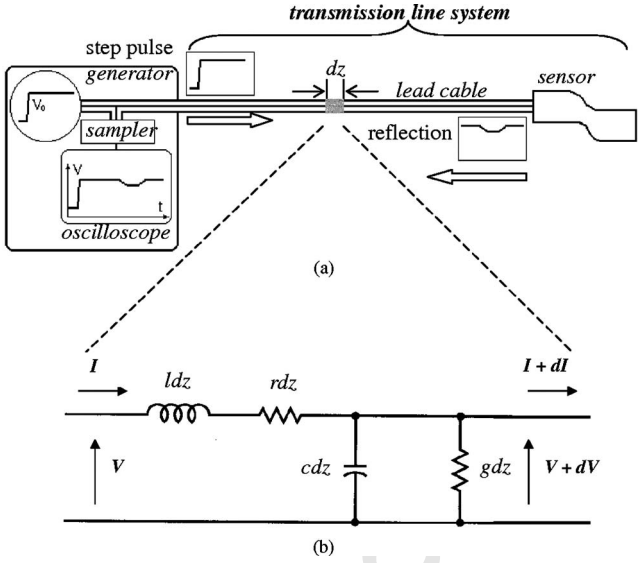

FIG. 1—(*a*) *A typical TDR configuration, and* (*b*) *the lumped circuit model for an infinitesimal section of the transmission line.*

form. Neglecting the resistance effect may lead to unreasonable interpretation, especially for surveillance with long TDR cable. Heimovaara et al. (2004) used the multi-section wave propagation model (Feng et al. 1999; Lin 2003a) to invert for the spatial distribution of water content along a TDR probe. They added the resistance term in calculating the wave propagation parameters of coaxial lines, but the resistance effect was overlooked for noncoaxial lines. In the context of monitoring deformation of rock masses, Dowding et al. (2002) developed a wave propagation model trying to account for cable resistance and multiple reflections. Dielectric dispersion was not considered since they only considered cable deformation. In their model, the wave equation is solved by the finite difference method and transformed into frequency domain. A frequency-dependent magnitude loss is subsequently applied in the frequency domain and the resistance-attenuated signal is then converted back into the time domain. The numerical model is very time-consuming and potentially unstable. Moreover, the cable resistance results in not only the magnitude modulation but also a phase distortion, which was not taken into account.

The purpose of this paper is to develop an efficient, complete, and general-purpose TDR model that accounts for multiple reflection, dielectric dispersion, and cable resistance in particular. The TDR model is parametrized and formulated to be concise and generic for all types of transmission line and sensing waveguide. The formulation and calibration of the model are introduced first. Simulations of groundwater level and deformation monitoring are used as examples to demonstrate the power of the model.

TDR Wave Propagation Model

TDR Physical System

A TDR measurement setup is composed of a TDR device and a transmission line system (see Fig. 1(*a*)). The TDR device generally consists of a pulse generator, a sampler, and an oscilloscope; the transmission line is composed of a lead coaxial cable and a sensing waveguide. The sensing waveguide may be a coaxial cable (e.g., for deformation and groundwater level monitoring) or a specially-designed multi-conductor waveguide. The pulse generator sends an electromagnetic pulse along the lead cable and the sensing waveguide directs the electromagnetic wave into the material under test or environment to be monitored. Impedance change occurs when the measurement waveguide is subjected to deformation or electrical properties of the surrounding material change. The reflections due to the impedance change are recorded for analyzing relevant influential parameters. TDR waveguides for geotechnical applications can be grouped into three categories according to the measuring principles.

1. Crimp type: The characteristic impedance of the cable is determined solely by its cross-sectional geometry if the insulating material between conductors remains unchanged. Reflections of the electromagnetic pulse are recorded if the coaxial cable is subjected to loadings and "crimped." When a coaxial cable is embedded in a rock or soil mass, it can be used to monitor the localized shear deformation of the rock or soil mass. It has been shown that the magnitude of the reflected pulse is related to the amount of displacement (Dowding et al. 1988; Dowding and Huang 1994).
2. Interface type: Reflections of the electromagnetic pulse occur at the interfaces of impedance mismatches due to changes in the dielectric properties of the insulating materials. These interfaces may represent groundwater level (air-water interface) or scouring depth (soil-water interface) depending on the design of the waveguide. TDR can efficiently be used to locate the positions of these interfaces (Dowding et al. 1996; Yankielun and Zabilansky 1999).
3. Dielectric type: A waveguide probe with impedance mismatches on both ends is inserted into the material of interest. The electromagnetic pulse is reflected at the beginning and end of the probe. The electrical properties of a material include frequency-dependent dielectric permittivity (ε) and electrical conductivity (σ). A travel time analysis of the two reflections can determine the apparent dielectric constant, while the electrical conductivity (σ) can be measured using the steady-state response, which is readily obtained from the reflected signal at long time. The apparent dielectric constant and electrical conductivity is related to the soil water content and density (Lin et al. 2000; Yu and Drnevich 2004). The complex dielectric permittivity represents the combined effect of frequency-dependent dielectric permittivity and electrical conductivity. The spectral analysis of the TDR signal allows dielectric spectroscopy (i.e., measurement of complex dielectric permittivity at various frequencies) for studying soil-water interaction (Heimovaara 1994; Lin 2003a).

TDR Mathematical Model—Lumped Circuit Model

The cable resistance becomes an important issue in practice. Although a TDR mathematical model has been formulated in various forms (Feng et al. 1999; Dowding et al. 2002; Lin 2003a), the effect of cable resistance has not been properly considered in the model. To complete the TDR mathematical model, a resistance correction factor is formulated within the modeling framework proposed by Lin (2003a). To begin with, the TDR physical system is mathematically described by the equivalent distributed parameter, lumped circuit (Ramo et al. 1994). We may characterize an infinitesimal sec-

tion of the transmission line with a per-unit-length (lumped) capacitance c (F/m), inductance l (H/m), conductance g (S/m), and resistance r (Ω/m), as shown in Fig. 1(b). The line current, I, and the voltage between the conductors, V, in a transmission line can be uniquely defined to describe the electromagnetic wave propagation because of the special field structure (i.e., transverse electromagnetic mode) inside the transmission line. The governing equation in phase form (i.e., in the frequency domain) can be derived as

$$\frac{dV(z)}{dz} = -(r + j2\pi fl)I(z) \tag{1a}$$

$$\frac{dI(z)}{dz} = -(g + j2\pi fc)V(z) \tag{1b}$$

in which z is the position along the line and f is the frequency. The per-unit-length parameters, r, l, g, and c, are functions of the cross-sectional geometry of the transmission line and electromagnetic properties of the media between conductors. The electromagnetic properties of a material is characterized by its dielectric permittivity (ε), electrical conductivity (σ), and magnetic permeability (μ). In general, these parameters are functions of frequency. The dielectric permittivity is often expressed in terms of dielectric permittivity of free space ($\varepsilon_0 = 8.854^{*}10^{-12}$ F/m) and relative dielectric permittivity (ε_r) as $\varepsilon(f) = \varepsilon_0\varepsilon_r(f)$, where ε_r is generally a function of frequency. For materials like soils, the magnetic permeability differs from magnetic permeability of free space ($\mu_0 = 4\pi^{*}10^{-7}$ H/m) by a negligible fraction and the frequency dependency of conductivity can be neglected. The per-unit-length parameters can be written in generic forms as

$$r = \frac{r_s(f)}{\Psi} \tag{2a}$$

$$l = \frac{\mu}{\Theta} + \frac{r}{2\pi f} \tag{2b}$$

$$g = \Theta\sigma \tag{2c}$$

$$c = \Theta\varepsilon(f) \tag{2d}$$

where $r_s(\Omega)$ is the surface resistivity of conductor, Ψ (m) is the geometric factor for resistance, and Θ (dimensionless) is the geometric factor for inductance, conductance, and capacitance. The surface resistivity is a function of frequency, $r_s = \alpha_s^{*}10^{-7}f^{1/2}(\Omega)$, where $\alpha_s(\Omega\sec^{0.5})$ is the characteristic of the conductor for the skin effect. Values of α_s for various typical conductors can be found in Ramo et al. (1994). The generic forms of per-unit-length parameters in Eq 2 are important for deriving the resistance correction factor.

The general solution of Eq 1 can be written as (Ramo et al. 1994)

$$V(z) = V^{+}e^{-\gamma z} + V^{-}e^{\gamma z} \tag{3a}$$

$$I(z) = \frac{V^{+}}{Z_c}e^{-\gamma z} - \frac{V^{-}}{Z_c}e^{\gamma z} \tag{3b}$$

where V^{+} and V^{-} are the two unknown constants in the general solution, γ is the propagation constant, and Z_c is the characteristic impedance. The terms γ and Z_c can be written as

$$\gamma = \sqrt{(r + j2\pi fl)(g + j2\pi fc)} \tag{4a}$$

$$Z_c = \sqrt{\frac{r + j2\pi fl}{g + j2\pi fc}} \tag{4b}$$

Resistance Correction Factor and Parameterization of TDR Model

Equation 4 can be found in most textbooks on electromagnetic waves. But the per-unit-length parameters, r, l, g, and c can be analytically determined from cross-sectional geometry only for special transmission lines (i.e., coaxial lines). Furthermore, these parameters are not independent, as shown in Eq 2. For general purpose, better-parametrized forms for γ and Z_c are derived by substituting Eq 2 into Eq 4, as

$$\gamma = \frac{j2\pi f}{v_0}\sqrt{\varepsilon_r^{*}} * A \tag{5a}$$

$$Z_c = \frac{Z_p}{\sqrt{\varepsilon_r^{*}}} * A \tag{5b}$$

in which v_0 is the speed of light, $\varepsilon_r^{*} = \varepsilon_r - j\sigma/(2\pi f\varepsilon_0)$ is the complex dielectric permittivity, Z_p is the geometric impedance defined as the characteristic impedance in free space, and A is the resistance correction factor accounting for the effect of cable resistance. Z_p and A can be written out as

$$Z_p = \frac{1}{\Theta}\sqrt{\frac{\mu_0}{\varepsilon_0}} \tag{6a}$$

$$A = \sqrt{1 + (1 - j)\left(\frac{\Theta}{\Psi}\right)\left(\frac{\alpha_s}{2\pi\mu_0 \times 10^7\sqrt{f}}\right)} = \sqrt{1 + (1 - j)\frac{\alpha_R}{\sqrt{f}}} \tag{6b}$$

Notably, Z_p is a function only of the geometric factor (Θ), and A is a function of the geometric factors and surface resistivity. The resistance loss factor $\alpha_R(\sec^{-0.5})$ is defined to represent the combined effect of geometric factors and surface resistivity. Equation 5 is the general form for propagation constant and characteristic impedance in TDR modeling. If cable resistance is ignored (i.e., $\alpha_s = 0$), A becomes 1.0 and γ and Z_p have expressions identical to that derived in previous studies (Clarkson et al. 1977; Heimovaara 1994; Feng et al. 1999, Lin 2003a).

The propagation constant (γ) and characteristic impedance (Z_c) are two intrinsic properties of the transmission line. The propagation constant controls the speed and decay of a wave traveling along the line. For a line with sections of different characteristic impedances, reflection and transmission of wave will occur at the section interfaces. Equation 5 was derived to explicitly separate effects of geometric characteristic (i.e., Z_p), material property (i.e., ε_r^{*}), and cable resistance (i.e., A) on the propagation constant and characteristic impedance. Since A is frequency dependent, α_R is defined as the controlling parameter for cable resistance. Both Z_p and α_R depend on probe dimensions. Although the geometric factors (Θ and Ψ) may be calculated theoretically from probe dimensions for simple configurations (i.e., coaxial line), Z_p and α_R are best calibrated from TDR measurements. Thus, the transmission line is uniquely characterized by Z_p, ε_r^{*}, and α_R.

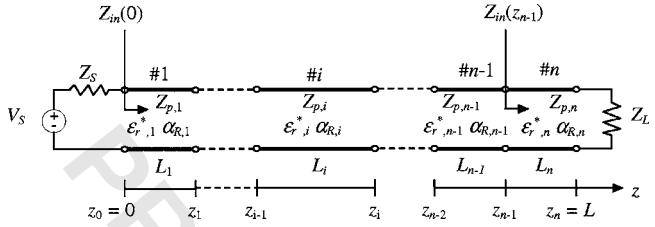

FIG. 2—*Representing a nonuniform line as a cascade of uniform sections, each section characterized by* L_i, $Z_{p,i}$, $\varepsilon^*_{r,i}$, *and* $\alpha_{R,i}$.

Simulation of TDR Waveforms

An actual TDR system consists of a cable tester and a nonuniform transmission line. The line is comprised of a coaxial cable, a transitional device (or probe head), and a sensing waveguide. The resulting transmission line equations became nonconstant-coefficient differential equations. However, a cascade of uniform sections, as shown in Fig. 2, could be used to discretize the nonuniform transmission line. Each uniform section is characterized by L_i, $Z_{p,i}$, $\varepsilon^*_{r,i}$, and $\alpha_{R,i}$. In a line with sections of different characteristic impedances, waves can be reflected and transmitted at the interfaces of the sections. The propagation velocity is a function of frequency since the dielectric permittivity of the insulating material depends on frequency. The TDR waveform recorded by the sampling oscilloscope is a result of multiple reflections and dispersion. Once the propagation constants and characteristic impedances of each uniform section are determined by Eq 5, the frequency response of the TDR sampling voltage $V(0)$ can be derived, following Lin (2003a), as

$$V(0) = \frac{Z_{in}(0)}{Z_{in}(0) + Z_S} V_S = HV_S \tag{7}$$

where $V(0)$ is the Fourier transform of the TDR waveform; V_s is the Fourier transform of the TDR step input; Z_s is the source impedance of the TDR instrument (typically Z_s=50 Ω), $Z_{in}(0)$ is the input impedance at z=0, and H=$Z_{in}(0)/(Z_{in}(0)+Z_S)$ is the system function. As shown in Fig. 2, the input impedance $Z_{in}(z)$ is the equivalent impedance when looking into the circuit from position z. The input impedance at z=0 (i.e., $Z_{in}(0)$) represents the total impedance of the entire nonuniform transmission line. It can be derived recursively from the characteristic impedance and the propagation constant of each uniform section, starting from the terminal impedance Z_L:

$$Z_{in}(z_n) = Z_L$$

$$Z_{in}(z_{n-1}) = Z_{c,n}\frac{Z_L + Z_{c,n}\tanh(\gamma_n l_n)}{Z_{c,n} + Z_L\tanh(\gamma_n l_n)}$$

$$Z_{in}(z_{n-2}) = Z_{c,n-1}\frac{Z_{in}(z_{n-1}) + Z_{c,n-1}\tanh(\gamma_{n-1} l_{n-1})}{Z_{c,n-1} + Z_{in}(z_{n-1})\tanh(\gamma_{n-1} l_{n-1})}$$

$$\vdots$$

$$Z_{in}(0) = Z_{c,1}\frac{Z_{in}(z_1) + Z_{c,1}\tanh(\gamma_1 l_1)}{Z_{c,1} + Z_{in}(z_1)\tanh(\gamma_1 l_1)} \tag{8}$$

where $Z_{c,i}$, γ_i, and l_i, are the characteristic impedance, propagation constant, and length of each section, respectively, and Z_L is the terminal impedance. A typical TDR measurement system uses an open loop (Z_L=∞) or a closed loop (Z_L=0). The form of system function (in Eqs 7 and 8) is identical to that presented in Lin (2003a). But, here the effect of cable resistance is taken into account and formulated as the resistance correction factor in Eqs 5 and 6, which will then be used for calculating the complete system function by Eqs 7 and 8. Both the resistance correction factor A and system function are complex numbers. The effect of cable resistance introduces not only a magnitude modulation but also phase modulus to the system function. The phase modulation was not taken into account in the wave propagation model introduced by Dowding et al. (2002).

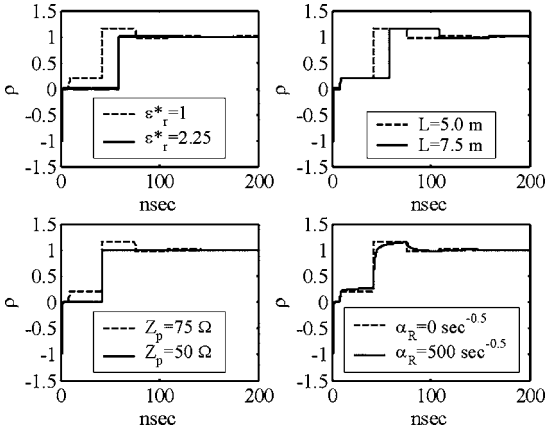

FIG. 3—*Numerical simulations showing the effect of TDR system parameters on the TDR waveforms for short-ended and open-ended condition* (*Reference case:* L=5 m, Z_p=50 Ω, ε^*_r=1.0, α_R=0).

Equations 7 and 8 provide the system function to simulate TDR waveforms of any TDR measurement system which may consist of different types of transmission lines and dielectric materials. For a given TDR measurement system, we need to know the length l_i, the geometric impedance $Z_{p,i}$, the cable resistance parameter $\alpha_{R,i}$, the equivalent dielectric permittivity $\varepsilon^*_{r,i}$ of each uniform section of the nonuniform transmission line, and the terminal impedances, Z_S and Z_L to predict the TDR waveform. Let the voltage source of the TDR be denoted by $v_S(t)$, the sampling voltage of the TDR be denoted by $v_{TDR}(t)$, and the FFT algorithm by function $FFT(\ )$. The simulation of a TDR waveform takes the following steps:

1. Determine the model parameters of each uniform section including L_i, $Z_{p,i}$, $\varepsilon^*_{r,i}$, and $\alpha_{R,i}$.
2. Determine appropriate window size for frequency and time to avoid aliasing in discrete Fourier Transform.
3. Apply the Fast Fourier Transform to the source voltage in frequency domain V_S=$FFT(v_S)$.
4. Subsequently applying Eqs 6, 5, 8, and 7 to determine $V(0)$ in frequency domain.
5. Perform an Inverse Fast Fourier Transform $v_{TDR}(t)$ =$IFFT(V(0))$.

The proposed algorithm is fairly efficient. Unlike the finite difference method, the transmission line is divided into sections only at places where line properties change. Only one element (with parameters L_i, $Z_{p,i}$, $\varepsilon^*_{r,i}$, and $\alpha_{R,i}$) is needed for a long section of uniform line, making it much more efficient than finite difference method (Dowding et al. 2002).

A few simple TDR simulations were performed to demonstrate how the model parameters (L, Z_p, ε^*_r, and α_R) affect the TDR signal (see Fig. 3). The synthetic waveforms represent a TDR device con-

nected to a transmission line with various combinations of model parameters. Frequency-independent material property (i.e., ε_r^* =constant) was assumed and the boundary conditions used were Z_s=50 Ω, Z_L=∞ Ω for an open end, and Z_L=0 Ω for a shorted end. A reference case was chosen as L=5 m, Z_p=50 Ω, ε_r^*=1.0, and α_R=0. To show how each model parameter affects the TDR signal, each model parameter was subsequently altered and the simulated waveforms (for open end and shorted end conditions) were compared to the reference case. As shown in Fig. 3, the time delay of reflection increases with L while Z_p affects the reflection magnitude. The material property (ε_r^*) affects both time delay and reflection magnitude. Therefore, different combinations of (L, Z_p, ε_r^*) can result in the same TDR waveform. This nonuniqueness can also be proved by the wave propagation theory. The cable resistance parameter α_R affects the waveform through the frequency-dependent term A. The rise time of the reflected pulse and the plateau of the step pulses increase as α_R increases. In addition, the steady-state response increases for nonopen terminal condition. The dielectric dispersion and electrical conductivity may also increase the rise time and steady-state response. However, the only parameter that affects the plateau of the step pulse is α_R.

Calibration of TDR Model Parameters

Depending on the TDR applications, one of the three parameters (L, Z_p, ε_r^*) are interpreted from the TDR measurement. For example, the position of an interface (L) is interpreted when TDR is used to monitor displacement (Lin and Tang 2005) or groundwater level (Dowding et al. 1996). The reflection amplitude, which is directly related to change of Z_p, is used to correlate with localized shear deformation (Dowding et al. 1988). $\varepsilon_r^*(f)$ or some features of $\varepsilon_r^*(f)$ are interpreted from TDR measurements when TDR is used to estimate soil physical properties (Topp et al. 1980; Dalton 1992; Heimovaara 1994). These conventional data interpretations are affected by several factors, such as the dielectric relaxation, multiple reflections, and cable resistance, aside from the parameter to be measured. The proposed TDR wave propagation model can be used to improve TDR interpretations for various geotechnical applications.

Instead of making assumptions to some of the system parameters as was done in conventional data interpretations, we can determine the system parameters through proper calibrations before the TDR system is used for measurements. As discussed in the previous section, one of the three parameters (L, Z_p, ε_r^*) needs to be known so that the other two parameters and α_R can be determined from the measured TDR waveform. In geotechnical monitoring, the length L is first determined and fixed. (Z_p, ε_r^*, α_R) is then calibrated from the measured waveform. Subsequent changes of L (due to displacement or groundwater level changes) can be accurately determined by back calculation with known (Z_p, ε_r^*, α_R). The changes of Z_p and L resulted from localized shear deformations can be quantified by back calculation with known (ε_r^*, α_R). For measurement of electrical property, (L, Z_p, α_R) is calibrated for a probe filled with known dielectric property (ε_r^*). Dielectric spectroscopy (i.e., estimation of $\varepsilon_r^*(f)$) can then be performed with the calibrated probe.

Consider a simple example where a 30-m long RG58A/U cable with nominal impedance of 50 Ω is connected to a TDR device (Tektronix 1502C). The cable itself can be a sensing waveguide for detecting localized shear deformation or can be used as a lead cable for various types of measurements. The precise properties (i.e., Z_p, ε_r^*, and α_R) of the cable are of interest before it is put into use for measurements. The dielectric permittivity of polyethylene inside the cable can be considered frequency-independent in the TDR frequency range (i.e., ε_r^*=constant). The open-ended and short-ended signals were measured. Initial values of the parameters to be inverted were assumed. Optimal values of the parameters were obtained by minimizing the residual sum of squares of the difference between the measured and simulated waveforms using the Simplex algorithm (Nelder and Mead 1965). The cable characteristics (Z_p, ε_r^*, and α_R) were backcalculated from the open-ended waveform as (Z_p=75 Ω, ε_r^*=1.9, and α_R=132 sec$^{-0.5}$). Figure 4 shows the measured waveforms and predicted waveforms using the inverted parameters for both open-end and shorted-end conditions. The great match between the measured and predicted waveforms validates the TDR wave propagation model and the calibration by full-waveform inversion. The simulated waveform in which cable resistance is ignored is also shown in Fig. 4. The difference between this waveform and the measured one manifests the importance of accounting for cable resistance. The rise time and the steady-state response are greatly affected by long cables. Errors may arise in the analysis of travel time, steady-state response, magnitude of reflection spike, or spectral response if the cable resistance is not taken into account. The following section will demonstrate the usefulness of the TDR wave propagation model for various geotechnical applications.

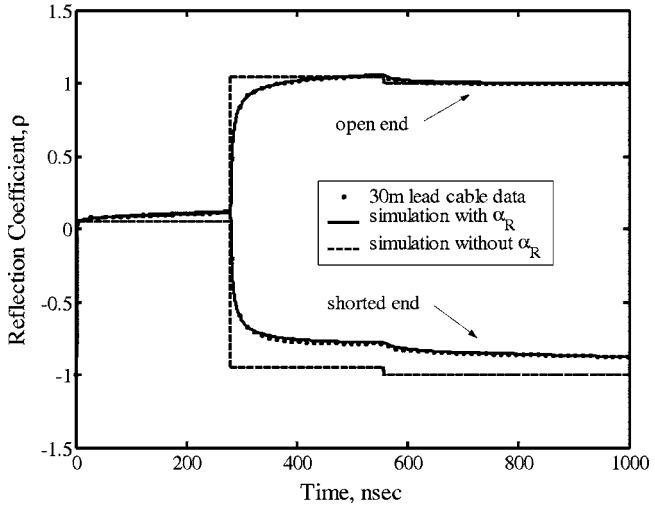

FIG. 4—*Calibrating the cable parameters of a* 30-m *long RG58A/U cable by matching the measured and simulated waveforms.*

Interpretation Based on TDR Wave Propagation Model

Interface and Dielectric Type Example

The dielectric property of the insulating material may vary along the transmission line in interface and dielectric type of applications. The parameter of interest in an interface-type application is the position where dielectric property changes (e.g., groundwater level or scouring depth), while the dielectric property is to be determined in the dielectric-type application where the interface is fixed. In general, waveform inversion based on the TDR wave propagation model can simultaneously determine the interface and the di-

AQ: #1

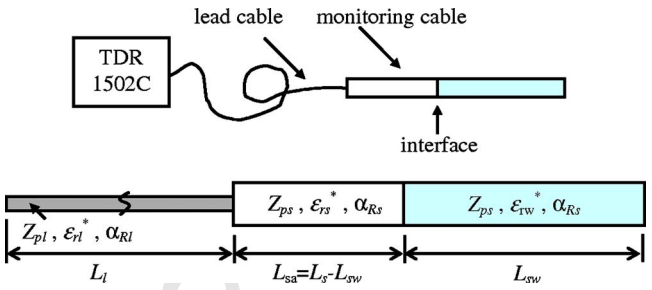

FIG. 5—*Schematic of the laboratory setup for water level monitoring and the associated multi-section transmission line model.*

electric property. As an example, Fig. 5 shows the laboratory setup for water level monitoring. A water level sensing waveguide made of an air-dielectric coaxial cable (Andrew HJ5-50) was connected to the 30-m lead cable described in the preceding section. A TDR measurement with the sensing waveguide simply in air was taken for calibrating the transmission-line parameters (Z_p, ε_r^*, and α_R) of the connector and the sensing waveguide. The sensing waveguide was then inserted into a water-filled tube. Two measurements were taken for water levels at 20 cm and 30 cm from the cable end.

Traditionally, the tangent-line method can be used to locate the air-water interface. A line parallel to the horizontal axis is drawn tangent to the trace at a local minimum around the reflection. A second tangent is drawn at the point of maximum gradient after the local minimum of the TDR waveform. The intersection of this line with the horizontal line determines the reflection point of the interface (Timlin and Pachepsky 1996; Klemunes et al. 1997). The water levels calculated by the tangent-line method are 22.31 cm for the 20-cm water level and 33.72 cm for the 30-cm water level. The discrepancy is attributed to the ambiguity of the empirical tangent-line method. As the cable length increases, the reflected waveform becomes smeared as a result of the cable resistance. Hence, water level cannot be accurately determined by the empirical tangent-line method.

Precise water level can be back calculated from the measured waveform using the wave propagation model with known transmission-line parameters ($Z_{ps}, \varepsilon_{rs}^*, \alpha_{Rs}$) of the sensing waveguide. The sensing waveguide is divided into two parts, one filled with air and the other filled with water. The complex dielectric permittivity (including the electrical conductivity) of groundwater may vary with temperature and contamination. Therefore, it is more general to treat ε_{rw}^* (complex dielectric permittivity of the water in the sensing waveguide) as an unknown. With the capability of full-waveform simulation, the water level and $\varepsilon_{rw}^*(f)$ can be simultaneously determined using the full-waveform inversion. In this case, the monitoring system is divided into three sections of uniform transmission line: the lead cable, sensing waveguide in air, and sensing waveguide in water (see Fig. 5). For simplicity, the connector is considered as part of the lead cable. Parameters ($L_l, Z_{pl}, \varepsilon_{rl}^*, \alpha_{Rl}$) and ($L_s, Z_{ps}, \varepsilon_{rs}^*, \alpha_{Rs}$) can be calibrated beforehand. The remaining unknowns are L_{sw} and ε_{rw}^*. Since the dielectric relaxation frequency of water is much higher than the TDR frequency range, dielectric permittivity of water can be considered frequency-independent in the TDR frequency range. The complex dielectric permittivity of the water can then be written as

$$\varepsilon_{rw}^*(f) = \varepsilon_{rw} - \frac{j\sigma_w}{2\pi f \varepsilon_0} \tag{9}$$

where ε_{rw} and σ_w are the dielectric permittivity and electrical conductivity of water, respectively.

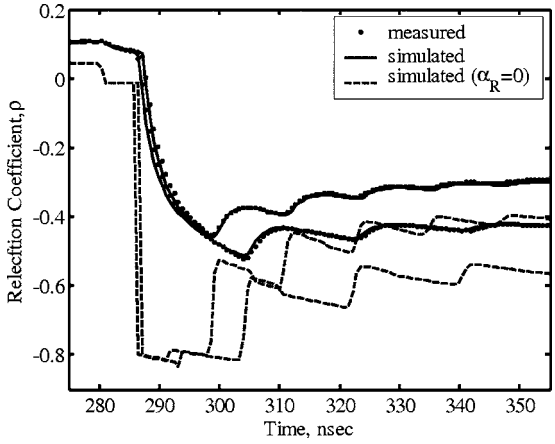

FIG. 6—*Comparison of the measured and predicted TDR waveforms in water level monitoring.*

Figure 6 shows the waveform matching when the inversion converged. Also shown for comparison in Fig. 6 are the simulated waveforms when cable resistance is ignored (α_R=0). The resulting estimations of water level (L_{sw}) were 20.01 cm for the 20-cm water level and 30.48 cm for the 30-cm water level, respectively. In addition, ε_{rw}=79.9 and σ_w=0.0323 S/m were obtained from the inversion, which compares well with the expected values (ε_{rw}=80.2 and σ_w=0.0323 S/m) determined by a three-prong TDR probe and conductivity meter. This example demonstrates the effectiveness of the wave propagation model to infer from the TDR waveform both the interface of impedance mismatch and electrical properties of the material in the sensing waveguide. The interpretation of scouring and sediment monitoring may be treated similarly. When a multi-conductor waveguide or TDR penetrometer is used for soil measurements, the accurate wave propagation model also serves as a precise kernel for inverting dielectric spectrum of soils. Long discussion of dielectric spectroscopy should be left for a separate paper.

Crimp Type Example

The cable is crimped when subjected to localized shear. Conventional data interpretation correlates amplitude of the reflection spike at the crimp with the localized shear deformation. However, the amplitude of the reflection spike is also greatly affected by the cable length and the width of the crimped zone. These factors can be effectively taken into account using the wave propagation model, as will be demonstrated on a direct shear test. Figure 7 illus-

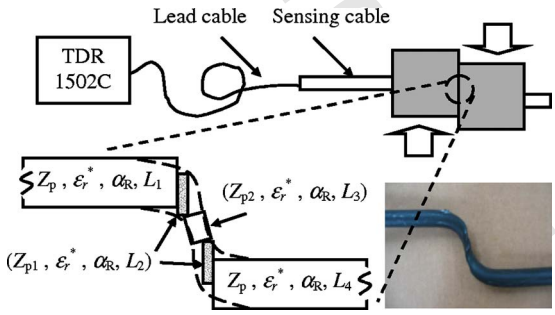

FIG. 7—*Schematic of the laboratory setup for monitoring of localized shear deformation and the associated multi-section transmission line model.*

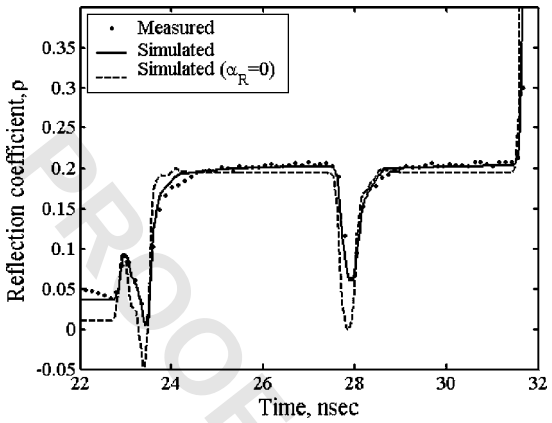

FIG. 8—*Comparison of the measured and predicted TDR waveforms at* 20-mm *shear deformation* (*length of lead cable=2 m*).

trates the direct shear test on a deformation-sensing cable cast in a direct shear box filled with gypsum. Commscope P3-500 was used as the sensing cable (75 Ω, solid aluminum tube swaged onto dielectric core, fully bonded copper clad center conductor). The sensing cable was connected to the TDR device through a 2-m and a 10-m RG58A/U lead cable, respectively.

With known cable length, the transmission-line parameters (Z_p, ε_r^*, and α_R) of the lead cable and sensing cable were first calibrated from measurements prior to shearing. The calibration gave (Z_p=76 Ω, ε_r^*=1.9, and α_R=135 $\text{sec}^{-0.5}$) for the lead cable and (Z_p=90 Ω, ε_r^*=1.5, and α_R=40 $\text{sec}^{-0.5}$) for the sensing cable. As shear deformation develops, the cross-sectional geometry, hence the geometric impedance Z_p, and cable length of the sensing cable changes accordingly, as shown by the photo in Fig. 7. The changes of Z_p and L due to localized shear deformations can be quantified by back calculation with known (ε_r^*, α_R). The sensing cable was discretized into five constant-parameter sections with three sections representing the deformed part, as shown in Fig. 7. The parameters (Z_p, ε_r^*, and α_R) of the undeformed cable are predetermined. After the cable is deformed, the parameters to be back calculated from the measured waveform are (L_1, L_2, L_3, Z_{p1}, and Z_{p2}). At the same shear deformation (e.g., 20 mm), Figs. 8 and 9 show the measured and simulated waveforms with 2-m and 10-m lead cable, respectively. The inverted parameters were (L_1 =0.52 m, L_2=0.0125 m, L_3=0.023 m, Z_{p1}=76.9 Ω, and Z_{p2} =69.6 Ω) for 2-m lead cable and (L_1=0.51 m, L_2=0.0126 m, L_3 =0.025 m, Z_{p1}=76.8 Ω, and Z_{p2}=69.3 Ω) for 10-m lead cable. The simulated waveforms using the inverted parameters (L_1, L_2, L_3, Z_{p1}, and Z_{p2}) match the measured waveforms extremely well. The wave propagation model successfully takes into account the effect of cable resistance and crimped width (i.e., L_2 and L_3,), resulting in a unique relationship between the shear deformation and geometric impedance Z_p.

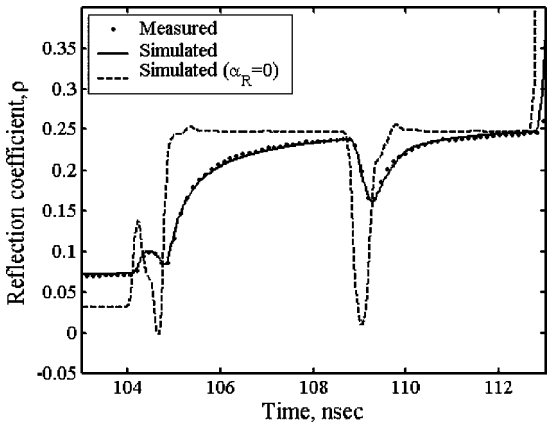

FIG. 9—*Comparison of the measured and predicted TDR waveforms at* 20-mm *shear deformation* (*length of lead cable=10 m*).

Also shown for comparison in Figs. 8 and 9 are the simulated waveforms when cable resistance is ignored (α_R=0). The rise time of the reflection spike increases and the reflection magnitude decreases as cable resistance (or length) increases. As a consequence, the spatial resolution and sensitivity decreases with increasing cable resistance. The high-loss RG58A/U lead cable was used to manifest the importance of accounting for cable resistance. In actual applications, low-loss cable should be used to minimize the reduction of resolution and sensitivity due to cable resistance.

This example demonstrates the accuracy and efficiency of the TDR wave propagation model developed. Similar simulations were also performed by Dowding et al. (2002) using the finite difference approach. However, the accuracy is not as satisfactory because the phase distortion due to cable resistance was not considered. Moreover, the efficiency and stability of the finite difference simulation depends on the time step Δt and spatial step Δz. Spatial resolution is limited by the stability criterion and computational time. Using our approach, very small shear bandwidth can be accurately modeled without stability problem or increasing computational time.

Conclusion

Time domain reflectometry (TDR) is finding more and more applications in geotechnical measurements and monitoring, driving the demand for an accurate TDR wave propagation model. In this study, an efficient, complete, and general-purpose TDR model was developed to account for multiple reflection, dielectric dispersion, and cable resistance all together. The multi-section wave propagation model is formulated in the frequency domain in which the dielectric dispersion and cable resistance can be easily incorporated based on the transmission line theory. A uniform section of transmission line is characterized by its length, cross-sectional geometry, dielectric property, and cable resistance. These properties are parametrized by the length (L), geometric impedance (Z_p), dielectric permittivity (ε_r^*), and resistance loss factor (α_R), respectively. A TDR waveform can be simulated if these four parameters are known for each section of the uniform transmission line. However, L, Z_p, and ε_r^* are found to be correlated in that different combinations of L, Z_p, and ε_r^* can result in the same TDR waveform. To calibrate the TDR system, one of the three parameters (L, Z_p, and ε_r^*) needs to be known a priori so that the other two parameters and α_R can be back calculated from the calibration measurement. One or two of the three parameters (L, Z_p, ε_r^*) will change with the physical parameter to be monitored, depending on the probe design and specific application. The changing parameters can be determined by inverse analysis of the measured waveform. Calibration of TDR cable and TDR interpretations for various geotechnical applications were demonstrated with laboratory experiments. The excellent match between the simulated and recorded waveforms indicates that the model is reliable and accurate. These examples, although simple, show that the proposed numerical procedure is a relatively simple, efficient, and high-resolution tool for probe design, parametric studies, data interpretation, and inverse analyses.

Many new applications and more reasonable data interpretations may be developed with the assistance of the TDR wave propagation model introduced in this study.

Acknowledgment

Funding for this research was provided by the National Science Council of ROC under contract No. 93-2211-E-009-013 and in part by the MOU-ATU program.

References

[1] Benson, C. H., and Bosscher, P. J., 1999, *Time-domain Reflectometry (TDR) in Geotechnics: A Review, Nondestructive and Automated Testing for Soil and Rock Properties, ASTM STP 1350*, W. A. Marr and C. E. Fairhurst, Eds., ASTM International, West Conshohocken, PA.

[2] Clarkson, T. S., Glasser, L., Tuxworth, R. W., and Williams, G., 1977, "An Appreciation of Experimental Factors in Time-Domain Spectroscopy," *J. Assoc. Adv. Med. Instrum.*, Vol. 10, pp. 173–202.

[3] Dalton, F. N., 1992, "Development of Time Domain Reflectometry for Measuring Soil Water Content and Bulk Soil Electrical Conductivity," *Advances in Measurement of Soil Properties: Bring Theory into Practice*, G. C. Topp et al., Eds, Soil Sci. Soc. Am., Madison, WI, SSSA Sp. Pub. 30, pp. 143–167.

[4] Dowding, C. H., and Huang, F.-C., 1994, "Early Detection of Rock Movement with Time Domain Reflectometry," *J. Geotech. Engrg.*, Vol. 120, pp. 1413–1427.

[5] Dowding, C. H., Huang, F.-H., and McComb, P. S., 1996, "Water Pressure Measurement with Time Domain Reflectometry," *Geotech. Test. J.*, Vol. 19, pp. 58–64.

[6] Dowding, C. H., Su, M. B., and O'Connor, K. M., 1988, "Principles of Time Domain Reflectometry Applied to Measurement of Rock Mass Deformation," *Int. J. Rock Mech. and Min. Sci.*, Vol. 25, pp. 287–297.

[7] Dowding, C. H., Summers, J. A., Taflove, A., and Kath, W. L., 2002, "Electromagnetic Wave Propagation Model for Differentiation of Geotechnical Disturbances Along Buried Cables," *Geotech. Test. J.*, Vol. 25, No. 4, pp. 449–458.

[8] Feng, W., Lin, C.-P., Deschamps, R. J., and Drnevich, V. P., 1999, "Theoretical Model of a Multisection Time Domain Reflectometry Measurement System," *Water Resour. Res.*, Vol. 35, No. 8, pp. 2321–2331.

[9] Heimovaara, T. J., 1994, "Frequency Domain Analysis of Time Domain Reflectometry Waveforms 1. Measurement of the Complex Dielectric Permittivity of Soils," *Water Resour. Res.*, Vol. 30, pp. 89–199.

[10] Heimovaara, T. J., Huisman, J. A., Vrugt, J. A., and Bouten, W., 2004, "Obtaining the Spatial Distribution of Water Content Along a TDR Probe Using the SCEM-UA Bayesian Inverse Modeling Scheme," *Vadose Zone J.* 3, pp. 1128–1145.

[11] Klemunes, J. A., Mathew, W. W., and Lopez, A., Jr., 1997, "Analysis of Methods Used in Time Domain Reflectometry Response," *Transp. Res. Rec.*, Vol. 1548, pp. 89–96.

[12] Lin, C.-P., 2003a, "Analysis of a Non-uniform and Dispersive TDR Measurement System with Application to Dielectric Spectroscopy of Soils," *Water Resour. Res.*, Vol. 39, art. no. 1012.

[13] Lin, C.-P., 2003b, "Frequency Domain Versus Traveltime Analyses of TDR Waveforms for Soil Moisture Measurements," *Soil Sci. Soc. Am. J.*, Vol. 67, pp. 720–729.

[14] Lin, C.-P., and Tang, S.-H., 2005, "Development and Calibration of a TDR Extensometer for Geotechnical Monitoring," *Geotech. Test. J.*, Vol. 28, No. 5, pp. 464–471.

[15] Lin, C.-P., Chung, C.-C., and Tang, S.-H., 2006a, "Development of TDR Penetrometer through Theoretical and Laboratory Investigations: 2. Measurement of Soil Electrical Conductivity," *Geotech. Test. J.*, Vol. 29, No. 4, (in press).

[16] Lin, C.-P., Drnevich, V. P., Feng, W., and Deschamps, R. J., 2000, "Time Domain Reflectometry for Compaction Quality Control," *Use of Geophysical Methods in Construction*, *Geotechnical Special Publication No. 108*, ASCE, pp. 15–34. AQ: #2

[17] Lin, C.-P., Tang, S.-H., and Chung, C.-C., 2006b, "Development of TDR Penetrometer Through Theoretical and Laboratory Investigations: 1. Measurement of Soil Dielectric Permittivity," *Geotech. Test. J.*, Vol. 29, No. 4, (in press). AQ: #3

[18] O'Connor, K. M., and Dowding, C. H., 1999, *Geomeasurements by Pulsing TDR and Probes*, CRC Press, Boca Raton.

[19] PermAlert ESP, 1995, Leak Detection/Location Systems, Niles, IL.

[20] Pierce, C. E., Bilaine, C., Huang, F.-C., and Dowding, C. H., 1994, "Effects of Multiple Crimps and Cable Length on Reflection Signatures from Long Cables," *Proceedings of the Symposium on Time Domain Reflectometry in Environmental, Infrastructure, and Mining Applications*, Evanston, IL, 7–9 Sept. 1994, pp. 540–554.

[21] Ramo, S., Whinnery, J. R., and Van Duzer, T., 1994, *Fields and Waves in Communication Electronics*, 3rd ed., John Wiley, New York.

[22] Reece, C. F., 1998, "Simple Method for Determining Cable Length Resistance in Time Domain Reflectometry Systems," *Soil Sci. Soc. Am. J.*, Vol. 62, pp. 314–317.

[23] Robinson, D. A., Jones, S. B., Wraith, J. M., Or, D., and Friedman, S. P., 2003, "A Review of Advances in Dielectric and Electrical Conductivity Measurement in Soils Using Time Domain Reflectometry," *Vadose Zone J.* 2, pp. 444–475.

[24] Siddiqui, S. I., Drnevich, V. P., and Deschamps, R. J., 2000, "Time Domain Reflectometry Development for Use in Geotechnical Engineering," *Geotech. Test. J.*, Vol. 23, No. 1, pp. 9–20.

[25] Timlin, D. J., and Pachepsky, Y. A., 1996, "Comparison of Three Methods to Obtain the Apparent Dielectric Constant from Time Domain Reflectometry Wave Traces," *Soil Sci. Soc. Am. J.*, Vol. 60, pp. 970–977.

[26] Topp, G. C., Davis, J. L., and Annan, A. P., 1980, "Electromagnetic Determination of Soil Water Content and Electrical Conductivity Measurement Using Time Domain Reflectometry," *Water Resour. Res.*, Vol. 16, pp. 574–582.

[27] Yankielun, N. E., and Zabilansky, L., 1999, "Laboratory Investigation of Time-Domain Reflectometry System for Monitoring Bridge Scour," *J. Hydraul. Eng.*, Vol. 125, pp. 1279–1283.

[28] Yu, X., and Drnevich, V. P., 2004, "Soil Water Content and Dry Density by Time Domain Reflectometry," *J. Geotech. Geoenviron. Eng.*, Vol. 130, No. 9, September.

AUTHOR QUERIES — 003702GTJ

#1 au: not in reference list
#2 Au: update.
#3 Au: update.

附錄B

Apparent Dielectric Constant and Effective Frequency of TDR Measurements: Influencing Factors and Comparison

C.-C. Chung and C.-P. Lin*

Department of Civil Engineering, National Chiao Tung University, Hsinchu, Taiwan.

(Paper accepted for publication in Vadose Zone Journal)

*** Corresponding Author:**

Chih-Ping Lin, Professor

Department of Civil Engineering, National Chiao Tung University

1001 Ta-Hsueh Rd., Hsinchu, Taiwan.

Tel. +886-3-513-1574; Fax. +886-3-571-6257

Email: cplin@mail.nctu.edu.tw

Abstract

When measuring soil water content by time domain reflectometry (TDR), several methods are available for determining the related apparent dielectric constant (K_a) from the TDR waveform. Their influencing factors and effective frequencies have not been extensively investigated and results obtained from different methods have not been critically compared. The purpose of this study was to use numerical simulations to systematically investigate the effects of electrical conductivity, cable length, and dielectric dispersion on K_a and the associated effective frequency. Not only does the dielectric dispersion significantly affect the measured K_a, it also plays an important role on how the K_a is affected by electrical conductivity and cable length. Three methods for determining K_a were compared, including the dual tangent, single tangent, and derivative methods. Their effective frequencies were carefully examined with emphasis on whether the effects of electrical conductivity, cable length, and dielectric dispersion can be accounted for by the estimated effective frequency. The results show that there is no consistent trend between the change in K_a and the change in effective frequency as the influencing factors vary. Compensating the effects of electrical conductivity, cable length, and dielectric dispersion by the effective frequency seems theoretically infeasible. To improve the accuracy of TDR soil water content measurements in the existence of these influencing factors, future studies are advocated towards the TDR dielectric spectroscopy or developing signal processing techniques for determining dielectric permittivity near the optimal frequency range.

1. Introduction

In light of great demand for soil moisture monitoring over a short time interval, the measurement of soil dielectric properties as a surrogate for soil water content has become the major technique for such a purpose, including time domain reflectometry (TDR) (Topp et al., 1980; Topp and Ferre, 2002; Robinson et al., 2003a) and capacitance methods (Dean et al., 1987; Paltineanu and Starr, 1997). TDR is typically more accurate due to its higher effective frequency, and often does not require a site-specific calibration. It can also provide accurate measurement of soil electrical conductivity in the same sampling volume (Lin et al., 2007; Lin et al., 2008). Conventional TDR probes using bifilar or trifilar TDR waveguides have limited penetration depth, but new TDR penetrometers have been developed to overcome this limitation (Vaz and Hopmans, 2001; Lin et al., 2006a; Lin et al., 2006b). Despite the success of current TDR technology, the travel time analysis algorithm that is used to extract apparent dielectric constant (K_a) has not been standardized, and there is room for further improving the accuracy of water content determination. Three aspects associated with the travel time analysis are: (a) determination of reflection arrivals, (b) probe calibration, and (c) physical meaning or effective frequency of travel time analysis. These three aspects are briefly reviewed as follows.

Different methods have been proposed to determine the reflection arrivals in travel time analysis. The first methodology is based on the so-called "tangent method" (Topp et al., 1980). The reflection arrival is located at the intersection of the two tangents to the curve, marked as point A in Fig. 1a and called "dual tangent method". While the second tangent line can be drawn at the point of maximum gradient in the rising limb, the location to draw the first tangent line often lacks a clear definition. To facilitate automation, Baker and Allmaras (1990) used a horizontal line tangent to the waveform

at the local minimum. The intersection of this line with the second tangent line is determined as the reflection arrival, marked as point B in Fig. 1a and called "single tangent method". The single tangent method appears to be less arbitrary than the dual tangent method because the points of the local minimum and the maximum gradient can be clearly defined mathematically. Timlin and Pachepsky (1996) and Klemunes et al. (1997) compared both methods and concluded that the single tangent method provided a more accurate calibration equation for water content determination. However, Or and Wraith (1999) concluded that the dual tangent method is more accurate for conditions of high electrical conductivity. The second methodology is based on the apex of the derivative, as marked by point C in Fig. 1b and called the "derivative method". This relatively new method was proposed in research studies discussing the probe calibration (Mattei et al., 2005) and effective frequency (Robinson et al., 2005). Calibration equation based on such a travel time definition has not been found.

The electrical length of the probe needs to be calibrated to convert the apparent travel time to apparent velocity (and thereby the apparent dielectric constant). Water is typically used for such a purpose since it has a well-known and high dielectric permittivity value. However, the start reflection at the interface between probe head and sensing rods typically can not be clearly defined due to mismatches in the probe head. Heimovaara (1993) defined a consistent first reflection point and denoted the round-trip travel time as t_p and the time difference between selected point and the actual start reflection point as t_0, as shown in Fig. 1a. The probe length and t_0 were then calibrated using measurements in air and water. The air-water calibration method was demonstrated by Robinson et al. (2003b) to be accurate across the range of permittivity values in non-dispersive media. They also showed that the calibration performed solely

in water (i.e. only for probe length) using the apex of the first reflection as the first reference start point could introduce a small error at low permittivity values. Locating start reflection by the dual tangent method and calibrating the probe length along, Mattei et al. (2006) showed that the dual tangent method (for locating the end reflection) gives inconsistent probe length calibration in air and water while the derivative method can yield consistent probe length calibration. The anomalous result provided by the dual tangent method was explained by dispersion effects. However, the dielectric dispersion of water is not significant in the TDR frequency range. We believe that the inconsistent probe length calibration with the dual tangent method was attributed to the error in defining the start reflection point. The approach proposed by Heimovaara (1993) using the air-water calibration is supported and used in this study.

The apparent dielectric constant traditionally determined by the travel time analysis using a tangent method does not have a clear physical meaning and is influenced by several system and material parameters. Logsdon (2000) experimentally demonstrated that cable length has a great effect on measurement in high surface area soils and suggested using the same cable length for calibration and measurements. Neglecting cable resistance, Lin (2003) examined how TDR bandwidth, probe length, dielectric relaxation, and electrical conductivity affect travel time analysis by the automated single tangent method. Effects of TDR bandwidth and probe length could be quantified and calibrated, but the calibration equation for soil moisture measurements is still affected by dielectric relaxation and electrical conductivity, due to differences in soil texture and density. Using spectral analysis, Lin (2003) suggested that the optimal frequency range, in which the dielectric permittivity is most invariant to soil texture, lies between 500 MHz and 1 GHz, as illustrated in Fig. 2. Robinson et al. (2005) investigated the effective frequencies, defined by the 10-90% rise time of the

reflected signal, of the dual tangent and derivative methods, considering only the special case of non-conductive and lossless TDR measurements. Their results indicated that the effective frequency corresponds with the permittivity determined from the derivative method and not from the conventional dual tangent method. Nevertheless, Evett et al. (2005) tried to incorporate bulk electrical conductivity and effective frequency, defined by the slope of the rising limb of the end reflection, into the water content calibration equation in a hypothesized form, and showed reduced calibration RMSE. However, the hypothesized form does not have a strong theoretical basis. The effects of dielectric dispersion, electrical conductivity, and cable length on the apparent dielectric constant and effective frequency need further investigation.

Several methods were proposed for determining the apparent dielectric constant (K_a) from a TDR waveform. Their influencing factors have not been extensively investigated and the apparent dielectric constant and effective frequency obtained from different methods have not been critically compared. The objectives of this paper are twofold: (1) to examine effects of electrical conductivity, dielectric dispersion, and cable length on apparent dielectric constant and effective frequency and (2) to investigate whether effects of those factors on the apparent dielectric constant can be accounted for by the effective frequency.

2. Materials and Methods

The wave phenomena in a TDR measurement include multiple reflections, dielectric dispersion, and attenuations due to conductive loss and cable resistance. A comprehensive TDR wave propagation model that accounts for all wave phenomena has been proposed and validated by Lin and Tang (2007). In the context of TDR electrical conductivity measurement, Lin et al. (2007) and Lin et al. (2008) utilized the

TDR wave propagation model to show the correct method for taking account of cable resistance and guideline for selecting proper recording time. With the proven capability to accurately simulate TDR measurements, the TDR wave propagation model can be used to systematically investigate effects of dielectric dispersion, electrical conductivity, and cable length on apparent dielectric constant and effective frequency. Synthetic TDR measurements (waveforms) were generated by varying the influential factors in a controlled fashion. The associated apparent dielectric constants and effective frequencies were calculated and compared.

2.1 Synthetic TDR Measurements (Waveforms)

The behavior of electromagnetic wave propagation in the frequency domain can be characterized by the propagation constant (γ) and the characteristic impedance (Z_c). The propagation constant controls the velocity and attenuation of electromagnetic wave propagation and the characteristic impedance controls the magnitude of reflection. The propagation constant (γ) and characteristic impedance (Z_c) taking into account dielectric dispersion, electrical conductivity, and cable resistance can be written as (Lin and Tang, 2007)

$$\gamma = \frac{j2\pi f}{c}\sqrt{\varepsilon_r^*} * A \qquad [1a]$$

$$Z_c = \frac{Z_p}{\sqrt{\varepsilon_r^*}} * A \qquad [1b]$$

$$A = \sqrt{1 + (1-j)\left(\frac{\eta_0}{Z_p}\right)\frac{\alpha_R}{\sqrt{f}}} \qquad [1c]$$

where c is the speed of light, $\varepsilon_r^* = \varepsilon_r - j\sigma/(2\pi f\varepsilon_0)$ is the complex dielectric permittivity (including the effect of dielectric permittivity ε_r and electrical conductivity σ, in which

ε_0 is the dielectric permittivity of free space), Z_p is the geometric impedance (characteristic impedance in air), A is the per-unit-length resistance correction factor, j is the complex unit, $\eta_0 = \sqrt{\mu_0 / \varepsilon_0} \approx 120\pi$ is the intrinsic impedance of free space (in which μ_0 is the magnetic permeability of free space), α_R ($\sec^{-0.5}$) is the resistance loss factor (a function of the cross-sectional geometry and surface resistivity due to skin effect), and f is the frequency. Each uniform section of a transmission line is characterized by its length, cross-sectional geometry, dielectric property, and cable resistance. These properties are parameterized by the length (L), geometric impedance (Z_p), dielectric permittivity (ε_r^*), and resistance loss factor (α_R). Once these parameters are known or calibrated, TDR waveforms can be simulated using Eq. [1] and the modeling framework proposed by Lin (2003). The propagation constants and characteristic impedances of each uniform section are first determined by Eq. [1]. The input impedance at location $z = 0$ (source end), $Z_{in}(0)$, represents the total impedance of the entire non-uniform transmission line. It can be derived recursively from the characteristic impedance and the propagation constant of each uniform section, starting from the terminal impedance Z_L:

$$
\begin{aligned}
Z_{in}(z_n) &= Z_L \\
Z_{in}(z_{n-1}) &= Z_{c,n}\frac{Z_L + Z_{c,n}\tanh(\gamma_n l_n)}{Z_{c,n} + Z_L\tanh(\gamma_n l_n)} \\
Z_{in}(z_{n-2}) &= Z_{c,n-1}\frac{Z_{in}(z_{n-1}) + Z_{c,n-1}\tanh(\gamma_{n-1} l_{n-1})}{Z_{c,n-1} + Z_{in}(z_{n-1})\tanh(\gamma_{n-1} l_{n-1})} \\
&\vdots \\
Z_{in}(0) &= Z_{c,1}\frac{Z_{in}(z_1) + Z_{c,1}\tanh(\gamma_1 l_1)}{Z_{c,1} + Z_{in}(z_1)\tanh(\gamma_1 l_1)}
\end{aligned}
\qquad [2]
$$

where $Z_{c,i}$, γ_i, and l_i, are the characteristic impedance, propagation constant, and length of each uniform section, respectively, and Z_L is the terminal impedance. A typical TDR

measurement system uses an open loop ($Z_L = \infty$). The frequency response of the TDR sampling voltage $V(0)$ can then be written in terms of the input impedance as

$$V(0) = \frac{Z_{in}(0)}{Z_{in}(0) + Z_S} V_S = H V_S \quad [3]$$

where $V(0)$ is the Fourier transform of the TDR waveform (v_t) ; V_s is the Fourier transform of the TDR step input; Z_s is the source impedance of the TDR instrument (typically Z_s = 50 Ω), $Z_{in}(0)$ is the input impedance at z = 0, and H=Z_{in} (0)/(Z_{in} (0)+Z_S) is the transfer function of the TDR response. The TDR waveform is the inverse Fourier transform of $V(0)$.

The synthetic TDR measurement system is composed of a TDR device, a RG-58 lead cable, and a sensing waveguide. Possible mismatches due to connectors and probe head are neglected since the simplification will not affect the apparent dielectric constant. Tap water and a silt loam modeled by the Cole-Cole equation were used as the basic materials. It is understood that the Cole-Cole equation may not be perfect for modeling dielectric dispersion of soils, since additional relaxations at lower frequencies might exist and multiple Cole-Cole relaxations would be more accurate. Although multiple Cole-Cole relaxations might be mandatory for dielectric spectroscopy, the simple Cole-Cole equation was used to parameterize the dielectric dispersion for the parametric study of dispersion effect. The transmission line parameters and dielectric properties used in the parametric study are listed in Table 1 and Table 2, respectively. Time interval $\Delta t = 2.5\times10^{-11}$ sec and time window $T = 8.2\times10^{-6}$ sec (slightly greater than the pulse length of 7×10^{-6} sec in a TDR 100) were used in the numerical simulations. The corresponding Nyquist frequency (half the sampling frequency, sometimes called the cut-off frequency) and frequency resolution are 20 GHz and 60 kHz, respectively. The Nyquist frequency is well above the frequency bandwidth of

TDR 100 and the long time window ensures that the steady state is obtained before onset of the next step pulse.

As shown in Table 2, two dielectric permittivity values representing water and a silt loam were mainly used in the parametric study to show how K_a and effective frequency are affected by EC, cable length, and dielectric dispersion. A similar study has been done by Robinson et al. (2005). But their study was limited to non-conductive materials and a lossless cable. To compare with what has been done, the same permittivity range (ε_{dc} values of 10, 25, 50, 75 and 100; and ε_{∞} values of 1.44, 2.18, 3.40, 4.63 and 5.85) with two different relaxation frequencies (0.1 GHz and 10 GHz) were used to reproduce the Fig. 3b in Robinson et al. (2005). The transmission line parameters used were the same as the parametric study's reference case listed in Table 1. Different EC and cable length values were used to show their influence and importance.

2.2 Travel Time Analysis and Effective Frequency

An arbitrary time in the reflection waveform was chosen as the reference time. The arrival time of the end reflection was determined by different methods including the single tangent, dual tangent, and derivative methods, as shown in Fig. 1. The time between these two points is denoted as t_p, which is a combination of the actual travel time in the sensing waveguide (t_s) and a constant time offset (t_0) between the reference time and the actual start point. The travel time t_p is related to the apparent dielectric constant (K_a) by the following relationship:

$$t_p = t_0 + t_s = t_0 + 2L\sqrt{K_a}/c \qquad [4]$$

where L is the electrical length of the probe. The time offset t_0 and the probe length L were calibrated by taking measurements in air and water with known values of

permittivity, as suggested by Heimovaara (1993). It should be noted that different values of system parameters (t_0 and L) may be obtained when different methods of travel time analysis are used.

Two methods have been used to investigate the "effective frequency" of the K_a measurement. One method compares the K_a from the travel time analysis with the permittivity obtained from the frequency domain dispersion curve (Or and Rasmussen, 1999; Lin, 2003). The other method is based on the 10-90% rise time of the end reflection (Logsdon, 2000; Robinson et al., 2005). To avoid confusion, the first approach is termed "equivalent frequency f_{eq}". It is determined by matching K_a estimated from travel time analysis methods to the frequency-dependent apparent dielectric permittivity $\varepsilon_a(f)$ (Von Hippel, 1954)：

$$K_a = \varepsilon_a(f_{eq}) = \frac{\varepsilon_r^{'}(f_{eq})}{2}\left(1+\sqrt{\left(\frac{\varepsilon_r^{''}(f_{eq})+\frac{\sigma}{2\pi f_{eq}\varepsilon_0}}{\varepsilon_r^{'}(f_{eq})}\right)^2}\right) \quad [5]$$

where $\varepsilon_r^{'}$ is the real part of the permittivity due to energy storage and $\varepsilon_r^{''}$ is the imaginary component due to dielectric loss. For determining equivalent frequencies in the parametric study, the real and imaginary permittivity as functions of frequency were known a priori from model parameters listed in Table 1 and Table 2. Unlike Or and Rasmussen (1999), the apparent dielectric permittivity $\varepsilon_a(f)$ is used instead of the real part of dielectric permittivity to take into account effects of dielectric loss and electrical conductivity on phase velocity. The second approach is termed "frequency bandwidth f_{bw}". It is defined by the 10%-90% rise time (t_r) of the end reflection as (Strickland, 1970)

$$f_{bw} = \frac{\ln\left(\frac{0.9}{0.1}\right)}{2\pi t_r} \approx 0.35 / t_r \qquad [6]$$

where t_r is measured in seconds. In actual TDR measurements, the equivalent frequency can not be uniquely determined since real and imaginary permittivities in Eq. [5] are also unknown. Therefore, the frequency bandwidth was defined in hopes that it can represent the equivalent frequency. In this paper, both the equivalent frequency and the frequency bandwidth as functions of the influencing factors are examined and compared.

3. Results and Discussion

3.1 Importance of EC and Cable Length

Robinson et al. (2005) investigated the frequency bandwidth (defined by Eq. [6]) of the dual tangent and derivative methods. Their results (Fig. 3b in Robinson et al., 2005) indicated that K_a of the derivative method is equivalent to the calculated permittivity by substituting the frequency bandwidth into the equivalent frequency in Eq. [5], providing physical meaning to the derivative method. However, their study was limited to zero EC and lossless cable. To see whether the neglected EC and cable resistance matters, the same procedure was followed but additionally bringing in the effect of EC and cable resistance. Figure 3, similar to Fig. 3b of Robinson et al. (2005), shows the apparent dielectric constant of the derivative method versus the calculated permittivity from the frequency bandwidth for various conditions. Figure 3a and 3b reveal the effect of EC for the reference cable length. The relation between K_a of the derivative method and calculated permittivity from the frequency bandwidth falls on 1:1 line in non-dispersive materials (with relaxation frequency greater than TDR bandwidth) regardless of EC value. As the material becomes dispersive and conductive,

the relation deviates from the 1:1 line. Figure 3c and 3d reveal the effect of cable length for zero EC. Similarly, cable resistance becomes an influencing factor when the material is dispersive. These results show that both EC and cable resistance play important roles for dispersive materials and Robinson et al. (2005)'s finding that the frequency bandwidth correspond with K_a of the derivative method holds only for limited EC and cable length values. In the context of soil moisture determination, whether K_a is the same as the calculated permittivity from the effective frequency is not critical, it is of more concern how K_a varies with influencing factors while the actual water content may remain the same. It is also of interest whether the effective frequency can provide useful information for compensating the effects of the influencing factors. Therefore, the subsequent discussions focus on variation of apparent dielectric constant and effective frequency as functions of EC, cable length, and dielectric dispersion.

3.2 Effect of Electrical Conductivity

The electrical conductivity is well known for having a smoothing effect on the reflected waveform and hence affecting the K_a determination. However, the degree of influence may depend on dielectric dispersion and the method of travel time analysis. Varying the value of electrical conductivity in water (as a non-dispersive case) and silt loam (as a dispersive case), Fig.4 shows the effects of electrical conductivity on K_a for different methods of travel time analyses. In the non-dispersive case, only the single tangent method is slightly affected by the electrical conductivity. Both the dual tangent method and derivative method are unexpectedly immune to changing electrical conductivity (see Fig. 4a). As the medium becomes dispersive within the TDR bandwidth, the apparent dielectric constant becomes sensitive to changing electrical

conductivity (see Fig. 4b). Among all methods, the dual tangent method is least affected by electrical conductivity. When EC is greater than 0.05 Sm^{-1}, the single tangent method and derivative method suddenly obtains higher apparent dielectric constants as EC increases. The K_a may even become greater than DC electric permittivity due to significant contribution of EC at low frequencies.

For each simulated waveform, the equivalent frequencies of different travel time analysis methods and the frequency bandwidth of the end reflection were determined by Eq. [5] and Eq. [6], respectively. The equivalent frequencies and frequency bandwidth associated with Fig. 4b (the dispersive case) is shown in Fig. 5. Only the dispersive case is shown since the equivalent frequencies in non-dispersive case is not meaningful. Against common perception, the frequency bandwidth is not significantly affected by electrical conductivity. The end reflection may appear smoothed due do decreased reflection magnitude as electrical conductivity increases. The 10%-90% rise time and hence the frequency bandwidth remains relatively constant. The equivalent frequencies decrease with increasing electrical conductivity as expected. In this particular case, the frequency bandwidth is close to the equivalent frequency of the derivative method in the middle range of EC. The dual tangent method leads to the highest equivalent frequency while the derivative method, as also pointed out by Robinson et al. (2005), results in the lowest equivalent frequency, which is closer to the frequency bandwidth. The dual tangent is advantageous in this regard since, at higher frequency, the apparent dielectric permittivity is less affected by changing electrical conductivity. But unfortunately, it's automation of data reduction is also most difficult.

3.3 Effect of Cable Resistance

The per-unit-length parameters that govern the TDR waveform include capacitance, inductance, conductance, and resistance. The first three parameters are

associated with electrical properties of the medium and cross-sectional geometry of the waveguide. The per-unit-length resistance is a result of surface resistivity and cross-sectional geometry of the waveguide (including cable, connector, and sensing probe), which is often ignored in early studies of TDR waveform by assuming a short cable. The cable resistance is practically important since significantly long cable is often used in monitoring (Lin and Tang, 2007; Lin et al., 2007). Not only does it affect the steady-state response and how fast the TDR waveform approaches the steady state, the cable resistance also interferes with the transient waveform related to the travel time analysis, as shown in Fig. 6 for measurements in water with different cable lengths. The "significant length" in which cable resistance becomes unnegligible depends on the cable type, which could range from lower quality RG-58, medium quality RG-8, to higher quality cables with solid outer conductor used in CATV industry. The RG-58 cable is used for simulation in this study to manifest the effect of cable resistance and since it has been widely used for its easy handling.

The measurements of water and the silt loam with various cable lengths were simulated. As an attempt to counteract the effects of cable length, the system parameters (i.e. t_0 and L) were obtained by air-water calibration for each cable length. The cable resistance significantly distorted the TDR waveform. Consequently, the calibrated probe length increases with increasing cable length, as shown in Table. 3. Figure 7 shows the effects of cable length on K_a for different methods of travel time analyses. In the non-dispersive case (Fig. 7a), all methods are not affected by cable length if air-water calibrations are performed for each cable length. As the medium becomes dispersive within the TDR bandwidth, the apparent dielectric constant becomes quite sensitive to changing cable length (see Fig. 7b), in particular for the derivative method, even though the probe parameters have been calibrated by the

air-water calibration procedure for each cable length. Figure 7 suggests that the empirical relationship between K_a and soil water content depends on cable length if the soil is significantly dielectric-dispersive. This is in agreement with the finding in Logsdon (2000). When studying the effect of cable length on K_a–water content calibration for high surface areas soils, Logsdon (2000) concluded that high surface area samples should be calibrated using the same cable length used for measurements. This is even more imperative if the derivate method is used.

The equivalent frequencies and frequency bandwidth associated with Fig. 7b (the dispersive case) is shown in Fig. 8. Both the equivalent frequency and frequency bandwidth decreases with increasing cable length. The single tangent and dual tangent methods have similar trends, while the derivative method is most sensitive to the cable length and results in the lowest equivalent frequency. Therefore, the derivative method can yield a K_a greater than DC dielectric permittivity due to existence of electrical conductivity and low equivalent frequency. In this particular case, the equivalent frequency of the derivative method corresponds to the frequency bandwidth only for cable length around 10~15 m.

3.4 Effect of Dielectric Relaxation Frequency

The apparent dielectric constant does not have a clear physical meaning when the dielectric permittivity is dispersive and conductive. Based on the Cole-Cole equation, the effects of dielectric relaxation frequency f_{rel} on K_a were investigated by varying f_{rel} in Table 2 while keeping other Cole-Cole parameters constant. The water-based cases represent cases with large difference between ε_∞ and ε_{dc} (defined as $\Delta\varepsilon = \varepsilon_{dc} - \varepsilon_\infty$), and the silt loam-based cases represent cases with relatively small $\Delta\varepsilon$. The apparent dielectric constants as affected by f_{rel} are shown in Fig. 9. The f_{rel} seems to have a lower

bound frequency below which the dielectric permittivity is equivalently non-dispersive and equal to ε_{∞}, and a higher bound frequency above which the dielectric permittivity is equivalently non-dispersive and equal to ε_{dc}. As f_{rel} increases from the lower bound frequency to the higher bound frequency, the apparent dielectric constant goes from ε_{∞} to ε_{dc}. In these relaxation frequencies, the derivative method yields higher K_a than tangent methods because its equivalent frequency is always lower than that of tangent methods. Comparing Fig. 9a with Fig. 9b, the lower bound frequency seems to decrease as $\Delta\varepsilon$ increases. That is, the higher the $\Delta\varepsilon$, the wider the relaxation frequency range is affected by the dielectric dispersion.

Also depicted in Fig. 9 are the associated frequency bandwidths as affected by the relaxation frequency. When the relaxation frequency is outside the frequency range spanned by the aforementioned lower bound and higher bound, the dielectric permittivity does not show dispersion in the TDR frequency range, and hence the corresponding frequency bandwidth is relatively independent of f_{rel}. The frequency bandwidth decreases as the relaxation frequency becomes "active" and reaches the lowest point near the middle of the "active" frequency range spanned by the lower bound and higher bound.

3.5 Apparent Dielectric Constant vs. Frequency Bandwidth

The effects of electrical conductivity, cable resistance, and dielectric dispersion were systematically investigated. These factors can significantly affect the measured apparent dielectric constant. The equivalent frequency would give some physical meaning to the measured apparent dielectric constant, but no method is available for its direct determination from the TDR measurement. Even if the equivalent frequency of the apparent dielectric constant can be determined, it may not correspond to the optimal

frequency range for water content measurement, as shown in Fig. 1. The frequency bandwidth, often referred to as the effective frequency in the literature, can be determined from the rise time of the end reflection. It was anticipated to correspond to the equivalent frequency of the derivative method. However, this correspondence is not generally true. Besides, the derivative method is quite sensitive to electrical conductivity and cable resistance, and hence would not be a good alternative to the conventional tangent line methods. Nevertheless, the frequency bandwidth of the TDR measurement offers an extra piece of information. An idea has been proposed to incorporate frequency bandwidth into the empirical relationship between apparent dielectric constant and soil water content (e.g. Evett et al., 2005). To examine whether this idea is generally feasible, the relationship between apparent dielectric constant from the dual tangent method and frequency bandwidth is plotted in Fig. 10 using the data obtained from previous three parametric studies. The electrical conductivity, cable length, and dielectric dispersion apparently have distinct effects on the K_a-f_{bw} relationship. In fact, the change in apparent dielectric constant vs. the change in frequency bandwidth as the influencing factors vary is divergent. When measuring soil water content, the same water content may measure different apparent dielectric constants due to different electrical conductivity (e.g. water salinity), cable length, and dielectric dispersion (e.g. soil texture). Since there is no consistent trend between the change in apparent dielectric constant and the change in frequency bandwidth, compensating the effects of electrical conductivity, cable length, and dielectric dispersion by the frequency bandwidth seem theoretically infeasible. As shown in Fig. 2, Lin (2003) suggested that there is an optimal frequency range, in which the dielectric permittivity is most invariant to soil texture (dielectric dispersion). To improve the accuracy of TDR soil water content in the existence of the influencing factors, the

actual real part of dielectric permittivity near the optimal frequency range should be measured and used to correlate with water content. Dielectric spectroscopy (measurement of frequency-dependent dielectric permittivity) based on the full waveform model that takes into account the electrical conductivity and cable resistance can be used for such a purpose. However, dielectric spectroscopy is still not the state of practice due to its complex computation and system calibration. Future studies are suggested to simplify the TDR dielectric spectroscopy or develop signal processing techniques for determining dielectric permittivity near the optimal frequency range.

4. Conclusions

The apparent dielectric constant (K_a) derived from various travel time analyses (e.g. duel tangent, single tangent, and derivative methods) does not have a clear physical meaning. Although earlier study showed that K_a of the derivative method corresponds with the effective frequency determined from the reflection rise time, this finding is true only for limited EC and cable length values. Using numerical simulations, this study systematically investigated the influencing factors, including electrical conductivity (EC), dielectric dispersion, and cable resistance, and the associated effective frequencies.

The material is perceivably dispersive in a TDR measurement when the dielectric relaxation frequency (f_{rel}) is within a frequency range. Within this frequency range, the apparent dielectric constant and frequency bandwidth (determined from the rise time of the end reflection) are sensitive to f_{rel}. Dielectric dispersion also plays an important role on how electrical conductivity and cable length affect K_a. In non-dispersive cases, K_a is not affected by EC, and effects of cable length on K_a can be accounted for by adjusting the probe parameters (i.e. the probe length and a constant time associated with arrival time of the incident wave) using air-water calibration for each cable length. In

dispersive cases, K_a becomes dependent on EC, particularly at high EC, and cable length, regardless of the effort of air-water calibration for each cable length.

Comparing methods of travel time analysis, the dual tangent method, although most difficult to be automated, yields a K_a with the highest equivalent frequency (i.e. a frequency at which the K_a is equal to the frequency-dependent dielectric permittivity) and is least sensitive to EC and cable length. The derivative method has the lowest equivalent frequency and is quite sensitive to EC and cable length for dispersive materials. Thus it is not a good alternative to the conventional tangent line methods.

There is no general correspondence between the frequency bandwidth and equivalent frequencies from various travel time analyses. Nevertheless, the frequency bandwidth of the TDR measurement does offer an extra piece of information. Simulation results were examined to see whether the effects of EC, cable length, and dielectric dispersion on the K_a can be reflected on and accounted for by the frequency bandwidth. The results show that there is no consistent trend between the change in K_a and the change in frequency bandwidth as the influencing factors vary. Therefore, compensating the effects of electrical conductivity, cable length, and dielectric dispersion by the frequency bandwidth seems theoretically infeasible. To improve the accuracy of soil water content measurement by TDR, future studies are suggested on TDR dielectric spectroscopy or developing signal processing techniques for determining dielectric permittivity within the optimal frequency range between 500 MHz to 1 GHz.

Reference

Baker, J. M., and R. R. Allmaras. 1990. System for automating and multiplexing soil moisture measurement by time-domain reflectometry. Soil Sci. Soc. Am. J. 54: 1-6.

Dean, T. J., J. P. Bell, and A. B. J. Baty. 1987. Soil moisture measurement by an improved capacitance technique: I Sensor design and performance. J. Hydrol. 93: 67-78.

Evett, S. R., J. A. Tolk, and T. A. Howell. 2005. Time domain reflectometry laboratory calibration in travel time, bulk electrical conductivity, and effective frequency. Vadose Zone Journal 4: 1020–1029.

Friel, R., and D. Or. 1999. Frequency analysis of time-domain reflectometry with application to dielectric spectroscopy of soil constituents. Geophysics 64: 707-718.

Heimovaara, T. J. 1992. Comments on “time domain reflectometry measurements of water content and electrical conductivity of layered soil columns”. Soil Sci. Soc. Am. J. 56: 1657-1658.

Heimovaara, T. J. 1993. Design of triple-wire time domain reflectometry probes in practice and theory. Soil Sci. Soc. Am. J. 57: 1410-1417.

Klemunes, J. A., W. W. Mathew, and A. Lopez, Jr. 1997. Analysis of methods used in time domain reflectometry response. Trans. Res. Rec. 1548: 89–96.

Lin, C. -P. 2003. Frequency domain versus travel time analyses of TDR waveforms for soil moisture measurements. Soil Sci. Soc. Am. J. 67: 720–729.

Lin, C. -P., C. -C. Chung, and S. -H. Tang. 2006b. Development of TDR penetrometer through theoretical and laboratory investigations: 2. measurement of soil electrical conductivity. Geotechnical Testing Journal 29: Paper ID GTJ 14315.

Lin, C. -P., C. -C. Chung, and S. -H. Tang. 2007. Accurate TDR measurement of electrical conductivity accounting for cable resistance and recording time. Soil Sci. Soc. Am. J. 71: 1278-1287.

Lin, C. -P., C. -C. Chung, J. A. Huisman, and S. -H. Tang. 2008. Clarification and

calibration of reflection coefficient for TDR electrical conductivity measurement. Soil Sci. Soc. Am. J. (in press).

Lin, C. -P., S. -H. Tang, and C. -C. Chung. 2006a. Development of TDR Penetrometer through Laboratory Investigations: 1. Measurement of Soil Dielectric Constant. Geotechnical Testing Journal 29: Paper ID: GTJ14093

Lin, C. -P., and S. -H. Tang. 2007. Comprehensive wave propagation model to improve TDR interpretations for geotechnical applications. Journal of Geotechnical and Geoenvironmental Engineering 30: Paper ID GTJ 100012.

Logsdon, S. D. 2000. Effect of cable length on time domain reflectometry calibration for high surface area soils. Soil Sci. Soc. Am. J. 64: 54-61.

Mattei, E., A. Di Matteo, A. De Santis, and E. Pettinelli. 2006. Role of dispersion effects in determining probe and electromagnetic parameters by time domain reflectometry. Water Resour. Res. 42: W08408.

Or, D. and V. P. Rasmussen. 1999. Effective frequency of TDR traveltime-based measurement of soil bulk dielectric permittivity. p. 257–260. *In* Third Workshop on Electromagnetic Wave Interaction with Water and Moist Substances. 11-13 Apr. 1999. Athens, GA.

Or, D., and J. M. Wraith. 1999. Temperature effects on soil bulk dielectric permittivity measured by time domain reflectometry: a physical model. Water Resour. Res. 35: 371–383.

Paltineanu, I. C., and J. L. Starr. 1997. Real-time water dynamics using multisensor capacitance probes: Laboratory capacitance probes. Soil Sci. Soc. Am. J. 61: 1576-1585.

Robinson, D. A., S. B. Jones, J. M. Wrath, D. Or, and S. P. Friedman. 2003a. A review of advances in dielectric and electrical conductivity measurements in soils using

time domain reflectometry. Vadose Zone J. 2: 444-475.

Robinson D. A., Schaap M., Jones S. B., Friedman S. P. and Gardner C. M. K. 2003b. Considerations for improving the accuracy of permittivity measurement using TDR: Air / water calibration, effects of cable length. Soil Sci. Soc. Am. J., 76: 62-70.

Robinson, D. A., M. G. Schaap, D. Or, and S. B. Jones. 2005. On the effective measurement frequency of time domain reflectometry in dispersive and non-conductive dielectric materials, Water Resour. Res. 40: W02007.

Strickland, J. A.. 1970. Time-domain reflectometry measurements. Tektronix Inc., Beaverton, Oregon.

Timlin, D. J., and Y. A. Pachepsky. 1996. Comparison of three methods to obtain the apparent dielectric constant from time domain reflectometry wave traces. Soil Sci. Soc. Am. J. 60: 970–977.

Topp, G.. C., J. L. Davis, and A. P. Annan. 1980. Electromagnetic determination of soil water content: measurements in coaxial transmission lines. Water Resour. Res. 16: 574-582.

Topp, G.. C., and P. A. Ferre. 2002. Water Content. pp.417-421. Dane, J. H. and G. C. Topp. *in* Methods of Soil Analysis. Part 4: Physical Methods. SSSA Book Ser. vol. 5. Soil Sci. Soc. of Am. Madison, Wis.

Vaz, C. M. P., and J. W. Hopmans. 2001. Simultaneous measurement of soil penetration resistance and water content with a combined penetrometer–TDR moisture probe, Soil Sci. Soc. Am. J., *65*, 4–12.

Von Hippel, A. R. 1954. Dielectrics and Waves. John Wiley. Hoboken, N. J.

List of Tables

Table 1. TDR system parameters used in the numerical simulations

Section	*Parameters*	*Reference value*	*Range*
Sensing waveguide	EC σ, S/m	0.01	0.005 ~ 0.1
	Dielectric permittivity ε_r	Tap water, and Silt loam†	with varying f_{rel}
	Geometric impedance Z_p , Ω	300	300
	Length L, m	0.3	0.3
	Resistance loss factor α_R , $sec^{-0.5}$	0	0
Lead cable (RG-58)	EC σ, S/m	0	0
	Dielectric permittivity ε_r	1.95	1.95
	Geometric impedance Z_p , Ω	77.5	77.5
	Length L, m	10	1 ~ 50
	Resistance loss factor α_R , $sec^{-0.5}$	19.8	19.8

† Referring to the Cole-Cole parameters listed in Table 2

Table 2. Cole-Cole† parameters for the materials used in the numerical simulations (modified after Friel and Or 1999)

Material	ε_{dc}	ε_{∞}	f_{rel}	β
Silt loam	26.0	18.0	0.2e9	0.01
Tap water	78.54††	4.22	17e9	0.0125

† Cole-Cole equation: $\varepsilon_r(f) = \varepsilon_{\infty} + \dfrac{\varepsilon_{dc} - \varepsilon_{\infty}}{1 + \left[j(f / f_{rel})\right]^{1-\beta}}$

†† Water temperature = 25°C

Table 3. The calibrated probe length (m) obtaied from the air-water calibration for different cable lengths and methods of travel time analysis

Methods	*Cable Length*			
	1 m	*10 m*	*25 m*	*50 m*
Single tangent method	0.2935	0.2968	0.3020	0.3049
Dual tangent method	0.2934	0.2968	0.3015	0.2993
Derivative method	0.3025	0.3062	0.3129	0.3352

List of Figures

compared for different cable lengths.

Fig. 7. The apparent dielectric constants as affected by cable length in (a) the non-dispersive case and (b) the dispersive case.

Fig. 8. The equivalent frequency and frequency bandwidth corresponding to Fig. 7(b).

Fig. 9. The apparent dielectric constant and frequency bandwidth obtained by changing the dielectric relaxation frequency while keeping other Cole-Cole parameters constant in (a) water and (b) silt loam.

Fig. 10. The relationship between apparent dielectric constant from the dual tangent method and frequency bandwidth.

Fig. 1.

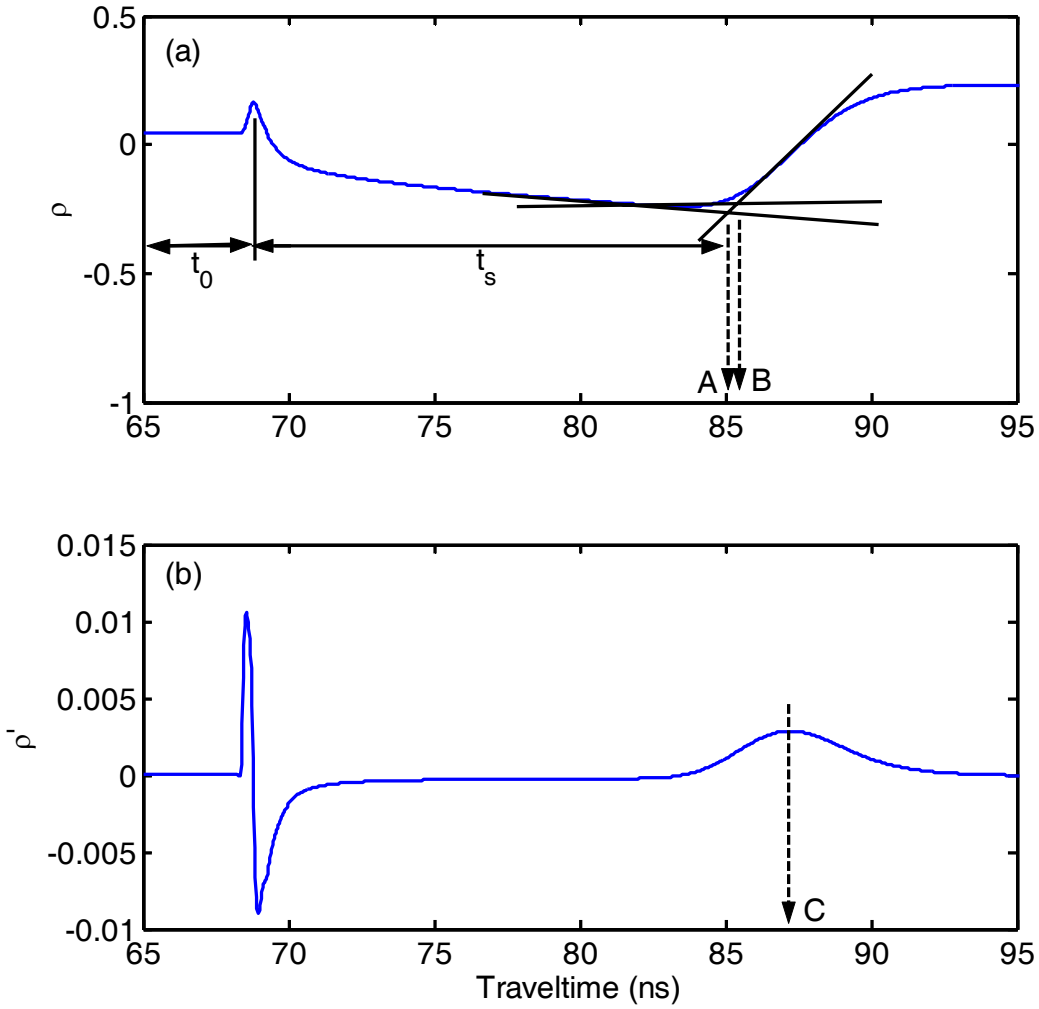
(a)
0.5
0
-0.5
-1
ρ
t0
ts
A
B
65
70
75
80
85
90
95
(b)
0.015
0.01
0.005
0
-0.005
-0.01
ρ'
C
Traveltime (ns)

Fig. 2.

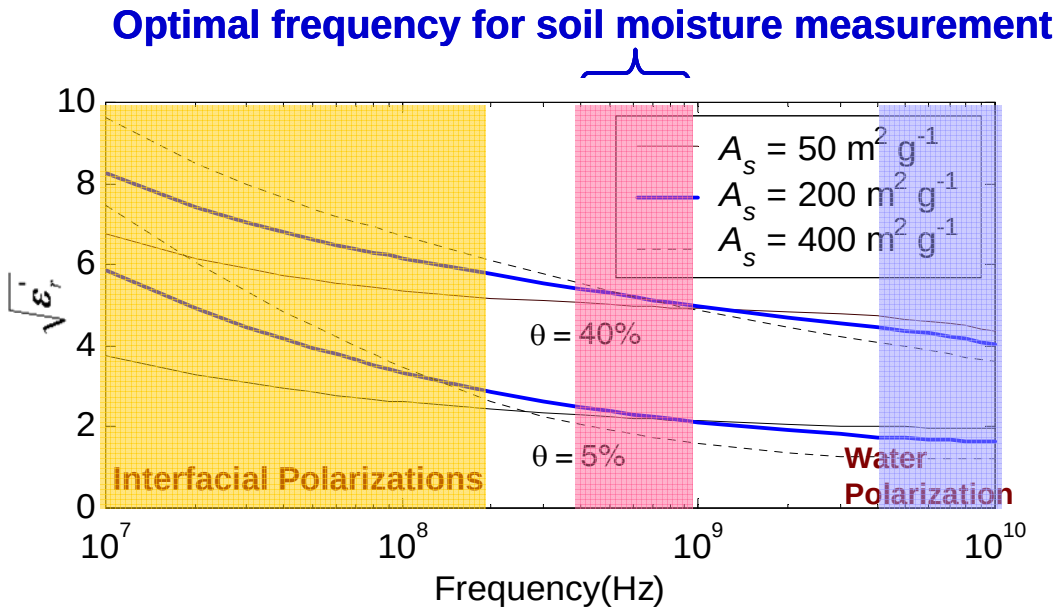
Optimal frequency for soil moisture measurement
10
8
6
4
2
0
$\sqrt{\varepsilon_r'}$
A_s = 50 m^2 g^{-1}
A_s = 200 m^2 g^{-1}
A_s = 400 m^2 g^{-1}
θ = 40%
θ = 5%
Interfacial Polarizations
Water Polarization
10^7
10^8
10^9
10^{10}
Frequency(Hz)

Fig. 3.

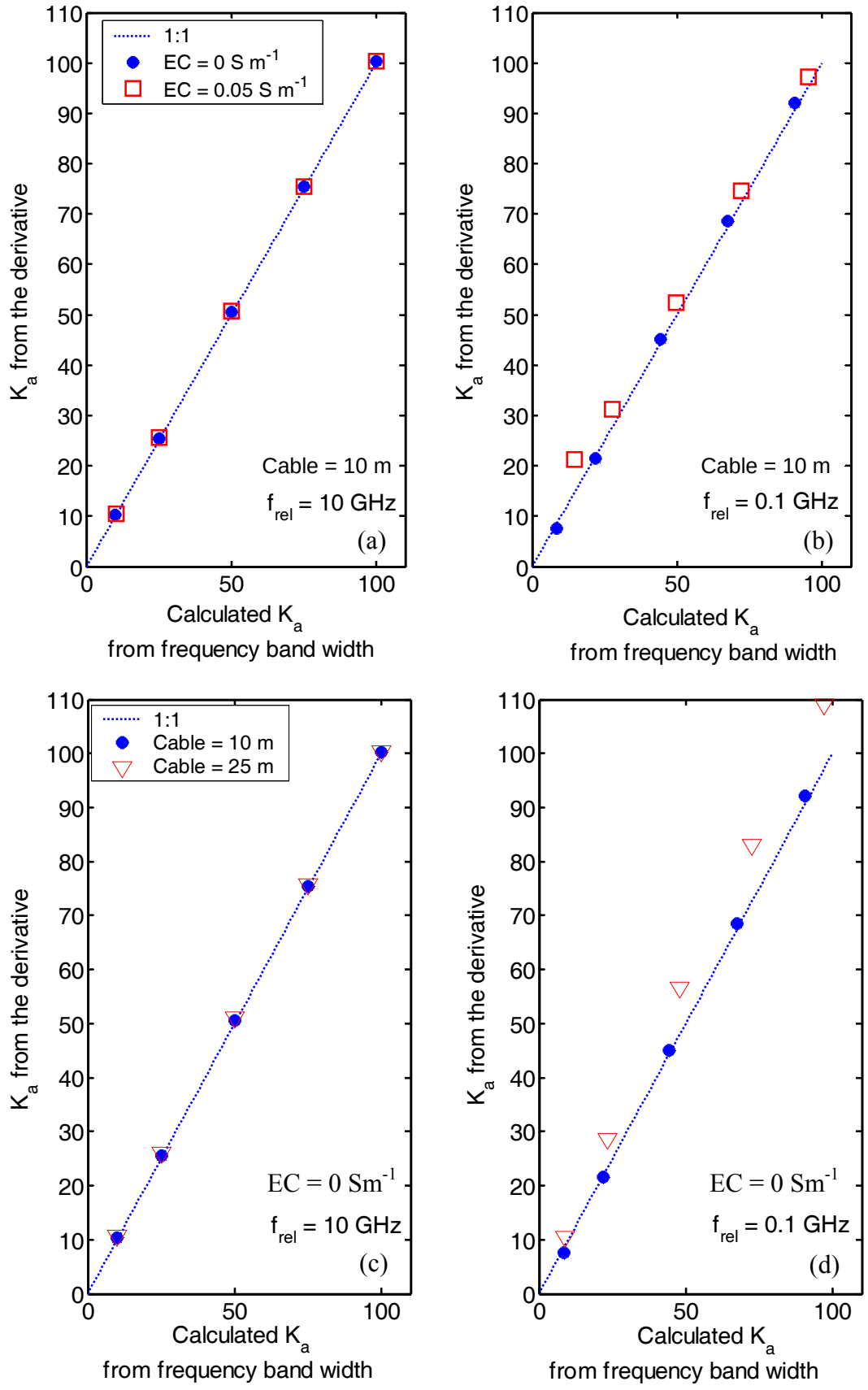
1:1
EC = 0 S m-1
EC = 0.05 S m-1
Cable = 10 m
frel = 10 GHz
(a)
Ka from the derivative
Calculated Ka
from frequency band width
Cable = 10 m
frel = 0.1 GHz
(b)
1:1
Cable = 10 m
Cable = 25 m
EC = 0 Sm-1
frel = 10 GHz
(c)
EC = 0 Sm-1
frel = 0.1 GHz
(d)

Fig. 4.

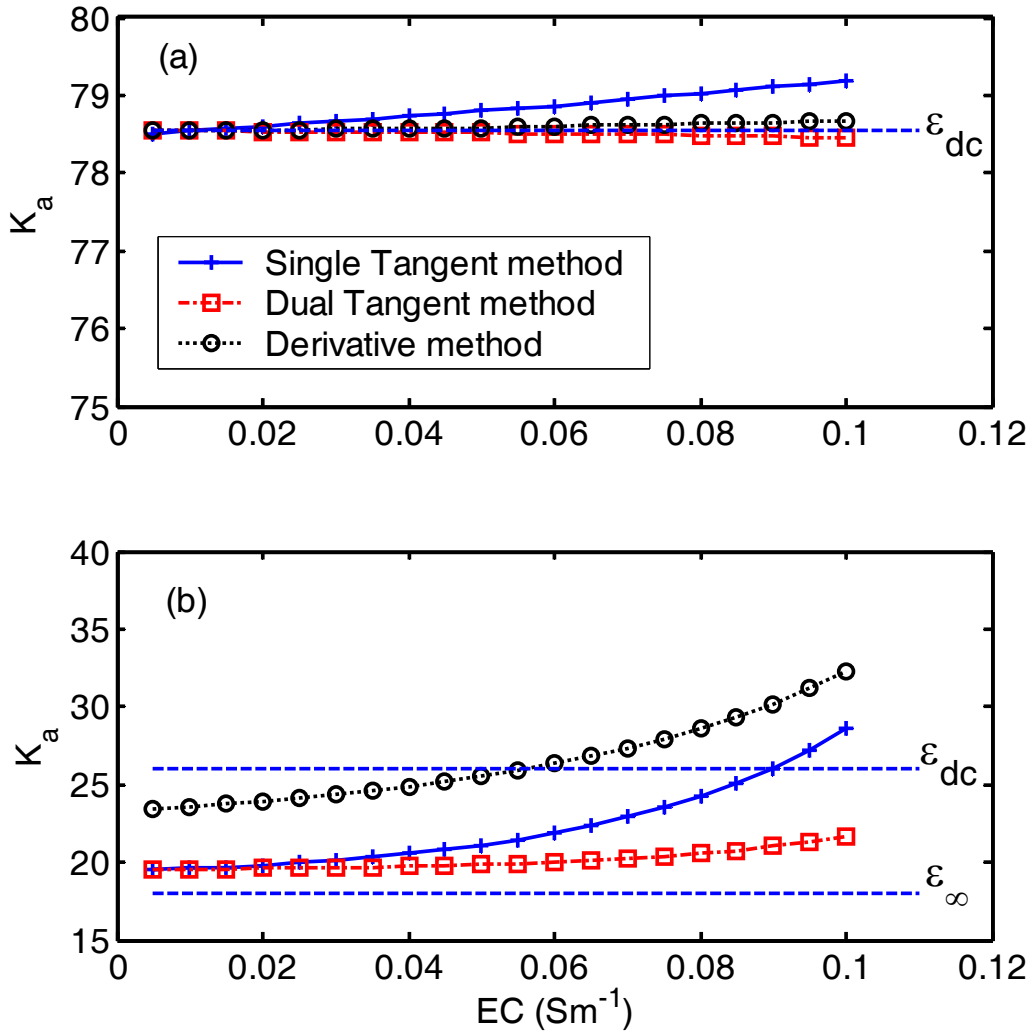
(a)
80
79
78
77
76
75
K_a
0
0.02
0.04
0.06
0.08
0.1
0.12
ε_{dc}
Single Tangent method
Dual Tangent method
Derivative method
(b)
40
35
30
25
20
15
K_a
ε_{dc}
ε_{∞}
EC (Sm^{-1})

Fig. 5.

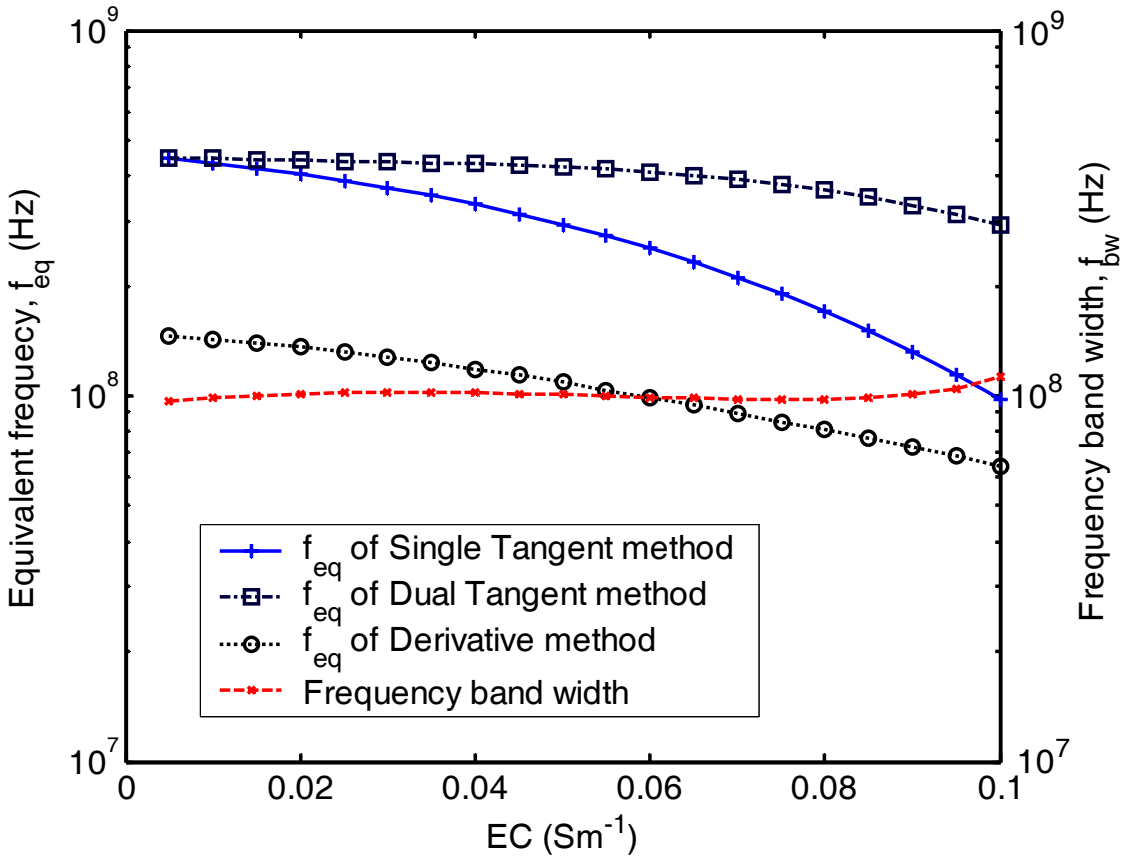
10^9
10^8
10^7
0
0.02
0.04
0.06
0.08
0.1
EC (Sm^{-1})
Equivalent frequecy, f_{eq} (Hz)
Frequency band width, f_{bw} (Hz)
f_{eq} of Single Tangent method
f_{eq} of Dual Tangent method
f_{eq} of Derivative method
Frequency band width

Fig. 6.

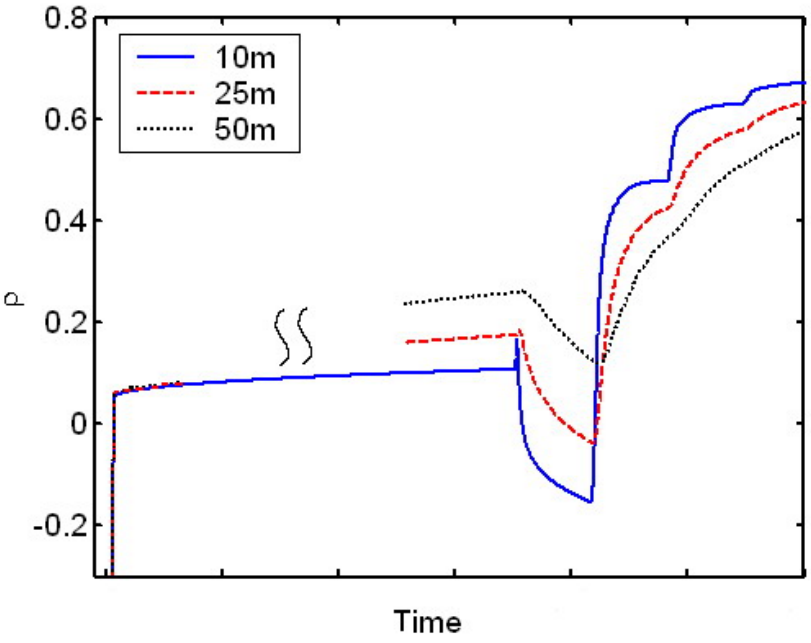

Fig. 7.

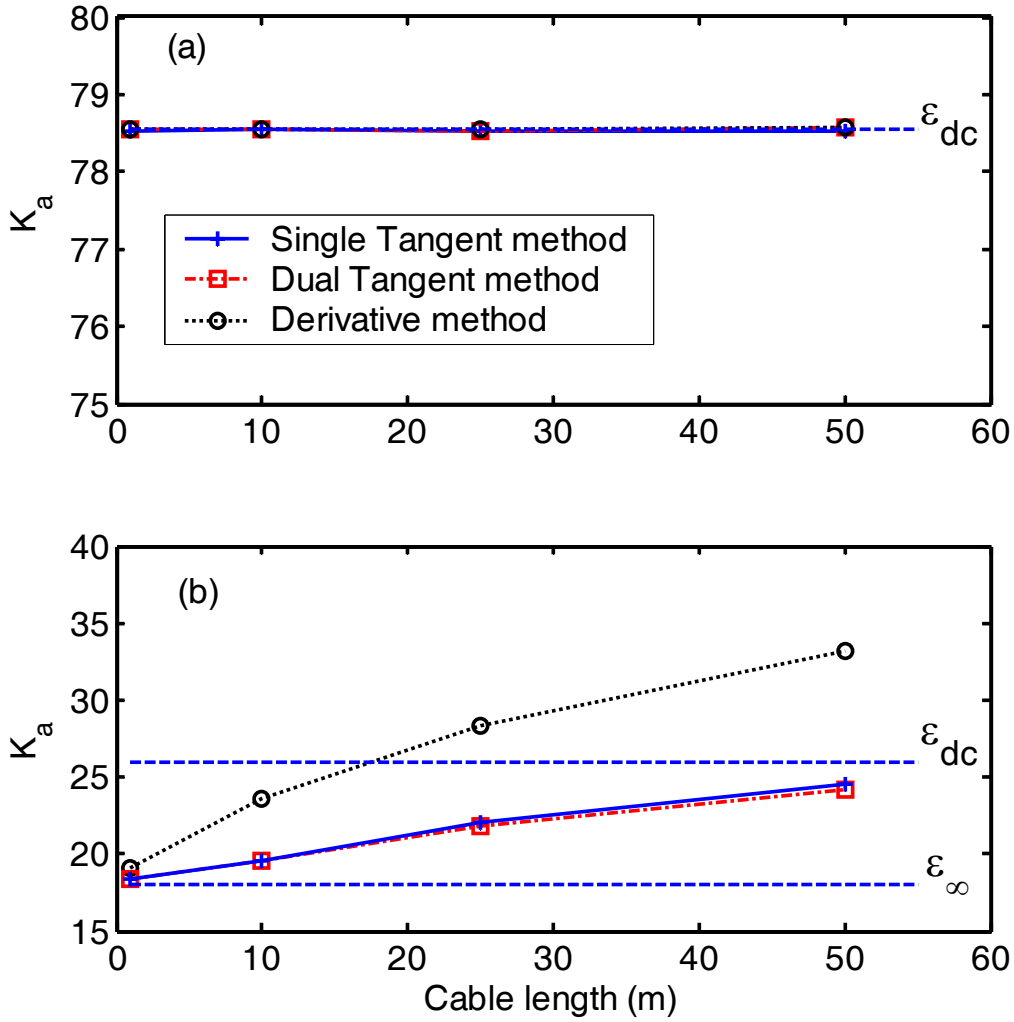
(a)
80
79
78
77
76
75
K_a
ε_{dc}
Single Tangent method
Dual Tangent method
Derivative method
0
10
20
30
40
50
60
(b)
40
35
30
25
20
15
K_a
ε_{dc}
ε_{∞}
Cable length (m)

Fig. 8.

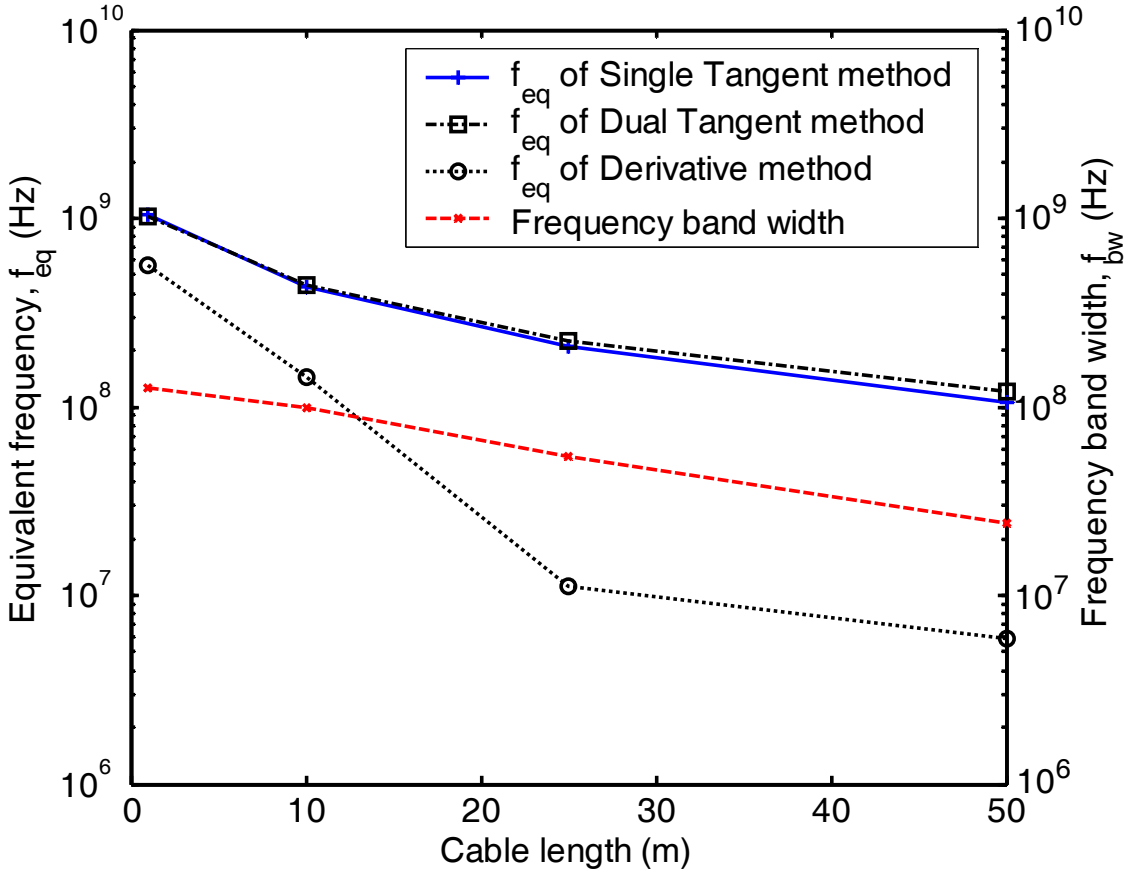
f_{eq} of Single Tangent method
f_{eq} of Dual Tangent method
f_{eq} of Derivative method
Frequency band width
Equivalent frequency, f_{eq} (Hz)
Frequency band width, f_{bw} (Hz)
Cable length (m)
10^{10}
10^{9}
10^{8}
10^{7}
10^{6}
0
10
20
30
40
50

Fig. 9.

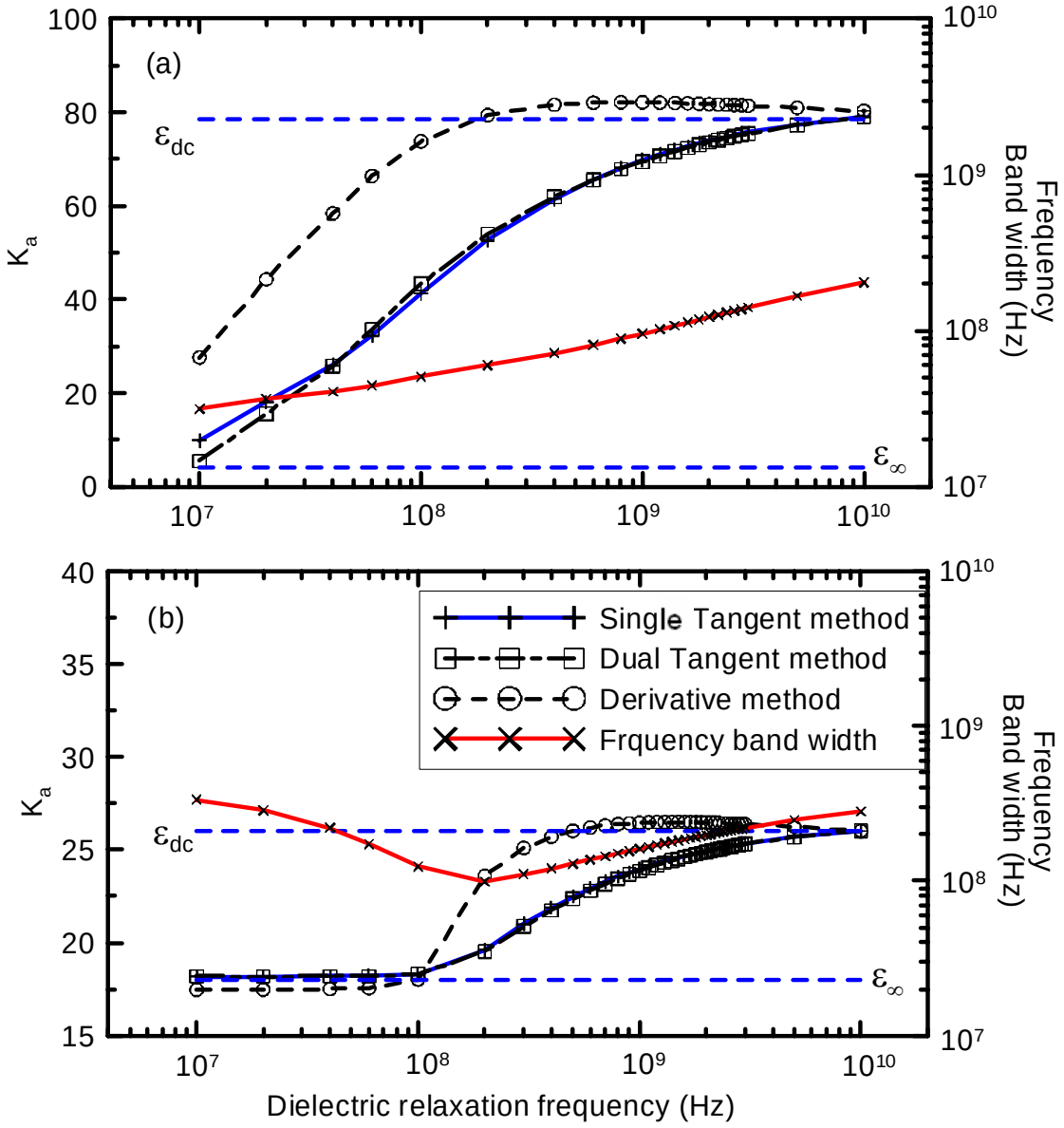
(a)
ε_{dc}
ε_{∞}
K_a
Frequency Band width (Hz)
100
80
60
40
20
0
10^{10}
10^{9}
10^{8}
10^{7}
(b)
Single Tangent method
Dual Tangent method
Derivative method
Frquency band width
ε_{dc}
ε_{∞}
K_a
Frequency Band width (Hz)
40
35
30
25
20
15
10^{10}
10^{9}
10^{8}
10^{7}
10^{7}
10^{8}
10^{9}
10^{10}
Dielectric relaxation frequency (Hz)

Fig. 10.

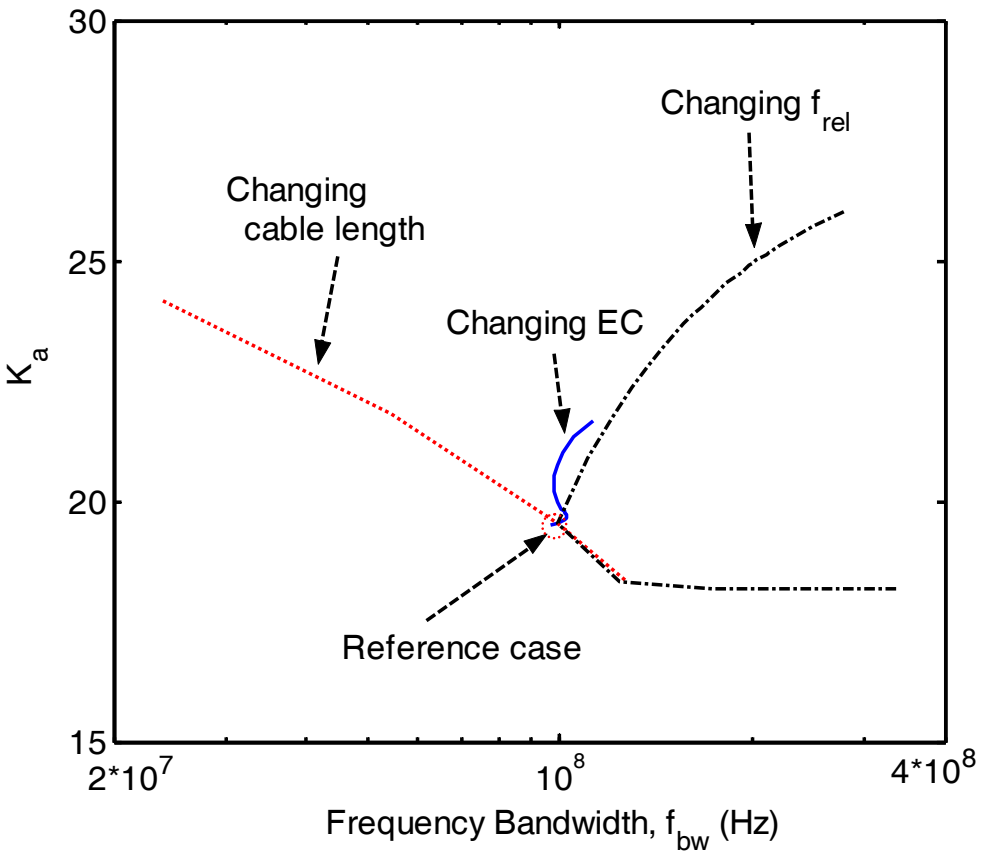
30
25
20
15
K_a
Changing f_{rel}
Changing
cable length
Changing EC
Reference case
$2*10^7$
10^8
$4*10^8$
Frequency Bandwidth, f_{bw} (Hz)

附錄C

Accurate Time Domain Reflectometry Measurement of Electrical Conductivity Accounting for Cable Resistance and Recording Time

C.-P. Lin*
C. C. Chung
S.-H. Tang
Dep. of Civil Engineering
National Chiao Tung Univ.
1001 Ta-Hsueh Rd.
Hsinchu, Taiwan.

Methods accounting for cable resistance in time domain reflectometry (TDR) based electrical conductivity measurements remain controversial, and the effect of TDR recording time has been underrated when long cables are used. A comprehensive full waveform model and the direct current (DC) analysis were used to show the correct method for taking cable resistance into account and guidelines for selecting proper recording time. The Castiglione–Shouse scaling method was found to be incorrect because the effect of cable resistance on the steady-state reflection coefficient is nonlinear. To account for cable resistance, the series resistors model is theoretically sound and should be used. The characteristic impedance of the lead cable has a frequency-dependent increase due to cable resistance, resulting in a rising step pulse and multiple reflections within the cable section. Hence, reaching the steady state takes much longer time than conventionally thought when long cables are used, in particular at very low and very high electrical conductivities. To determine the electrical conductivity accurately, the recording time should be taken after 10 multiple reflections within the probe and three multiple reflections within the lead cable.

Abbreviations: DC, direct current; EC, electrical conductivity; TDR, time domain electrical conductivity.

The bulk electrical conductivity (EC) of a soil is an important physical parameter for salinity assessment (Rhoades et al., 1989), studying solute transport (Kachanoski et al., 1992; Ward et al., 1994; Vanclooster et al., 1995), and correlating with hydraulic conductivity (Mualem and Friedman, 1991; Friedman and Seaton, 1998; Purvance and Andricevic, 2000). Contaminants also influence soil EC as they change the electrical properties of the pore fluid (Campanella and Weemees, 1990); however, soil water content plays an important role in these problems as well. Due to the ability to measure dielectric permittivity, which in turn can be used to estimate soil water content, and electrical conductivity in the same sampling volume, it is advantageous to measure soil EC based on TDR rather than the conventional DC resistivity method.

Time domain reflectometry is based on transmitting an electromagnetic pulse into a coaxial cable connected to a sensing waveguide and watching for reflections of this transmission due to impedance mismatches at the start and end of the sensing waveguide. The round-trip travel time in the sensing waveguide is related to the dielectric constant and the signal attenuation is associated with the EC of the material surrounding the sensing waveguide. In soil science, early attempts to measure soil EC with TDR used the magnitudes of first reflections from the start and end of the probe (Dalton et al., 1984; Topp et al., 1988; Zegelin et al., 1989), whose locations were somewhat arbitrary due to frequency-dependent attenuation. Later studies replaced the magnitude of the first end reflection with the steady-state reflection magnitude in the algorithm for calculating EC (Yanuka et al., 1988; Zegelin et al., 1989). These early algorithms suffered from several oversimplified assumptions, including the neglect of cable resistance, dielectric dispersion, and multiple reflections in a conductive medium. Topp et al. (1988) and Zegelin et al. (1989) presented the Giese–Tiemann method obtained from the thin sample theory (Giese and Tiemann, 1975) as an alternative method for EC measurement. The applicability of the thin sample theory was not ascertained but the experimental results indicated that it gives more reliable estimates than other methods. Nadler et al. (1991) rediscovered the Giese–Tiemann method, as pointed out by Heimovaara (1992) and Baker and Spaans (1993). Since then, the Giese–Tiemann method has become the standard equation for calculating EC from TDR measurements. At low frequency, as is the case for DC conductivity measurement, the thin sample theory is justified and the effects of dielectric dispersion and multiple reflections can be neglected. The cable resistance is not taken into account in the Giese-Tiemann method, however, and this assumption may become invalid when long cables are used in the field.

Heimovaara et al. (1995) observed that TDR EC measurements were increasingly underestimated as EC increased above 200 mS m^{-1}. These errors were attributed to neglecting series resistance of the cable, connectors, and cable tester as a parameter in the EC calculation. They suggested modeling the coaxial cable and the sample as two resistors in series and the Giese–Tiemann method was modified accordingly. Calibration parameters involved in calculating the TDR EC include the geometric factor (probe constant) and the cable resistance (including resistance loss in connectors and cable tester). These parameters may be calibrated using least square fitting of TDR EC measurements in

Soil Sci. Soc. Am. J. 71:XXX-XXX
doi:10.2136/sssaj2006.0383
Received 7 Nov. 2006.
*Corresponding author (cplin@mail.nctu.edu.tw).

solutions of different concentrations to EC measurements made with a conventional conductivity meter. To expedite calibrations for probes of different lengths, Reece (1998) proposed a method that measures cable resistance directly. Unexplained differences in EC accuracy between the calibration method and the direct measurement method for cable resistance was observed, however, in Heimovaara et al. (1995) and Huisman and Bouten (1999). They suggested that the series resistors theory may be slightly incomplete and the fitting procedure corrects the deviation from theory. More recently, Castiglione and Shouse (2003) demonstrated, both theoretically and experimentally, that the formulation based on the series resistors model is incorrect; however, their disturbing arguments, while seeming logical at a first glance, were in fact troubled by wrong assumptions and incorrect data. The assumption that the steady-state voltage varies exponentially along the cable (their Eq. [17]) and the data (their Fig. 5b) showing the effect of cable resistance on TDR waveforms are not correct. In light of the wrongly claimed insufficiency of the series resistors model, they presented an intuitive method, in which the measured steady-state reflection coefficients are linearly scaled between −1.0 and 1.0 with respect to the range expanded by the measurements in air (EC = 0) and under the short-circuited condition (EC =∞) before applying the Giese–Tiemann method. Despite the lack of a theoretical basis, the effect of cable resistance is inactivated through this linear scaling process and the method is becoming widely accepted (e.g., Robinson et al., 2003). It should be pointed out, however, that the effect of cable resistance on the steady-state reflection coefficient has never been proven to be linear.

The EC measurement by TDR, as easy as it may seem, remains a controversial issue, particularly when long cables are used. It should be noted that TDR is a high-frequency measurement technique with frequency ranging from kiloHertz to gigaHertz. The pulse length (i.e., duration of a single step pulse) is in the order of several microseconds. When TDR is used for determining DC electrical conductivity, it can only work for cases where the time required to reach the steady state is less than the pulse length. The time required to reach steady state strongly depends on the cable resistance. An arbitrary "long" time is usually used without close examination of its legitimacy. No work has been done on the effect of recording time, particularly in the context of long cables. In this study, a comprehensive full waveform analysis and the DC analysis were conducted in a well-parameterized manner. The full waveform analysis was used to examine the theoretical validity of the series resistors model and Castiglione–Shouse method, and to investigate the effect of recording time on these methods. It will be shown that the series resistors model is theoretically sound; the unexplained observations and disputes in the literature may be explained by the time effect.

THEORY

Full-Waveform Analysis

While dielectric spectroscopy requires the full waveform, only the steady-state reflection magnitude is needed for determining EC. With the capability of modeling the full TDR waveform, however, the theoretical validity of DC methods can be objectively examined. The effect of recording time on the DC analysis can also be investigated numerically.

The wave phenomena in a TDR measurement include multiple reflection, dielectric dispersion, and attenuation due to conductive loss and cable resistance. Wave propagation models for TDR have been formulated in various forms (Feng et al., 1999; Lin, 2003), in which multiple reflections, dielectric dispersion, and conductive loss are taken into account. Neglecting cable resistance in these models was justified by the short lead cable used. Cable resistance becomes an important issue in practice, however, when long cables are used. To complete the TDR mathematical model, Lin and Tang (2007) formulated a resistance correction factor (A) within the modeling framework proposed by Lin (2003). The frequency-dependent resistance correction factor is put in a different form here to express the individual contributions of geometric impedance and surface resistivity of conductors.

The behavior of electromagnetic wave propagation in the frequency domain can be characterized by the propagation constant (γ) and the characteristic impedance (Z_c). The propagation constant controls the velocity and attenuation of electromagnetic wave propagation and the characteristic impedance controls the magnitude of reflection. The γ and Z_c, taking into account the cable resistance, can be written as (Lin and Tang, 2007)

$$\gamma = \frac{j2\pi f}{c}\sqrt{\varepsilon_r^*}A \qquad [1a]$$

$$Z_c = \frac{Z_p}{\sqrt{\varepsilon_r^*}}A \qquad [1b]$$

$$A = \sqrt{1+(1-j)\left(\frac{\eta_0}{Z_p}\right)\frac{\alpha_R}{\sqrt{f}}} \qquad [1c]$$

where c is the speed of light, $\varepsilon_r^* = \varepsilon_r - j\sigma/(2\pi f\varepsilon_0)$ is the complex dielectric permittivity (including the effect of dielectric permittivity ε_r and electrical conductivity σ, in which ε_0 is the dielectric permittivity of free space), Z_p is the geometric impedance (characteristic impedance in air), A is the (per-unit-length) resistance correction factor, j is the complex unit, $\eta_0 = \sqrt{(\mu_0/\varepsilon_0)} \sim 120\pi$ is the intrinsic impedance of free space (in which α_0 is the magnetic permeability of free space), α_R ($s^{-0.5}$) is the resistance loss factor (a function of the cross-sectional geometry and surface resistivity due to skin effect), and f is the frequency. If cable resistance is ignored (i.e., $\alpha_R = 0$), A becomes 1.0 and γ and Z_c have expressions identical to the nonresistance formulations (Feng et al., 1999; Lin, 2003). Each uniform section of a transmission line is characterized by its length, cross-sectional geometry, dielectric property, and cable resistance. These properties are parameterized by the length (L), geometric impedance (Z_p), dielectric permittivity (ε_r^*), and resistance loss factor (α_R), as shown in Fig. 1a. Once these parameters are known or calibrated, TDR waveforms can be simulated using Eq. [1] and the modeling framework proposed by Lin (2003). The propagation constants and characteristic impedances of each uniform section are first determined by Eq. [1]. As illustrated in Fig. 1a, the input impedance at $z = 0$, i.e., $Z_{in}(0)$, represents the total impedance of the entire nonuniform transmission line. It can be derived recursively from the characteristic impedance and the propagation constant of each uniform section, starting from the terminal impedance Z_L:

$$\begin{aligned}
Z_{in}(z_n) &= Z_L \\
Z_{in}(z_{n-1}) &= Z_{c,n}\frac{Z_L + Z_{c,n}\tanh(\gamma_n l_n)}{Z_{c,n} + Z_L\tanh(\gamma_n l_n)} \\
Z_{in}(z_{n-2}) &= Z_{c,n-1}\frac{Z_{in}(z_{n-1}) + Z_{c,n-1}\tanh(\gamma_{n-1} l_{n-1})}{Z_{c,n-1} + Z_{in}(z_{n-1})\tanh(\gamma_{n-1} l_{n-1})} \\
&\vdots \\
Z_{in}(0) &= Z_{c,1}\frac{Z_{in}(z_1) + Z_{c,1}\tanh(\gamma_1 l_1)}{Z_{c,1} + Z_{in}(z_1)\tanh(\gamma_1 l_1)}
\end{aligned} \qquad [2]$$

where $Z_{c,i}$, γ_i, and l_i, are the characteristic impedance, propagation constant, and length of each section, respectively, and Z_L is the terminal impedance. A typical TDR measurement system uses an open loop ($Z_L = \infty$). The frequency response of the TDR sampling voltage $V(0)$ can then be written in terms of the input impedance as

$$V(0) = \frac{Z_{in}(0)}{Z_{in}(0) + Z_s} V_s = HV_s \qquad [3]$$

where $V(0)$ is the Fourier transform of the TDR waveform (v_t); V_s is the Fourier transform of the TDR step input; Z_s is the source impedance of the TDR instrument (typically $Z_s = 50\ \Omega$), $Z_{in}(0)$ is the input impedance at $z = 0$, and $H = Z_{in}(0)/[Z_{in}(0) + Z_s]$ is the transfer function of the TDR response. The TDR waveform is the inverse Fourier transform of $V(0)$. Inversion for transmission line parameters or material properties can be done based on this full waveform modeling.

Direct Current Circuit Analysis

From basic circuit theory, the transmission line can be modeled as a lumped circuit when the wavelength is significantly greater than the electrical length. At zero frequency, the lumped circuit is shown in Fig. 1b, equivalent to the assumptions made by Heimovaara et al. (1995) and Reece (1998). The DC lumped circuit model includes the voltage source v_s (double of the pulse step v_0), the inner resistance R_s (equal to the source impedance Z_s), and cable resistance R_{cable} (in fact, the combined series resistance of probe, cable, connector, and cable tester) and soil sample resistance R. The steady-state reflection voltage can be derived from circuit theory as

$$v_\infty = \frac{R + R_{cable}}{R + (R_s + R_{cable})} v_s \qquad [4]$$

where the sample resistance is related to the EC by

$$R = \frac{K_p}{\sigma} \qquad [5]$$

in which K_p is a geometric factor. Substituting Eq. [5] into Eq. [4] and noting $\rho_\infty = (v_\infty - v_0)/v_0$, in which $v_0 = 2v_s$ since the source impedance is typically designed to be identical to the characteristic impedance of the connected transmission line, as shown in Lin (2003), the EC of the sample can be derived as a function of the steady-state reflection coefficient ρ_∞:

$$\sigma = \frac{K_p}{R_s}\left(\frac{1-\rho_\infty}{1+\rho_\infty}\right)\left[\frac{1}{1-\left(\frac{R_{cable}}{R_s}\frac{1-\rho_\infty}{1+\rho_\infty}\right)}\right]$$

$$= \beta\left(\frac{1-\rho_\infty}{1+\rho_\infty}\right) k\left(R_{cable}, \rho_\infty\right) \qquad [6]$$

where β ($=K_p/R_s$) is a probe constant and k is the correction factor for cable resistance, called the *cable correction factor* (to be distinguished from the per-unit-length resistance correction factor A in Eq. [1]). The term $R_{cable}/R_s(1-\rho_\infty)/(1+\rho_\infty)$ is ≤ 1 (which can be proved by substituting R_{cable} from Eq. [11]), so the cable correction factor k can also be written as a power series:

$$k = \frac{1}{1-\left(\frac{R_{cable}}{R_s}\frac{1-\rho_\infty}{1+\rho_\infty}\right)}$$

$$= \left[1 + \left(\frac{R_{cable}}{R_s}\frac{1-\rho_\infty}{1+\rho_\infty}\right) + \left(\frac{R_{cable}}{R_s}\frac{1-\rho_\infty}{1+\rho_\infty}\right)^2 + \left(\frac{R_{cable}}{R_s}\frac{1-\rho_\infty}{1+\rho_\infty}\right)^3 + \ldots\right] \qquad [7]$$

It should be noted that the cable correction factor k depends not only on R_{cable} but also on the EC of the sample, since it is a function of ρ_∞. The effect of cable resistance increases with increasing EC (i.e., as ρ_∞ decreases).

To correctly determine the EC from a TDR measurement, both the probe constant β and cable resistance R_{cable} need to be known.

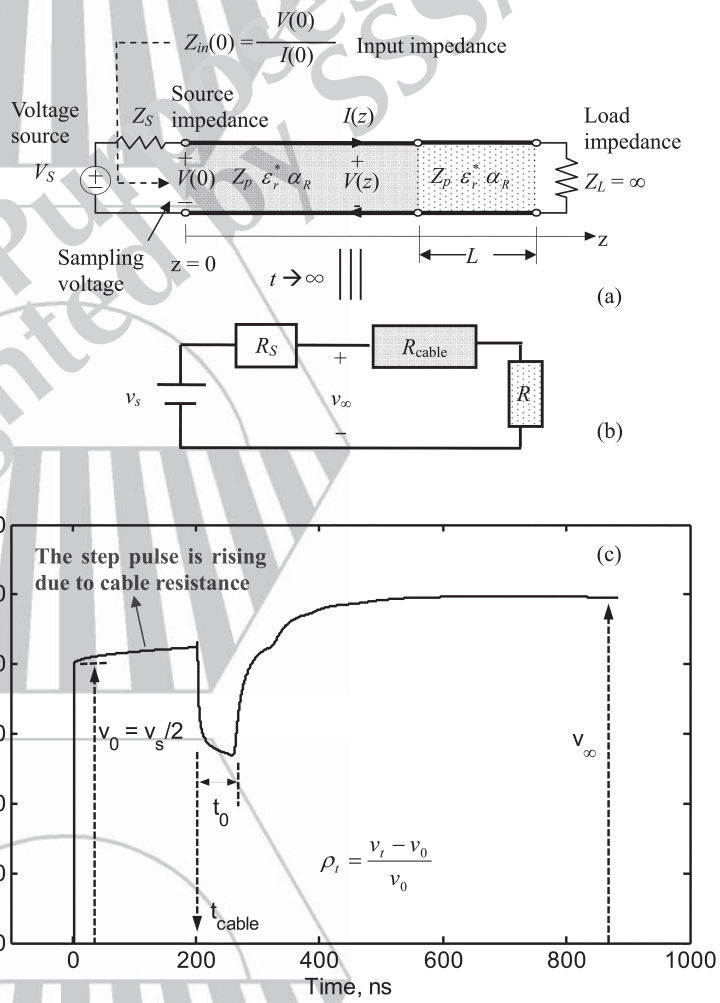

Fig. 1. (a) The multisection transmission line model of the time domain reflectometry (TDR) measurement system, in which each uniform section is characterized by the geometric impedance (Z_p), resistance loss factor (α_R), complex dielectric permittivity (ε_r^*), and waveguide length (L). The transmission line is driven by a source voltage (V_s) with a source impedance (Z_s) and terminated in a load (Z_L). The input impedance (Z_{in}) is defined as the ratio of line voltage (V) to the line current (I). (b) The associated direct current circuit model, in which R_s is the inner resistance (equal to the source impedance Z_s), R_{cable} is the cable resistance, R is sample resistance, v_s is the source voltage (in time domain), and v_∞ is the TDR steady-state voltage. (c) A typical TDR waveform showing definition of reflection coefficient (ρ), where t_0 is the roundtrip travel time in the probe section, and t_{cable} is the roundtrip travel time in the cable section.

Giese and Tiemann (1975) analytically derived the TDR EC from transmission line and thin sample theory in the case of lossless cable (i.e., $R_{cable} = 0$):

$$\sigma_{GT} = \left(\frac{\varepsilon_0 c Z_p}{Z_s L}\right)\left(\frac{1-\rho_\infty}{1+\rho_\infty}\right) = \beta\left(\frac{1-\rho_\infty}{1+\rho_\infty}\right) \quad [8]$$

where ε_0 is the dielectric permittivity of free space, c is the speed of light, Z_p is the geometric impedance of the probe, Z_s is the source impedance, and L is the probe length. As R_{cable} approaches zero, the cable correction factor k in Eq. [7] becomes unity and Eq. [6] has an expression equivalent to the Giese–Tiemann equation (Eq. [8]). Equating Eq. [8] to Eq. [6] with $R_{cable} = 0$, the probe constant can be found as

$$\beta = \left(\frac{\varepsilon_0 c Z_p}{Z_s L}\right) \quad [9]$$

where the only unknown value in practice is the probe geometric impedance Z_p, which can be analytically determined for coaxial and various multiconductor probes (Ball, 2002). The cable resistance depends on α_R (a cable property), the cable length, and the geometric impedance. Their relationship is induced from full waveform simulations as

$$R_{cable} = \sum_i 10^{-4}\frac{\alpha_{R,i} L_i}{\varepsilon_0 c Z_{p,i}} \quad [10]$$

where $\alpha_{R,i}$, $Z_{p,i}$ and L_i are the resistance loss factor, geometric impedance, and transmission line length for each uniform section. The unknown values in Eq. [10] are $\alpha_{R,i}$ and $Z_{p,i}$.

Although the probe constant β and cable resistance R_{cable} can be determined analytically from Eq. [9] and [10], $Z_{p,i}$ and $\alpha_{R,i}$ are typically not known a priori. Using the full waveform propagation model, $Z_{p,i}$ and $\alpha_{R,i}$ can be obtained (calibrated) from an inverse analysis of a single measurement in a sample with known electrical properties (such as air or pure water). Alternatively and more practically, R_{cable} can be directly determined from a measurement on a sample with known R, as suggested by Reece (1998). In the limiting case of a sample with $R = 0$ (i.e., TDR waveguide probe whose conductors are shorted together), the R_{cable} can be determined as

$$R_{cable} = \frac{R_s}{\left(1-\rho_{\infty,SC}/1+\rho_{\infty,SC}\right)} \quad [11]$$

where $\rho_{\infty,SC}$ is the steady-state reflection coefficient of the measurement in which the conductors are shorted together. With known R_{cable}, the probe constant β can be obtained using Eq. [6] and at least one calibration test in a salt solution with known EC.

The series resistors model should be theoretically sound according to the well-established circuit theory. Castiglione and Shouse (2003) presented an alternative approach for taking cable resistance into account, however, in which the steady-state reflection coefficients are linearly scaled between −1.0 and 1.0 with respect to the range expanded by the measurements in air (EC = 0) and the short-circuited condition (EC = ∞):

$$\rho_{scaled} = 2\frac{\rho_{sample} - \rho_{open}}{\rho_{open} - \rho_{short}} + 1 \quad [12]$$

where ρ_{scaled} is the TDR measurement corrected for cable resistance by the scaling process; ρ_{open} and ρ_{short} are the reflection coefficients with the probe in open air and short-circuited, respectively. The value of ρ_{scaled} represents the TDR measurement as if there is no cable resistance, so the Giese–Tiemann equation (Eq. [8]) can be used for calculating the EC. Castiglione and Shouse (2003) claimed that the series resistors model is incorrect and Eq. [12] leads to better agreement with experimental results. It should be pointed out, however, that the scaling process is linear while the effect of cable resistance on the steady-state reflection coefficient will be shown to be nonlinear. We examined both the series resistors model and the Castiglione–Shouse method using full waveform analysis and experiments.

MATERIALS AND METHODS

The ability of the TDR wave propagation model to capture the resistance effect was first verified by several TDR measurements with a 30-m RG58A/U cable. The TDR measurements were made by attaching the TDR probe (12-cm two-rod probe with conductors 3 mm in diameter with 20-mm spacing) to a Campbell Scientific TDR 100 (Campbell Scientific, Logan, UT) via the 30-m-long lead cable and a SDMX multiplexer. Any uniform transmission line section can be parameterized by the length (L), geometric impedance (Z_p), dielectric permittivity (ε_r^*), and resistance loss factor (α_R). One of the three parameters (L, Z_p, or ε_r^*) needs to be known so that the other two parameters and α_R can be calibrated from a measured TDR waveform (Lin and Tang, 2007). With known lengths, the transmission line parameters (Z_p, ε_r^*, and α_R) of the lead cable and multiplexer section were calibrated by a measurement with the lead cable open ended. The transmission line parameters (Z_p, L, and α_R) of the TDR probe were then calibrated by a measurement with the probe immersed in deionized water, whose dielectric property is known. Using the calibrated transmission line parameters, TDR waveforms were simulated and compared with measured waveforms for the probe in open air, immersed in tap water, and short-circuited. Time interval $\Delta t = 2.5 \times 10^{-11}$ s and number of data points $N = 65{,}536$ were used in the numerical simulations (for details, see Lin and Tang, 2007). The resulting effective time window $0.5N\Delta t = 8192\ (40\Delta t) = 8.2 \times 10^{-6}$ s is slightly greater than the pulse length of 7×10^{-6} s in a TDR 100. The corresponding Nyquist frequency and frequency resolution are 20 GHz and 60 kHz, respectively. The Nyquist frequency is well above the frequency bandwidth of the TDR 100 and the long time window ensures that a steady state is obtained.

Using the verified TDR wave propagation model, the theoretical validity of the series resistors model and the Castiglione–Shouse method can be examined. The EC was numerically controlled and compared with that estimated from the synthetic waveforms using the Giese–Tiemann method, series resistors model, and Castiglione–Shouse method. The time window used for these numerical simulations was excessively large to ensure that a steady state was obtained and DC analysis was examined. As will be seen, the cable resistance can have a great effect on how the reflection approaches the steady state. Intermediate reflection plateaus at long times may be mistakenly taken as the steady-state reflection coefficient. The effect of recording time on the series resistors model and the Castiglione–Shouse method was investigated through a parametric study. Factors considered include lead cable length, probe length, probe impedance, and electrical properties of the material being tested. The simulation parameters used in the parametric study are listed in Tables 1 and 2. The resistance loss factor (α_R) of the waveguide was set as 0.0 for all cases, since it has a negligible effect on the TDR waveform due to the short probe length.

The numerical findings were verified by experimental data. Time domain reflectometry measurements were made on seven NaCl electrolytic solutions, with σ varying from 0 to 0.15 S m^{-1}, using the 30-m RG58A/U cable and 12-cm two-rod probe. The EC was measured independently with a standard EC meter (YSI-32, Yellow Springs Inc., Yellow Springs, OH). When directly determining R_{cable} using Eq. [11], the measurements were performed by shorting the cable end with a short wire. The resistance in the probe section was found to be negligible from Eq. [10] and a theoretical α_R value computed from the probe geometry and conductor property. The cross-section of the probe is much larger than that of the coaxial cable. Shorting the probe end with a wire may introduce extra resistance. We suggest shorting the cable end with a short wire or the probe end with a metal plate.

Table 1. Simulation parameters.

Section	Parameter	Range
Waveguide	electrical conductivity (σ), S/m	0.005 ∼ 0.2
	dielectric permittivity (ε_r)	Tap water, ethanol, and silt loam†
	geometric impedance (Z_p), Ω	150 ∼ 300
	length L, m	0.1 ∼ 0.3
	resistance loss factor (α_R), $s^{-0.5}$	0
Lead cable	σ, S/m	0
	ε_r	1.95
	Z_p, Ω	77.5
	length, m	0 ∼ 200
	α_R, $s^{-0.5}$	0, 19.8

† Referring to the Cole–Cole parameters listed in Table 2.

RESULTS AND DISCUSSION

Effect of Cable Resistance on Time Domain Reflectometry Waveforms

The effect of cable resistance on TDR waveforms is illustrated by TDR measurements with a 30-m RG58A/U cable and modeled by the full waveform analysis. The characteristics of the lead cable (Z_p = 77.5 Ω, ε_r^* = 1.95, and α_R = 19.8 $s^{-0.5}$) were backcalculated from the measured waveform with the lead cable open ended, while the characteristics of the probe (Z_p = 290 Ω, L = 0.126 m, and α_R = 153 $s^{-0.5}$) were obtained from a measurement with the probe immersed in deionized water. Figure 2a shows the measured and predicted waveforms using the backcalculated parameters for the probe in open air, immersed in tap water, and short-circuited. The full waveform analysis takes into account the multiple reflections, dielectric dispersion, and attenuation due to conductive loss and cable resistance altogether. The excellent match between the measured and predicted waveforms validates the TDR wave propagation model and the calibration by full-waveform inversion. The predicted waveforms in which cable resistance is ignored are also shown in Fig. 2a for comparison. Of most importance to EC measurements is how cable resistance affects the steady-state response. As depicted in Fig. 2a, cable resistance gives rise to an increase in the steady-state response, causing an underestimation of EC if cable resistance is not taken into account. The amount of increase in the steady-state response depends on the EC, with no increase when EC = 0 (i.e., probe in open air) and maximum increase when EC = ∞. Therefore, the TDR EC measurements are increasingly underestimated as EC increases, as also observed by Heimovaara et al. (1995) and Reece (1998). This monotonic behavior is different from that revealed by Castiglione and Shouse (2003) in their Fig. 5b, reproduced in Fig. 2b for comparison. The reflection coefficient in air (i.e., EC = 0) should be 1.0 regardless of the lead cable length, as also suggested by Eq. [6]. The data shown in Castiglione and Shouse (2003) seems abnormal. The error was probably caused by the data acquisition program, and was overlooked due to the misconception that the long-time reflection coefficient is reduced in absolute value due to cable attenuation (i.e., a positive long-time reflection coefficient decreases at low EC, while a negative long-time reflection coefficient increases at high EC, as shown in Fig. 2b).

In addition to the steady-state response, it is also interesting to note how cable resistance affects the time required to reach the steady state. The characteristic impedance of the cable used is actually 55 Ω, not precisely 50 Ω. The unmatched cable gives rise to multiple reflections within the cable section, as can be observed from the reflections around 560 ns in Fig. 2a. Even if the cable has a nominal characteristic impedance perfectly matched with the source impedance of the TDR device (typically 50 Ω), the characteristic impedance of the cable is in fact a function of frequency and cable resistance, as suggested in Eq. [1]. This is evidenced by the rising step pulse, as shown in Fig. 2a and illustrated in Fig. 1. Therefore, the multiple reflections within the cable section are inevitable. The magnitude of the multiple reflections within the cable depends not only on cable resistance but also on the EC. It is most prominent when the probe is in open air or shorted. The rising plateau of the step pulse and the rise time of the reflected pulse increase as $_R$ or cable length increases. Hence, it takes a much longer time to reach steady state for long cables. The reflection coefficient beyond 400 ns may be mistakenly taken as the steady state if the waveform is not recorded long enough, as shown in Fig. 2a. This problem has been overlooked and may have a significant effect on TDR EC measurements.

Theoretical Assessment of Direct Current Analysis Methods (without Time Error)

Using the verified TDR wave propagation model, the theoretical validity of the series resistors model and the Castiglione–Shouse method can be examined. A very long time (8.2×10^{-6} s) was used in the numerical simulations to ensure that the assessment is performed under the true steady-state responses. The deficiency of the scaling process proposed by Castiglione and Shouse (2003) is illustrated in Fig. 3. To enhance visual illustration, a long

Table 2. Cole–Cole† parameters for materials used in numerical simulations.

Material	ε_{dc}	ε_∞	f_{rel}	α
Tap water	79.9	4.22	17×10^9	0.0125
Ethanol	25.2	4.5	0.78×10^9	0.0
Silt loam	26.0	18.0	0.2×10^9	0.01

† Cole–Cole equation: $\varepsilon_r(f) = \varepsilon_\infty + (\varepsilon_{dc} - \varepsilon_\infty)/\{1 + [j(f/f_{rel})]^{1-\alpha}\}$, where $\varepsilon_r(f)$ is the complex dielectric permittivity, ε_{dc} is the dielectric constant at zero frequency, ε_∞ is the dielectric constant at infinite frequency, f_{rel} is the relaxation frequency, α is a parameter characterizing a spread in the relaxation frequencies, j is the complex unity $\sqrt{(-1)}$, and f is the frequency.

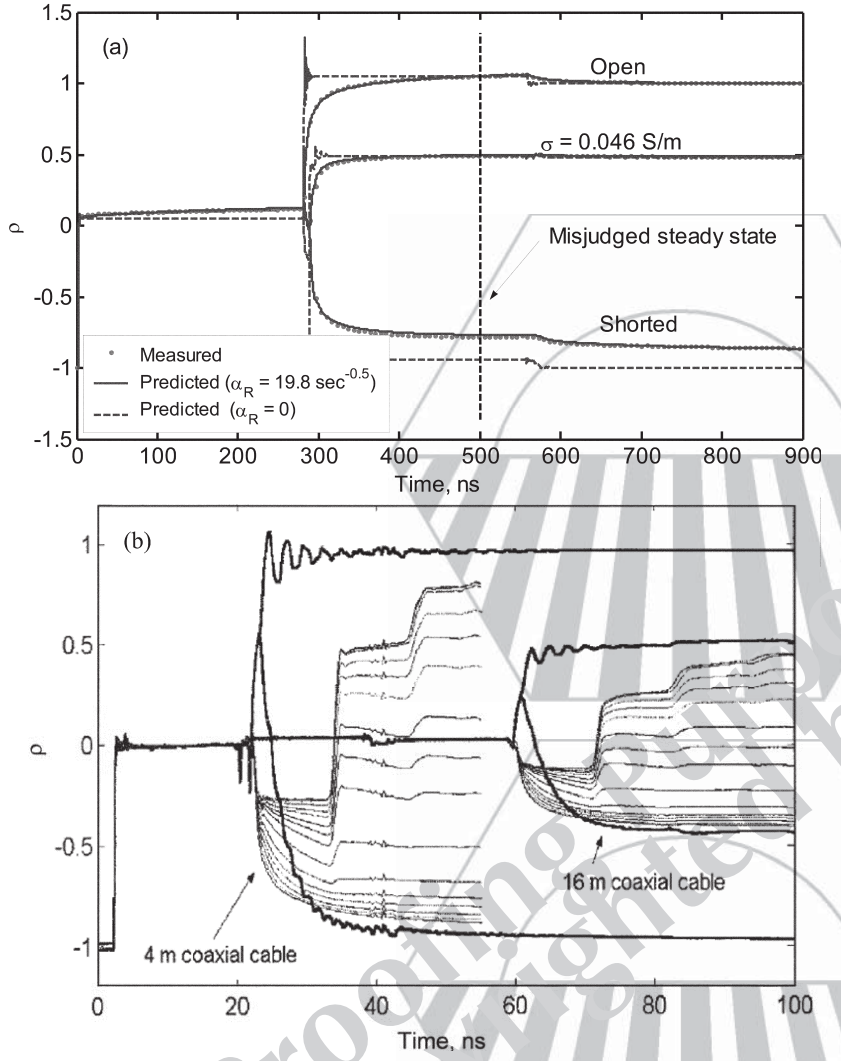

Fig. 2. Effect of cable resistance on time domain reflectometry (TDR) waveforms for a variety of electrical conductivities (σ): (a) measured TDR waveforms compared with that predicted by the full waveform model in this study; (b) measured TDR waveforms in Fig. 5b of Castiglione and Shouse (2003).

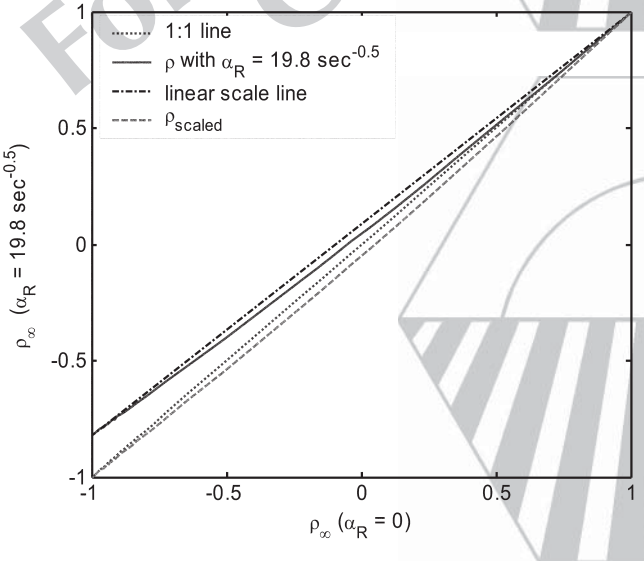

Fig. 3. Illustration of the nonlinear relationship between the steady-state reflection coefficient with 200-m RG-58 cable and that without cable resistance, in which ρ_{scaled} is the scaled reflection coefficient by the Castiglione–Shouse method (Eq. [12]).

RG-58 cable (200 m) was used for the numerical simulation. The steady-state reflection coefficient with the 200-m RG-58 cable (α_R = 19.8 $s^{-0.5}$) is plotted against that without cable loss (α_R = 0 $s^{-0.5}$), as shown by the solid line in Fig. 3. This curve is not a linear line and the scaled line by applying Eq. [11] is a nonlinear line rather than the 1:1 linear line. This disparity reveals that the Castiglione–Shouse method is correct only for EC = 0 and EC = ∞, since the effect of cable resistance on the steady-state reflection coefficient is nonlinear while the scaling process is linear.

In Fig. 4, the electrical conductivity in the measurement system was numerically controlled and compared with that estimated from the synthetic waveforms using three different DC analysis methods. The result shows that the series resistor model is theoretically correct (if the true steady-state response is obtained), while the Giese–Tiemann method and Castiglione–Shouse methods result in underestimation and overestimation, respectively. The overestimation by the Castiglione–Shouse method linearly increases with EC, while the underestimation by the Giese–Tiemann method nonlinearly increases with EC. In Fig. 4, the probe constant β is determined by Eq. [9], which is only a function of probe geometry and independent of cable resistance. If the probe constant β is obtained using least square fitting of TDR EC measurements in salt solutions of different concentrations to conductivity measurements made with a conventional conductivity meter, the result becomes that shown in Fig. 5. The linear overestimation by the Castiglione–Shouse method is completely compensated for by the fitted probe constant, while the nonlinear underestimation by the Giese–Tiemann

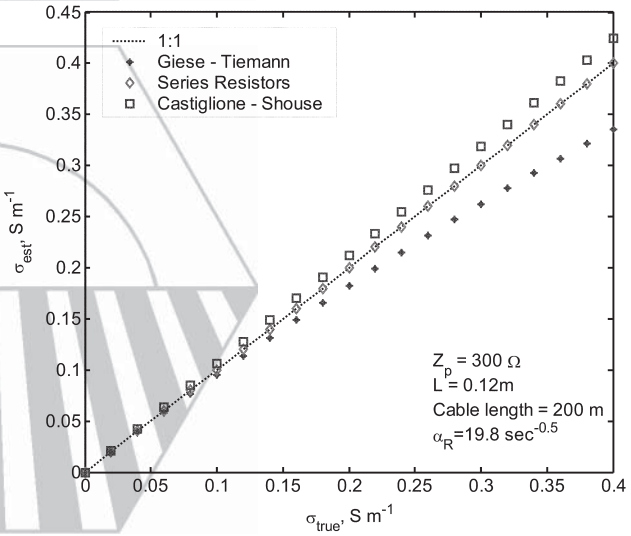

Fig. 4. The estimated electrical conductivity (σ_{est}) using the actual probe constant in three different methods compared with the numerically controlled true electrical conductivity (σ_{true}).

method is only minimized in a least square sense, resulting in slight overestimation at low EC and underestimation at high EC in the fitting range. It should be noted that the fitted probe constant depends not only on the probe geometry but also on the cable resistance. Hence, probes with the same probe geometry but different cable length should be individually calibrated when the Castiglione–Shouse method or the Giese–Tiemann method are used. This is not very practical for field monitoring with many probes. In practice, the series resistors model should be used. It has a unique probe constant for each type of probe, and the cable resistance can be easily determined by Eq. [11] without further calibrations.

Effect of Recording Time

The assessment of DC analysis methods assumes that steady state is obtained. In practice, an arbitrary "long" time is usually assumed for the steady state without close examination of its legitimacy. The parametric study shows that the time required to reach the steady state depends on the cable resistance, the electrical properties of the medium, and probe characteristics. In the case of negligible cable resistance, Fig. 6 shows how EC, probe characteristics, and dielectric permittivity affect the time required to reach the steady state. The recording time is expressed as the time that includes multiples of roundtrip travel time in the probe section (t_0). The reflection voltage at a very long time (8.2×10^{-6} s, slightly greater than the pulse length of 7×10^{-6} s in a TDR 100) was used to represent v_∞. The time required to reach the steady state increases with decreasing EC, decreasing characteristic impedance, and increasing dielectric constant. But without cable resistance, reflection coefficients all converge to the steady state ($v_t/v_\infty = 1$) in fewer than 10 multiple reflections within the probe, a time often used to represent the steady state in practice.

For the 12-cm probe, Fig. 7 shows the effect of recording time for different lengths of RG58 cable and electrical conductivities. The time required to reach the steady state increases with cable resistance. But the way the reflection coefficient

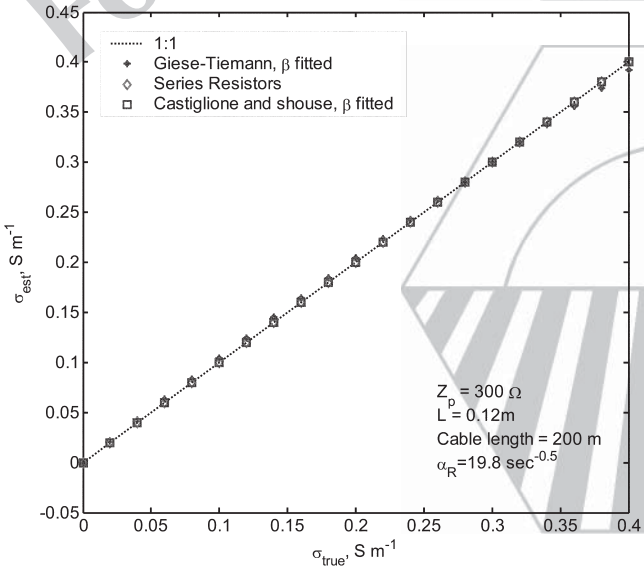

Fig. 5. The estimated electrical conductivity (σ_{est}) using the fitted probe constant (β) in three different methods compared with the numerically controlled true electrical conductivity (σ_{true}).

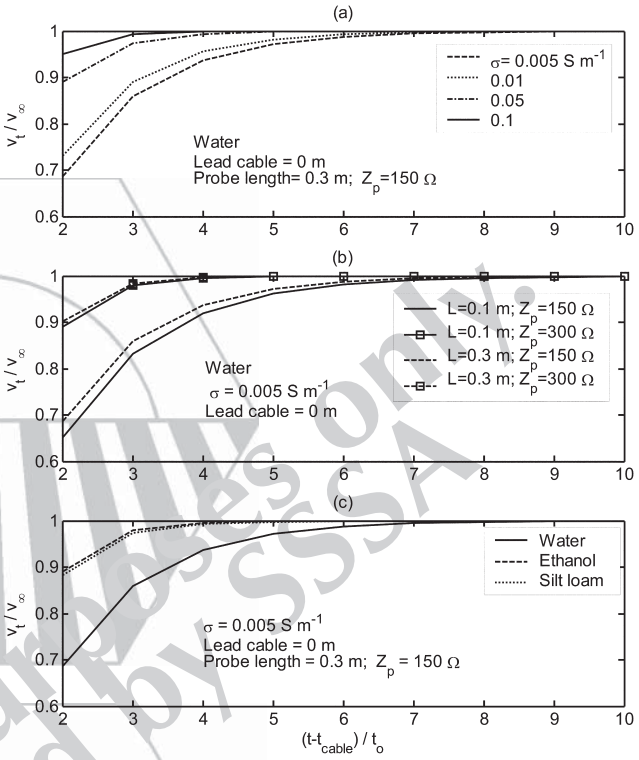

Fig. 6. Examples showing how (a) electrical conductivity σ, (b) geometric impedance Z_p and length L, and (c) dielectric permittivity affect the time required to reach the steady state, with time expressed as the time that includes multiples of roundtrip travel time in the probe section (t_0).

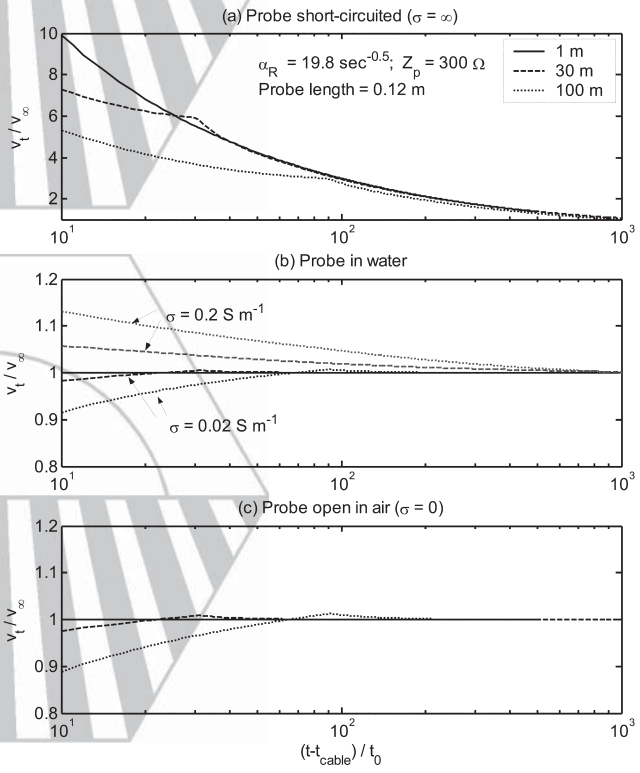

Fig. 7. Recording time required for the voltage (v_t) to reach steady state (v_∞) for probes that are (a) short-circuited, (b) in water of two electrical conductivities, and (c) in open air.

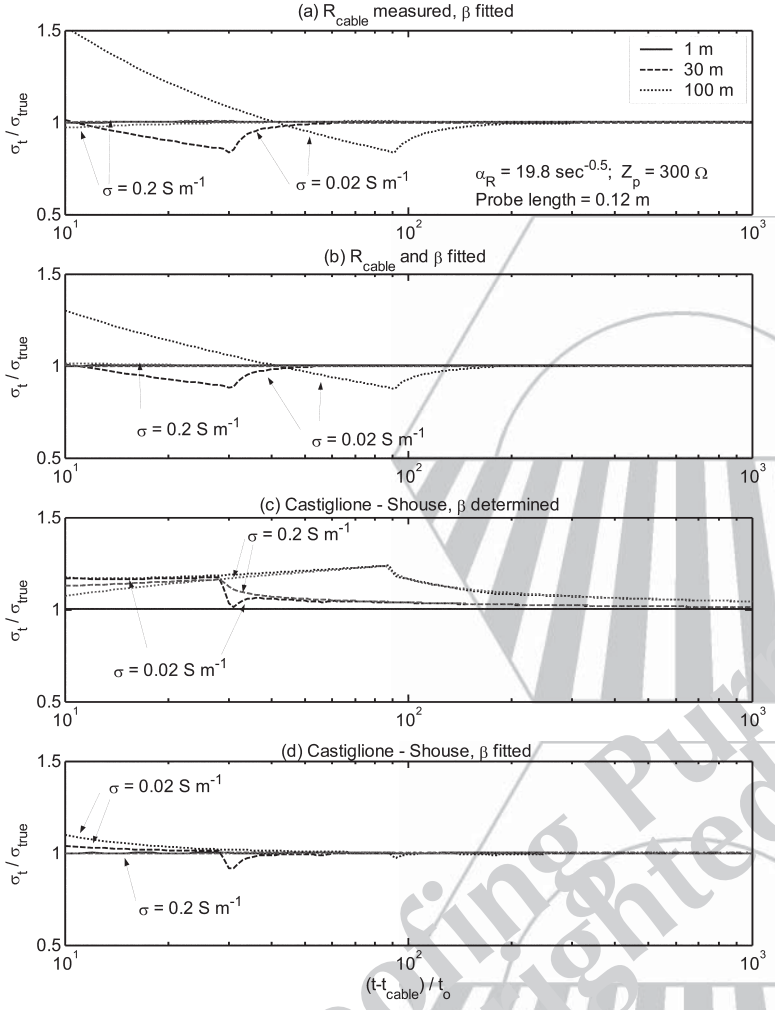

Fig. 8. The effect of recording time (t), expressed as the time that includes multiples of roundtrip travel time in the probe section (t_0), on the estimated electrical conductivity (σ_t) using the series resistors model with (a) cable resistance R_{cable} measured and probe constant β fitted, and (b) R_{cable} and β fitted, or using the Castiglione–Shouse method with (c) actual β determined, and (d) β fitted.

approaches the steady state strongly depends on the EC, as also suggested by Fig. 2. Two extreme cases, the probe in open air (EC = 0) and the probe with conductors shorted together (EC = ∞), are shown in Fig. 7a and 7c. Figure 7b shows the results for two electrical conductivities in between the two extreme cases. At high EC, the ratio v_t/v_∞ decreases monotonically and gradually approaches the steady state, while at low EC, v_t/v_∞ increases slightly above 1.0 and then quickly approaches the steady state. The medium EC is least affected by the recording time. The definition of "high," "medium," and "low" EC here means EC that results in reflection coefficient near −1.0, 0, and 1.0, respectively. This property depends on the probe characteristics (i.e., geometric impedance and probe length), as can be inferred from Eq. [9]. For example, the EC may be considered "high" for a long probe but is considered "medium" for a short probe. When the waveguide is short-circuited, it takes a much longer time to reach the steady state even with small cable resistance, as shown in Fig. 7a. Hence, cautions should be taken when determining the cable resistance from the TDR measurement of a short-circuited probe using Eq. [11].

Four approaches may be used to determine the TDR EC from the steady-state response: (i) using the series resistor model with cable resistance directly measured by the short-circuited probe (Eq. [11]) and a probe constant fitted to calibration tests; (ii) using the series resistor model with both cable resistance and the probe constant fitted to calibration tests; (iii) using the Castglione–Shouse method with an actual probe constant determined by Eq. [9] or calibrated with a very short cable; and (iv) using the Castiglione–Shouse method with a probe constant fitted to calibration tests. Figure 8 reveals the effect of recording time on estimated EC using these four different approaches, in which the estimated EC of any recording time is expressed as σ_t. In this illustration, calibrations were performed with EC ranging from 0 to 0.2 S m^{-1} with 0.02 S m^{-1} spacing. The fitted probe constant is the probe constant that results in the minimum least square error between estimated and actual EC in the fitting range. It coincides with the theoretical probe constant only when the series resistors model is used and the recording time is representative of the steady state. As shown in Fig. 8, the estimated EC by the series resistors model eventually converges to the true value, but the rate of convergence depends on the calibration method, the cable length, and the EC. The results for fitting both the probe constant and cable resistance (Fig. 8b) increase the estimation accuracy slightly for each recording time, but the convergence trend is similar to that for fitting only the probe constant, with cable resistance directly measured by the short-circuited probe (Fig. 8a). The time window required to have accurate estimation of EC increases with cable length, as expected, and is generally less than that required to reach the steady state due to the fitted probe constant. Unlike what Fig. 7b may suggest, however, high EC converges to the true value faster than low EC does. This is due to the fact that TDR EC measurements are affected by the recording time not only when making measurements but also when fitting the probe constant and cable resistance. As shown in Fig. 7, the TDR response approaches the steady state in different ways for different electrical conductivities. Depending on the fitting range and data sampling, the fitted probe constant may work in favor of some electrical conductivities. But of most importance is how to obtain accurate estimation for all electrical conductivities. The recording time is expressed as the time that includes multiples of roundtrip travel time in the probe section (t_0) in Fig. 8. The same result is plotted in Fig. 9 with recording time expressed as multiples of roundtrip travel time in the lead cable (t_{cable}). Except for the case of a very short lead cable, accurate estimation of EC can be obtained with a recording time greater than $3t_{cable}$, regardless of the fitting range for the probe constant. The characteristic impedance of the lead cable increases with increasing cable length, giving rise to multiple reflections within the lead cable, as shown in Fig. 2a. The convergence of EC estimation is governed by multiple reflections in the sensing probe for a short lead cable, while it becomes dominated by multiple reflections in the lead cable for a long lead cable. A simple guideline for selecting an appropriate recording time can be drawn from the parametric study. To determine the EC accurately, the recording time should be taken after 10 multiple reflections within the probe and three multiple reflections within the lead cable. Errors

found in the literature using the series resistor model with cable resistance directly measured by the short-circuited probe may be explained by the time effect, an imperfect shorting element, or the wrong acquisition program.

The effect of recording time on the Castiglione–Shouse method is shown in Fig. 8c, 8d, 9c and 9d for comparison. If the probe constant is fitted (Fig. 8d and 9d), the estimated EC by the Castiglione–Shouse method also converges to the true value with reduced time effect. But if the actual probe constant is determined and used (Fig. 8c and 9c), it takes a much longer time for the estimated EC by the Castiglione–Shouse method to become invariant with time. When the recording time is $>6t_{cable}$, the estimated EC still gradually decreases with time. The asymptotic value overestimates the EC. The overestimation increases with cable length and the asymptotic σ_t/σ_{true} is independent of the EC, as also suggested in Fig. 4.

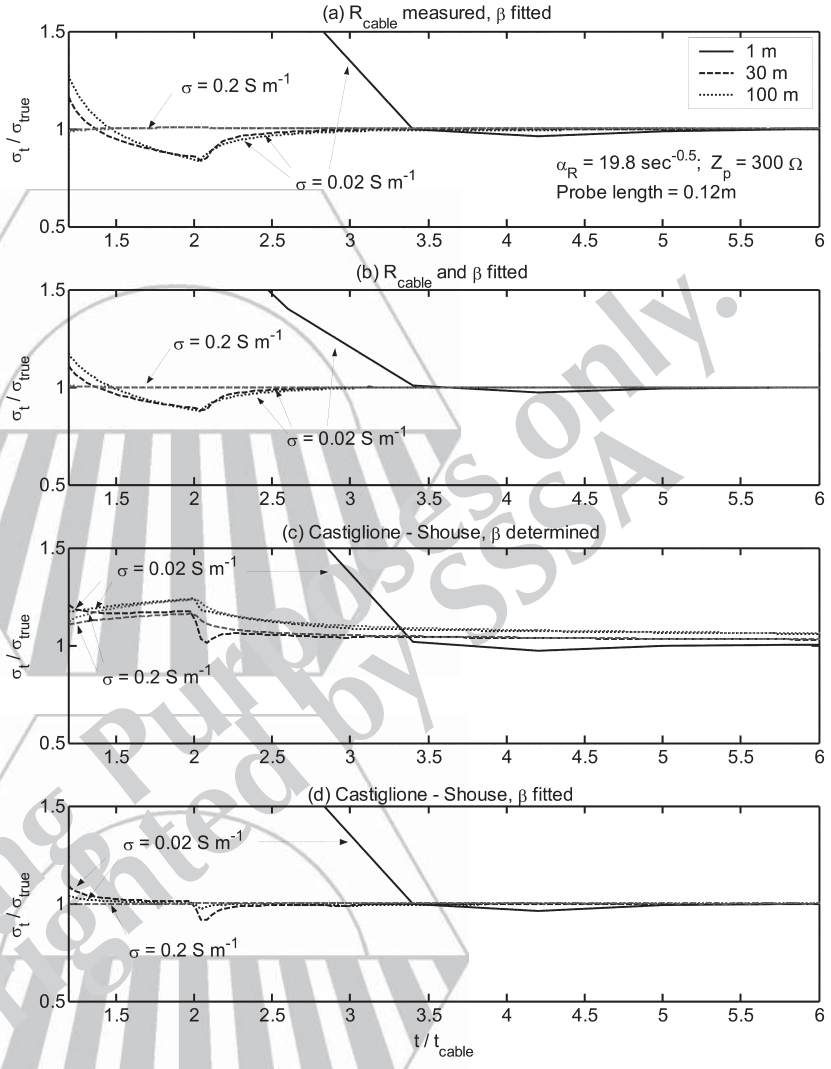

Fig. 9. The effect of recording time (t), expressed as multiples of roundtrip travel time in the lead cable (t_{cable}), on the estimated electrical conductivity (σ_t) using the series resistors model with (a) cable resistance R_{cable} measured and probe constant β fitted, (b) R_{cable} and β fitted, or using the Castiglione–Shouse method with (c) actual β determined, and (d) β fitted.

Experimental Verifications

To further verify the numerical findings, a few TDR measurements were made on NaCl electrolytic solutions, with σ varying from 0 to 0.15 S m^{-1}, using the 30-m RG58A/U cable and 12-cm two-rod probe. The TDR measurements were interpreted by the Giese–Tiemann method, Castiglione–Shouse method, and the series resistors model with cable resistance directly measured by the short-circuited probe. The steady-state responses were recorded at the time around $4.5t_{cable}$ that includes 80 multiple reflections within the probe, satisfying the criteria for the steady state. The same data were used for calibrating the probe constant. Figure 10 compares the TDR EC with that measured by a conventional EC meter. The results are in good agreement with that found in Fig. 4 and 5. When the probe constant is fitted, both the series resistors model and the Castiglione–Shouse method provide accurate EC measurements in the full EC range, while the Giese–Tiemann method slightly overestimates at low EC and underestimates at high EC in the fitting range. The fitted probe constants are equal to the actual probe constant when the lead cable is very short. For long lead cables, the fitted probe constant is identical to the actual one only in the series resistors model. If the actual probe constant is used, linear overestimation by the Castiglione–Shouse method and nonlinear underestimation by the Giese–Tiemann method are obvious, agreeing well with the numerical findings.

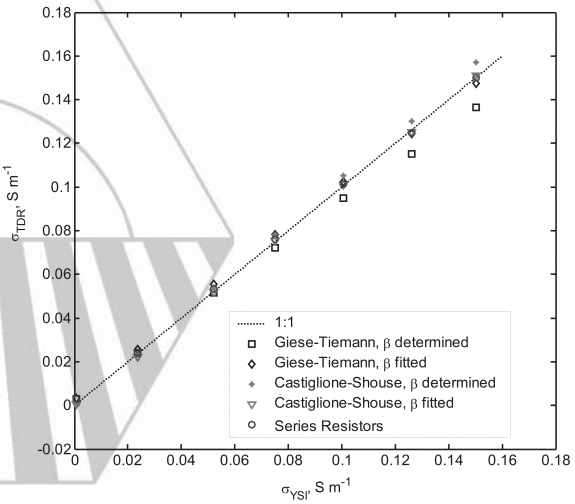

Fig. 10. Electrical conductivity measured by time domain reflectometry (σ_{TDR}) compared with that measured by a YSI conductivity meter (σ_{YSI}) using three different models with the probe constant β measured or fitted.

CONCLUSIONS

Cable resistance and recording time are important factors in TDR EC measurements when long lead cables are used. In this study, a rigorous full waveform analysis and the DC analysis were used to show the correct method for taking cable resistance into account and guidelines for selecting the proper recording time.

At EC = 0, the steady-state response is not affected by the cable resistance. But as EC increases, cable resistance gives rise to a growing increase in the steady-state response. Hence, the TDR EC measurements are increasingly underestimated by the Giese–Tiemann method as EC increases. This effect of cable resistance can be precisely captured and taken into account by the series resistors model, which is theoretically sound according to the well-established circuit theory and verified by the full waveform analysis. The alternative Castiglione–Shouse method, in which the measured steady-state reflection coefficients are linearly scaled between −1.0 and 1.0 with respect to the range expanded by the measurements in air (EC = 0) and under the short-circuited condition (EC = ∞), on the other hand, was shown to be incorrect. This can be explained by the fact that the effect of cable resistance on the steady-state reflection coefficient is nonlinear while the scaling process is linear. The error using the Castiglione–Shouse method may be completely compensated for if the probe constant β is obtained using least square fitting of TDR EC measurements to known EC values or to EC measurements made with a conventional conductivity meter. The fitted probe constant then becomes a function of cable length (resistance).

The cable resistance affects not only the steady-state response but also the time required to approach the steady state. The characteristic impedance of the lead cable has a frequency-dependent increase due to cable resistance, resulting in a rising step pulse and multiple reflections within the cable section. Hence, it takes a much longer time than conventionally thought to reach the steady state when long cables are used, in particular at very low and very high EC. To determine the electrical conductivity accurately, the recording time should be taken after 10 multiple reflections within the probe and three multiple reflections within the lead cable.

ACKNOWLEDGMENTS

This research is supported in part by the National Science Council of ROC under Contract no. 94-2211-E-009-044 and the MOU-ATU program at National Chiao Tung University. This support is greatly appreciated.

REFERENCES

Baker, J.M., and E.J.A. Spaans. 1993. Comments on "Time domain reflectometry measurements of water content and electrical conductivity of layered soil columns". Soil Sci. Soc. Am. J. 57:1395–1396.

Ball, J.A.R. 2002. Characteristic impedance of unbalanced TDR probes. IEEE Trans. Instrum. Meas. 51:532–536.

Campanella, R.G., and I. Weemees. 1990. Development and use of an electrical resistivity cone for groundwater contamination studies. Can. Geotech. J. 27:557–567.

Castiglione, P., and P.J. Shouse. 2003. The effect of ohmic cable losses on time-domain reflectometry measurements of electrical conductivity. Soil Sci. Soc. Am. J. 67:414–424.

Dalton, F.N., W.N. Herkelrath, D.S. Rawlins, and J.D. Rhoades. 1984. Time-domain reflectometry: Simultaneous measurement of soil water content and electrical conductivity with a single probe. Science 224:989–990.

Feng, W., C.-P. Lin, R.J. Deschamps, and V.P. Drnevich. 1999. Theoretical model of a multisection time domain reflectometry measurement system. Water Resour. Res. 35:2321–2331.

Friedman, S.P., and N.A. Seaton. 1998. Critical path analysis of the relationship between permeability and electrical conductivity of three-dimensional pore networks. Water Resour. Res. 34:1703–1710.

Giese, K., and R. Tiemann. 1975. Determination of the complex permittivity from thin-sample time domain reflectometry improved analysis of the step waveform. Adv. Mol. Relax. Processes 7:45–59.

Heimovaara, T.J. 1992. Comments on "Time domain reflectometry measurements of water content and electrical conductivity of layered soil columns". Soil Sci. Soc. Am. J. 56:1657–1658.

Heimovaara, T.J., A.G. Focke, W. Bouten, and J.M. Verstraten. 1995. Assessimg temporal variation in soil water composition with time domain reflectometry. Soil Sci. Soc. Am. J. 59:689–698.

Huisman, J.A., and W. Bouten. 1999. Comparison of calibration and direct measurement of cable and probe properties in time domain reflectometry. Soil Sci. Soc. Am. J. 63:1615–1617.

Kachanoski, R.G., E. Pringle, and A. Ward. 1992. Field measurement of solute travel times using time domain reflectometry. Soil Sci. Soc. Am. J. 56:47–52.

Lin, C., and S. Tang. 2007. Comprehensive wave propagation model to improve TDR interpretations for geotechnical applications. Geotech. Testing J. 30(2), doi:10.1520/GTJ100012.

Lin, C.-P. 2003. Analysis of non-uniform and dispersive time domain reflectometry measurement systems with application to dielectric spectroscopy of soils. Water Resour. Res. 39(1):1012, doi:10.1029/2002WR001418.

Mualem, Y., and S.P. Friedman. 1991. Theoretical prediction of electrical conductivity in saturated and unsaturated soil. Water Resour. Res. 27:2771–2777.

Nadler, A., S. Dasberg, and I. Lapid. 1991. Time domain reflectometry measurements of water content and electrical conductivity of layered soil columns. Soil Sci. Soc. Am. J. 55:938–943.

Purvance, D.T., and R. Andricevic. 2000. On the electrical–hydraulic conductivity correlation in aquifers. Water Resour. Res. 36:2905–2913.

Reece, C.F. 1998. Simple method for determining cable length resistance in time domain reflectometry systems. Soil Sci. Soc. Am. J. 62:314–317.

Rhoades, J.D., N.A. Manteghi, P.J. Shouse, and W.J. Alves. 1989. Soil electrical conductivity and soil salinity: New formulation and calibrations. Soil Sci. Soc. Am. J. 53:433–439.

Robinson, D.A., S.B. Jones, J.M. Wraith, D. Or, and S.P. Friedman. 2003. A review of advances in dielectric and electrical conductivity measurement in soils using time domain reflectometry. Vadose Zone J. 2:444–475.

Topp, G.C., M. Yanuka, W.D. Zebchuk, and S. Zegelin. 1988. Determination of electrical conductivity using time domain reflectometry: Soil and water experiments in coaxial lines. Water Resour. Res. 24:945–952.

Vanclooster, M., D. Mallants, J. Vanderborght, J. Diels, J. van Orshoven, and J. Feyen. 1995. Monitoring solute transport in a multi-layered sandy lysimeter using time domain reflectometry. Soil Sci. Soc. Am. J. 59:337–344.

Ward, A.L., R.G. Kachanoski, and D.E. Elrick. 1994. Laboratory measurements of solute transport using time domain reflectometry. Soil Sci. Soc. Am. J. 58:1031–1039.

Yanuka, M., G.C. Topp, S. Zegelin, and W.D. Zebchuk. 1988. Multiple reflection and attenuation of time domain reflectometry pulses: Theoretical consideration for application to soil and water. Water Resour. Res. 24:939–944.

Zegelin, S., I. White, and D.R. Jenkins. 1989. Improved filed probes for soil water content and electrical conductivity measurement using time domain reflectometry. Water Resour. Res. 25:2367–2376.

附錄D

Clarification and Calibration of Reflection Coefficient for Electrical Conductivity Measurement by Time Domain Reflectometry

C.-P. Lin*
C.-C. Chung
Dep. of Civil Engineering
National Chiao Tung Univ.
Hsinchu
Taiwan

J. A. Huisman
Inst. of Chemistry and Dynamics of the Geosphere
Institute 4: Agrosphere
Forschungszentrum Jülich
Jülich, Germany

S.-H. Tang
Dep. of Civil Engineering
National Chiao Tung Univ.
Hsinchu
Taiwan

Measurement of electrical conductivity by time domain reflectometry (TDR) requires knowledge of the source step voltage, which is often implicitly accounted for in the measured reflection coefficient. Errors may arise, however, from imperfect amplitude calibration when transforming the voltage signal into the reflection coefficient signal. This instrument error was identified as a considerable source of error in addition to cable resistance for TDR electrical conductivity measurements. The effect of the instrument error due to imperfect amplitude calibration was theoretically examined by the direct current circuit model and experimentally verified. The instrument error resulted in an overestimation of electrical conductivity while the cable resistance led to an underestimation. We clarified that the series resistors model for correction of cable resistance is accurate if the measured reflection coefficient is corrected for the instrument error. A calibration (correction) method for the measured reflection coefficient was proposed to account for both the instrument error and the effect of cable resistance, leading to a simple, accurate, and theoretically sound procedure for TDR electrical conductivity measurements.

Abbreviations: EC, electrical conductivity; TDR, time domain reflectometry.

Time domain reflectometry is a powerful tool for soil water content measurement. It has become even more popular as later findings have shown that it can be used to simultaneously measure soil water content and bulk electrical conductivity (EC or σ). After several years of exploration in the late 1980s, TDR electrical conductivity measurements are now universally calculated from the steady-state reflection coefficient (ρ_∞), known as the Giese–Tiemann method (Giese and Tiemann, 1975). The effect of cable resistance was not taken into account in the original Giese–Tiemann equation, resulting in increasing underestimation as cable length and EC increase. Heimovaara et al. (1995) modified the Giese–Tiemann equation to account for the cable resistance using a series resistors model. They also suggested that cable resistance and the probe constant should be calibrated with measurements made in liquids with known EC. Alternatively, the cable resistance can be directly determined from a measurement in which the conductors are shorted, as suggested by Reece (1998). Unexplained differences in EC accuracy between the calibration method and the direct measurement method were observed, however, in Heimovaara et al. (1995) and Huisman and Bouten (1999). They suggested that the series resistors theory might be slightly incomplete and the fitting procedure corrects the deviation from theory. Castiglione and Shouse (2003) presented an alternative method, in which the measured steady-state reflection coefficient is linearly rescaled between −1.0 and 1.0 based on a measurement in air (σ = 0) and a short-circuited condition (σ = ∞). After rescaling, the original Giese–Tiemann method is applied. It was believed that this scaling procedure eliminates the effect of cable resistance. For a while, the Castiglione–Shouse method became widely accepted and advocated (e.g., Robinson et al., 2003).

Recently, Lin et al. (2007) showed that the Castiglione–Shouse scaling method is incorrect because the effect of cable resistance on ρ_∞ is nonlinear. The error introduced by the Castiglione–Shouse method can be completely compensated, however, by fitting the probe constant to known EC values measured with a conventional conductivity meter. Because of this error compensation, the fitted probe constant becomes a function of cable length (resistance), which is theoretically incorrect. To account for the cable resistance, Lin et al. (2007) showed that the series resistors model is theoretically sound and should be preferred over the incorrect Castiglione–Shouse scaling method. A modified Giese–Tiemann equation was explicitly derived. The unexplained deviations from theory discussed in the literature regarding the series resistors model

Soil Sci. Soc. Am. J. 72:XXX-XXX
doi:10.2136/sssaj2007.0185
Received 21 May 2007.
*Corresponding author (cplin@mail.nctu.edu.tw).

were attributed to the time effect. It takes much longer time than conventionally thought to reach a steady state when long cables are used, in particular at very high EC. To determine the EC accurately, the recording time should be taken after 10 multiple reflections within the probe and three multiple reflections within the lead cable for EC ranging from 0 to 0.2 S m^{-1} (Lin et al., 2007). Much longer time is required to directly determine the cable resistance using the short-circuited probe.

Some errors may still be observed, particularly at low EC, using the procedure suggested by Lin et al. (2007). Typically, these errors are not obvious because calibration of the cable resistance requires measurements at high EC. It is not reasonable to attribute these errors and unexplained observations in the literature regarding the series resistors model to the time effect alone. In this study, we argue that these errors are related to inaccuracy in determining the reflection coefficient. The ρ_∞ of a measurement in air (i.e., open circuit without any conduction) is theoretically 1.0 regardless of the cable length; however, this is not the case for many TDR devices, resulting in nonzero EC at the zero-EC condition. For example, the ρ_∞ of our TDR100 units open in air range from 0.95 to 0.97. Typical fluctuations between 0.96 and 1.00 are the best the manufacturer can do with the technology they are using (Campbell Scientific, personal communication, 2007). The objective of this study was to complement Lin et al. (2007) to clarify that the series resistors model is indeed accurate and that the nonzero EC problem in air is due to something else—instrument error in defining the reflection coefficient for TDR EC measurement. A calibration (correction) method is proposed, leading to an accurate and theoretically sound procedure for TDR EC measurement.

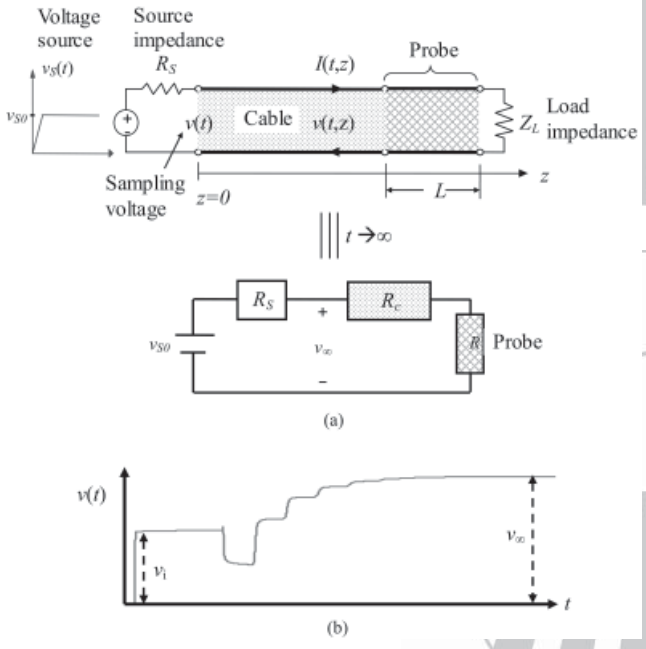

Fig. 1. (a) The classical transmission line model and the associated direct-current circuit model. The transmission line is driven by a source voltage (v_S) with a source impedance (R_S) and terminated in a load (Z_L). At zero frequency ($t \to \infty$), the source voltage is v_{S0} and the probe section is characterized by sample resistance R; (b) a typical time domain reflectometry waveform showing the incident step (v_i) and steady-state response (v_∞).

THEORY

The transmission line in a TDR measurement system is composed of a lead coaxial cable (including connectors) and a sensing waveguide, as shown in the classical model in Fig. 1a. The transmission line is driven by a step source voltage $v_S(t)$ of height v_{S0} with a source impedance R_S and terminated in a load Z_L. A typical TDR measurement system uses a 50 Ω source impedance and has an open termination with $Z_L = \infty$.

Incident Step Pulse and Reflection Coefficient

The TDR waveform is the voltage $v(t)$ sampled at the beginning of the transmission line. A typical TDR waveform is shown in Fig. 1b. It starts with an incident step of height v_i followed by added reflections and eventually reaches the steady state v_∞. Consider the characteristic impedance of the leading transmission line a constant Z_c (i.e., no dielectric dispersion or conductive loss) and let its length be infinitely long (i.e., the condition of no subsequent reflections). Then, the incident step as a function of the source step can be derived as (by substituting $l = \infty$ into Eq. [4] or $Z_{in}(0) = Z_c$ into Eq. [5] in Lin [2003])

$$v_i = \frac{Z_c}{Z_c + R_S} v_{S0} \qquad [1]$$

where Z_c is the characteristic impedance of the leading transmission line, R_S is the source impedance, and v_{S0} is the height of the source step voltage. The characteristic impedance of the leading transmission line is typically designed to match the source impedance such that $v_i = v_{S0}/2$.

If there is a mismatch in the transmission line, a reflected wave will originate at the mismatch interface and propagate back up the line toward the source, as shown in Fig. 2a. The degree of mismatch is indicated by the ratio of the reflected wave to the incident wave. This ratio is called the voltage reflection coefficient, ρ, and is related to the transmission line impedance by

$$\rho = \frac{v_r}{v_i} = \frac{v - v_i}{v_i} = \frac{Z_c' - Z_c}{Z_c' + Z_c} \qquad [2]$$

where v_r is the reflected voltage, and Z_c and Z_c' are the mismatched impedances. The reflection coefficient is an indication of the quality

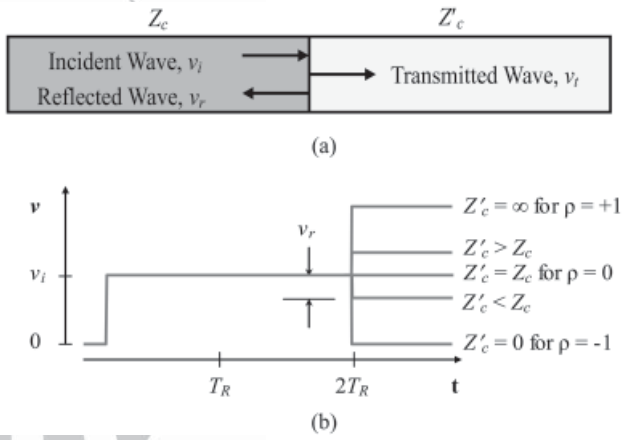

Fig. 2. (a) The reflected wave (v_r) and transmitted wave (v_t) at the mismatch interface; and (b) ideal time domain reflectometry signals for various impedance mismatches, where Z_c is the characteristic impedance of the leading transmission line, Z_c and Z_c' are the mismatched impedances, and ρ is the voltage reflection coefficient.

of the transmission system and is often used as the default form of the TDR signal. Ideal TDR signals for various impedance mismatches are shown in Fig. 2b. If there is no impedance mismatch (i.e., $Z_c = Z_c'$), $\rho = 0$ and no reflection will take place. The open circuit ($Z_c' = \infty$) and short circuit ($Z_c' = 0$) result in $\rho = 1$ and $\rho = -1$, respectively.

The original TDR waveform $v(t)$ is converted to $\rho(t)$ by applying Eq. [2]. The incident step v_i in Eq. [2] is determined by using a 50 Ω internal cable or a 50 Ω terminating block as the impedance reference and for amplitude calibration. According to Eq. [1], the determined incident step v_i is equal to $v_{S0}/2$ only if the source impedance is perfectly matched with the calibration impedance; however, it will be shown that an ideal match is seldom achieved in practice.

Reflection Coefficient for TDR Electrical Conductivity Measurement

The steady-state voltage of a TDR signal is related to the direct current EC of the material in the probe. At zero frequency ($t \to \infty$), the transmission line can be modeled as a lumped circuit composed of the voltage source v_{S0}, the inner resistance R_S, cable resistance R_{cable}, and soil sample resistance R, as shown in Fig. 1a. The steady-state voltage can be derived from circuit theory as (Lin et al., 2007)

$$v_\infty = \frac{R + R_{cable}}{R + (R_S + R_{cable})} v_{S0} \qquad [3]$$

where soil sample resistance is related to the soil bulk EC by $R = K_p/\sigma$, in which K_p is a geometric factor often referred to as a probe constant. Hence, the soil bulk EC can be written as a function of the steady-state voltage as

$$\sigma = \frac{K_p}{R_S}\left(\frac{1}{v_\infty/v_{S0}} - 1\right)\left[\frac{1}{1 - \frac{R_{cable}}{R_S}\left(\frac{1}{v_\infty/v_{S0}} - 1\right)}\right] \qquad [4]$$

where cable resistance can be calibrated along with the probe constant by measurements made in liquids with known EC or directly determined from the TDR measurement with the probe short-circuited as

$$R_{cable} = \frac{R_S}{\left(\frac{1}{v_{\infty,SC}/v_{S0}} - 1\right)} \qquad [5]$$

where $v_{\infty,SC}$ is the steady-state voltage of the short-circuited probe. Lin et al. (2007) used the complete transmission line theory and full waveform analysis to show that the series resistors model is theoretically sound.

In theory, it is the ratio of the steady-state voltage to the source-step voltage that determines the TDR EC measurement. Letting $v_0 = v_{S0}/2$ be the ideal incident voltage, the reflection coefficient for TDR EC measurement (ρ') is defined as

$$\rho' = \frac{v - v_0}{v_0} \qquad [6]$$

The TDR EC measurement (Eq. [4] and [5]) can be written in the more familiar form as

$$\sigma = \frac{K_p}{R_S}\left(\frac{1-\rho'_\infty}{1+\rho'_\infty}\right)\left[\frac{1}{1 - \frac{R_{cable}}{R_S}\left(\frac{1-\rho'_\infty}{1+\rho'_\infty}\right)}\right] \qquad [7a]$$

$$R_{cable} = \frac{R_S}{\left(\frac{1-\rho'_{\infty,SC}}{1+\rho'_{\infty,SC}}\right)} \qquad [7b]$$

While the reflection coefficient ρ in Fig. 2 reflects the degree of impedance mismatch between Z_c and Z_c', the steady-state reflection coefficient ρ'_∞ indicates how conductive the medium is. According to Eq. [7a], ρ'_∞ is a function of R_S but independent of Z_c and impedance mismatches in the probe head. Figure 3 shows theoretical values of ρ'_∞ for three distinct electrical conductivities, $\sigma = 0$, $\sigma = K_p/R_S$, and $\sigma = \infty$. At constant EC, ρ'_∞ increases as the cable resistance increases. The amount of increase in ρ'_∞ due to cable resistance decreases as EC decreases. In a nonconductive medium ($\sigma = 0$), the steady-state reflection coefficient ρ'_∞ is 1.0 regardless of cable resistance.

Calibration of Reflection Coefficient for TDR Electrical Conductivity Measurement

It should be noted that $\rho_\infty = \rho'_\infty$ only when $v_i = v_0$. Unfortunately, small differences between v_i and v_0 often occur in practice due to imperfect amplitude calibration at the 50 Ω level. Although the small error is insignificant when the reflection coefficient is used as an indication of the quality of the transmission system, it may introduce significant errors in TDR EC measurements at low electrical conductivities. Let $v_i = v_0 + \delta$, in which δ is a small error. The relationship between the instrument (measured) reflection coefficient ρ and the EC-associated reflection coefficient ρ' can be written as

$$\rho = \frac{v - v_i}{v_i} = \frac{v - (v_0 + \delta)}{v_0 + \delta} = \left(\frac{v_0}{v_0 + \delta}\right)\rho' - \frac{\delta}{v_0 + \delta} \qquad [8]$$

The relationship is graphically shown in Fig. 4a, in which $\rho_{\infty,air} = 0.95$. The instrument reflection coefficient ρ underestimates the EC-associated reflection coefficient ρ'. The underestimation linearly decreases with decreasing reflection coefficient and vanishes at $\rho' = -1$.

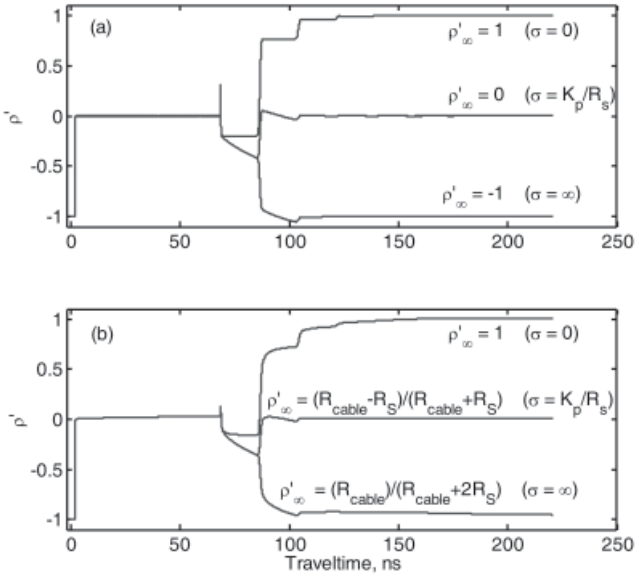

Fig. 3. Theoretical values of electrical-conductivity-associated reflection coefficient ρ'_∞ for three distinct electrical conductivities in the case of (a) zero cable resistance and (b) nonzero cable resistance.

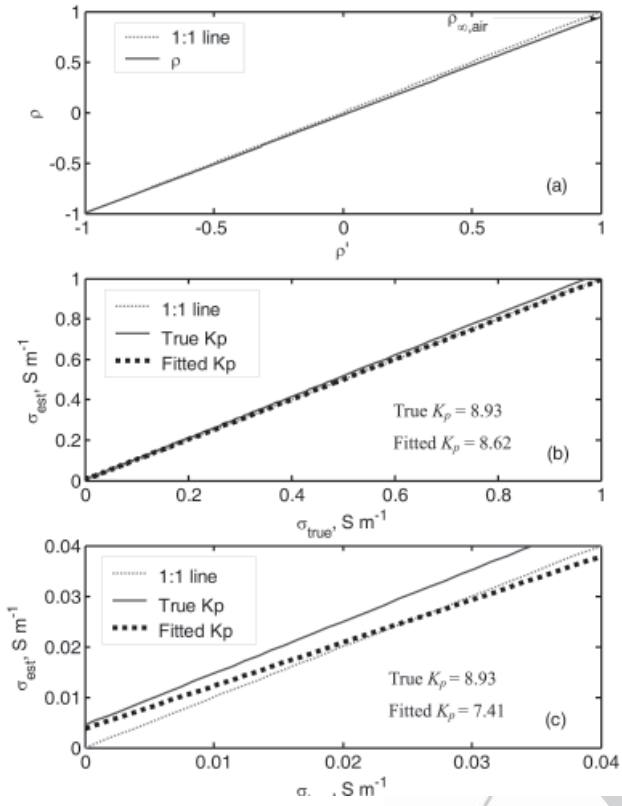

Fig. 4. (a) The relationship between the instrument reflection coefficient ρ and electrical-conductivity (EC)-associated reflection coefficient ρ′ when incident voltage $v_i \neq v_0$ (half of the source voltage) due to imperfect amplitude calibration at the 50 Ω level; and the effect of instrument error on EC determined by time domain reflectometry in (b) the high-EC range and (c) the low-EC range.

The underestimation is maximal at zero EC (e.g., TDR probe open in air) when ρ′ = 1. This phenomenon is often mistakenly interpreted as the effect of cable resistance. The effect of instrument error on the estimated TDR EC is shown in Fig. 4b and Fig. 4c for high and low EC, respectively. Using the actual probe constant (e.g., K_p = 8.93 for the probe used in this study) and condition of zero cable resistance in Eq. [7], the instrument error results in an overestimation of EC. This is particularly evident in the low-EC range. The overestimation may be minimized by fitting the probe constant instead of using the actual probe constant. However, the fitted K_p will now depend on the EC range used for calibration (see Fig. 4b and 4c). Although the fitted K_p is only slightly lower than the actual one and small errors of the estimated TDR EC are not noticeable in the high-EC range, the fitted K_p is significantly lower and errors of the estimated TDR EC are obvious in the low-EC range. Typically, one would determine the K_p with the high-EC measurements (e.g., K_p = 8.62) and apply it also to the low-EC data, resulting in considerable errors in the low-EC range, as shown in Fig. 4c.

From Eq. [7a], the EC-associated reflection coefficient ρ'_∞ in the case of zero EC should be 1.0 regardless of cable resistance. Therefore, the zero-EC ρ_∞ obtained by a measurement with the TDR probe in air or simply disconnected, denoted by $\rho_{\infty,air}$, can be used to correct the instrument reflection coefficient. The calibration equation to transform instrument reflection coefficients into EC-associated reflection coefficients can be derived from Fig. 4 as

$$\rho' = 2\frac{\rho - \rho_{\infty,air}}{\rho_{\infty,air} + 1} + 1 \qquad [9]$$

Scaled Reflection Coefficient for Giese–Tiemann Equation

Once the instrument reflection coefficient is calibrated by Eq. [9], Eq. [7] can be used directly for determining EC. In another form, the steady-state reflection coefficient can be scaled taking into account the instrument error and cable resistance such that the Giese–Tiemann equation (Giese and Tiemann, 1975) can be used:

$$\sigma = \frac{K_p}{R_s}\left(\frac{1-\rho_{\infty,Scale}}{1+\rho_{\infty,Scale}}\right) \qquad [10]$$

where $\rho_{\infty,Scale}$ is the scaled steady-state reflection coefficient corresponding to the ideal condition in which there is no instrument error or cable resistance. Castiglione and Shouse (2003) presented an approach for scaling the steady-state reflection coefficient in which the steady-state reflection coefficient is linearly scaled between −1.0 and 1.0 based on a measurement in air (σ = 0) and a short-circuited condition (σ = ∞):

$$\rho_{\infty,Scale(CS)} = 2\frac{\rho_\infty - \rho_{\infty,air}}{\rho_{\infty,air} - \rho_{\infty,SC}} + 1 \qquad [11]$$

where $\rho_{\infty,Scale(CS)}$ is the scaled steady-state reflection coefficient by the Castiglione–Shouse method; ρ_∞ is the instrument steady-state reflection coefficient of the sample; and $\rho_{\infty,air}$ and $\rho_{\infty,SC}$ are the reflection coefficients with the probe open in air and short-circuited, respectively. This approach can correct the instrument error due to imperfect amplitude calibration, but was shown to be unable to correctly account for cable resistance (Lin et al., 2007). Equating Eq. [10] to Eq. [7a], the correct scaled steady-state reflection coefficient can be found as

$$\rho_{\infty,Scale(SR)} = 2\frac{\left(1-\rho'_{\infty,SC}\right)\left(1-\rho'_\infty\right)}{\left(1+\rho'_{\infty,SC}\right)\left(1-\rho'_\infty\right) - 2\left(1-\rho'_{\infty,SC}\right)} + 1 \qquad [12]$$

where $\rho_{\infty,Scale(SR)}$ represents the scaled reflection coefficient by the series resistors model; ρ'_∞ and $\rho'_{\infty,SC}$ are the measured and short-circuited reflection coefficients calibrated by Eq. [9]. Assuming a cable resistance equal to that of a 20-m-long RG58 cable (e.g., R_{cable} = 0.723 Ω) and no instrument error ($\rho'_\infty = \rho_\infty$), Fig. 5a shows the effect of cable resistance on ρ'_∞ and the scaled steady-state reflection coefficient by the Castiglione–Shouse method (Eq. [11]) and the series resistors model (Eq. [12]). To enhance visual illustration, Fig. 5 plots deviations from the expected values on the *y* axis in stead of absolute values as in Fig. 4. In contrast to the instrument error due to imperfect amplitude calibration, the cable resistance causes an increase in ρ'_∞; however, the amount of increase reduces nonlinearly with increasing ρ'_∞ and vanishes at zero EC (ρ'_∞ = 1). This nonlinear effect cannot be correctly accounted for by the linear scaling method proposed by Castiglione and Shouse (2003). Figure 5b shows the deviation of estimated EC from true EC for the Castiglione–Shouse method and series resistors model using the actual probe constant (e.g., K_p = 8.93). The linear scaling method proposed by Castiglione and Shouse (2003) overestimates the EC by a constant rate, the magnitude of

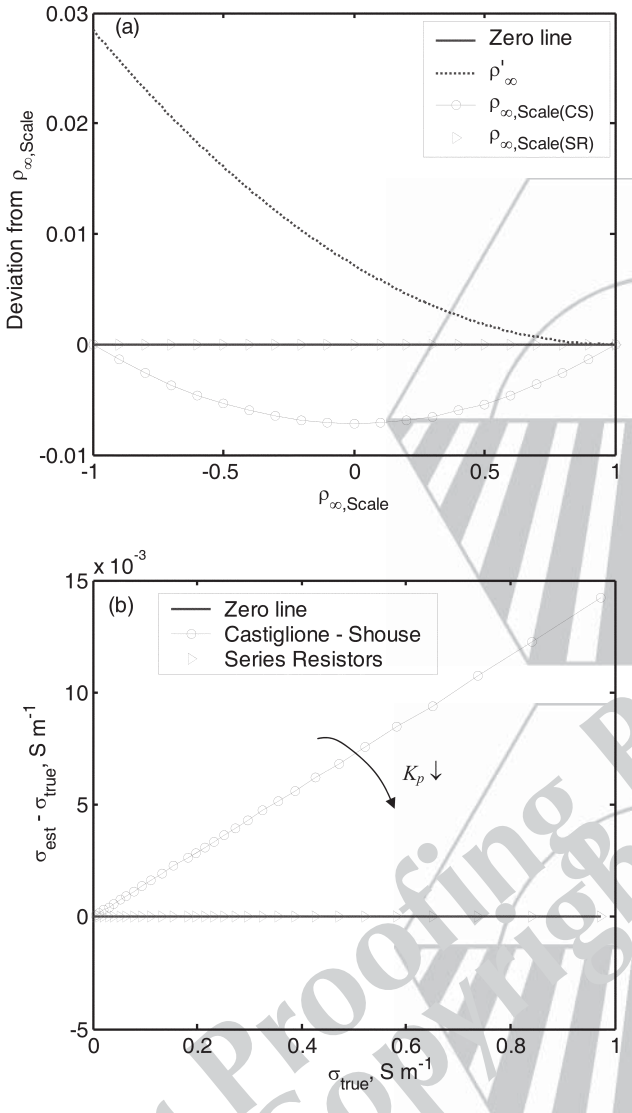

Fig. 5. (a) Effect of cable resistance (equal to that of a 20-m-long RG58 cable) on the steady-state reflection coefficient ρ'_∞ and the scaled steady-state reflection coefficient $\rho_{\infty,Scale}$ by the Castiglione–Shouse method and series resistors model; (b) deviation of the estimated electrical conductivity (σ) from the true σ for the Castiglione–Shouse method and series resistors model using the actual probe constant.

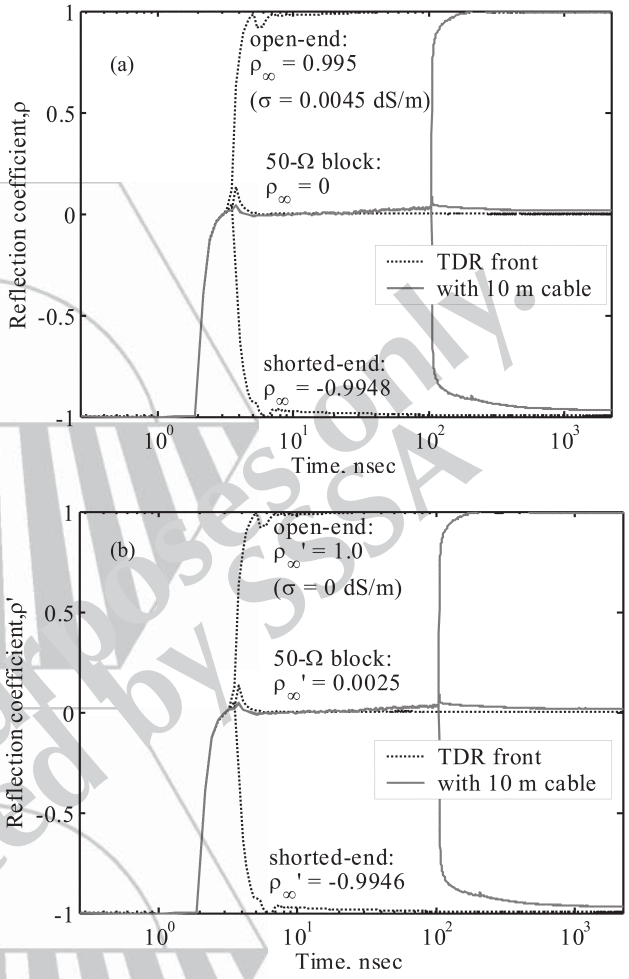

Fig. 6. (a) Original time domain reflectometry (TDR) waveforms from a Tektronix 1502C and (b) the associated corrected waveforms using calibration Eq. [9].

which depends on cable resistance. As pointed out above and by Lin et al. (2007), the linear overestimation by the Castiglione–Shouse method can be completely compensated for if the probe constant is adjusted (e.g., the fitted K_p becomes 8.78 in this case) such that calculated TDR EC matches the known EC; however, the fitted probe constant will depend not only on the probe geometry but also on the cable resistance. Hence, probes with different cable lengths should be individually calibrated when the Castiglione–Shouse method is used. The series resistors model is more consistent. It has a unique probe constant for each type of probe regardless of the cable length.

MATERIALS AND METHODS

The instrument errors due to imperfect amplitude calibration were examined for a Campbell Scientific TDR100 and a Tektronix 1502C. Three measurements were taken in which the front panel connector was open, shorted, and terminated by a 50 Ω block, respectively. To further demonstrate that the instrument error is not related to cable resistance, the three measurements were repeated with a 10-m RG58 cable connected to the TDR devices.

To experimentally investigate the effect of the imperfect amplitude calibration, TDR EC measurements were made on seven NaCl solutions, with ECs varying in the low-EC range from 0 to 0.04 S m^{-1}. The low-EC range was used to clearly illustrate the effect of instrument error due to imperfect amplitude calibration. The measurements were conducted using a TDR probe (10-cm two-rod probe with conductors 4 mm in diameter and 20 mm in spacing) connected to a Campbell Scientific TDR100 via a 2-m-long RG58 cable. The EC of each electrolytic solution was measured independently with a standard EC meter (YSI-32 Yellow Springs Instruments, Yellow Springs, OH). When determining the R_{cable} using Eq. [7b], the measurements were performed by shorting the cable end with a short wire. The steady-state responses were recorded near the end of the TDR pulse to better approximate the steady state. This is, in fact, mandatory for measurements in the high-EC range or for the short-circuited probe. The computation of TDR EC involves Eq. [9], [12], and [10] successively for the series resistors model and Eq. [11] and [10] for the Castiglione–Shouse method. To calculate the TDR EC using Eq. [10], the probe constant K_p is first obtained using least square fitting of TDR ECs to EC measurements made with the conventional conductivity meter. The TDR EC measurements of electrolytic solutions

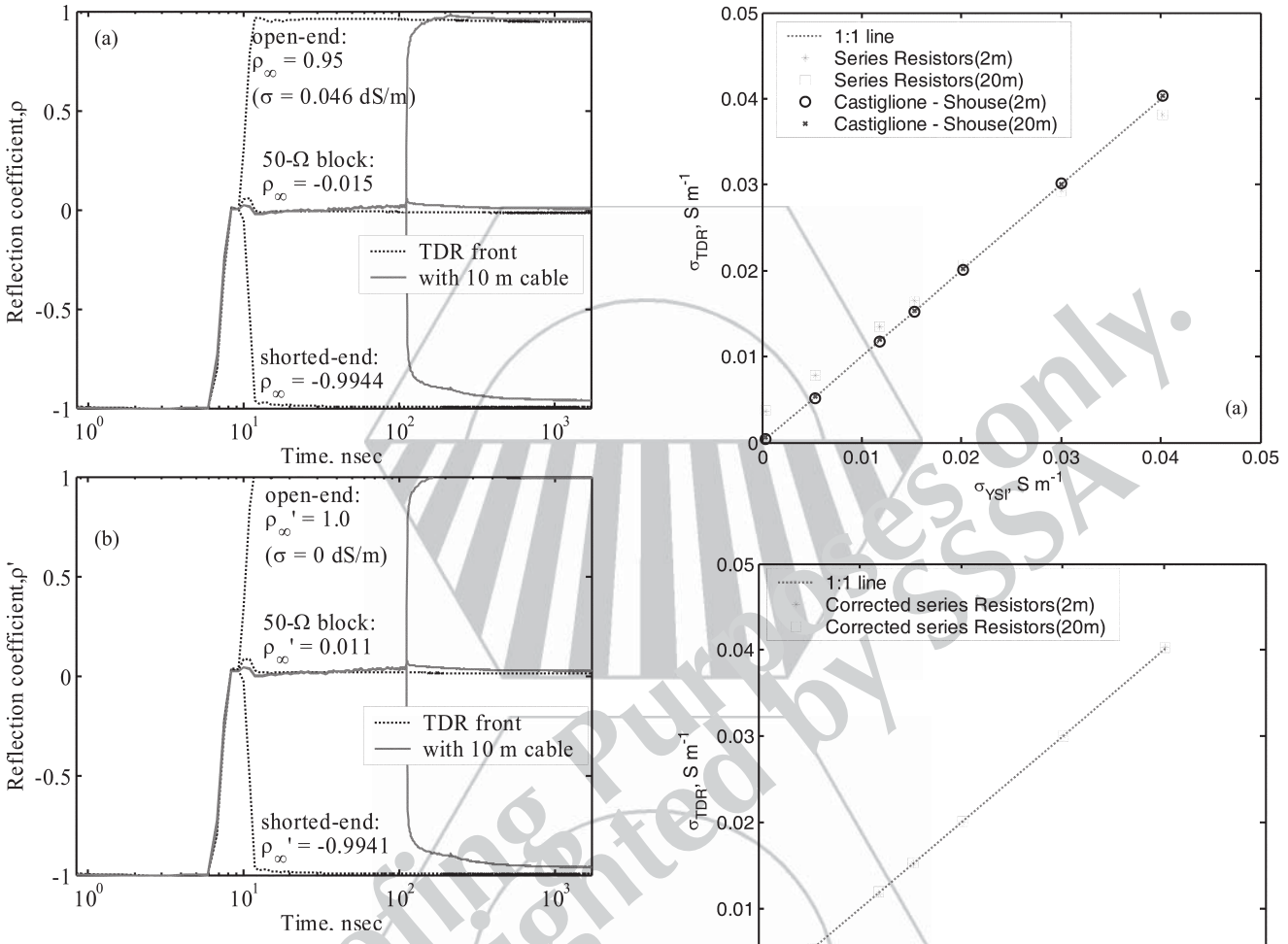

Fig. 7. (a) Original time domain reflectometry (TDR) waveforms from a Campbell Scientific TDR100 and (b) the associated corrected waveforms using calibration Eq. [9].

Fig. 8. Measurements of electrical conductivity by time domain reflectometry made by a Campbell Scientific TDR100 (a) without reflection coefficient calibration and (b) with reflection coefficient calibration using Eq. [9].

were repeated using a 20-m-long RG58 cable to show the effect of cable resistance on the fitted probe constants.

RESULTS AND DISCUSSION

A TDR device may output voltage (e.g., a Tektronix 1502C) or the reflection coefficient (e.g., a Campbell Scientific TDR100). To determine EC, v_∞/v_{S0} in Eq. [4] or ρ'_∞ in Eq. [7a] should be known. The source-step voltage v_{S0} of a voltage-output TDR device is simply equal to the v_∞ when the TDR probe is open in air, which then serves as the reference voltage for computing the EC. The original TDR waveform $v(t)$ of a voltage-output TDR device is often converted to $\rho(t)$ by applying Eq. [2], in which the incident step v_i is determined by using a 50-Ω cable or terminating block as the impedance reference and for amplitude calibration. Figure 6a shows a group of TDR waveforms $\rho(t)$ from the 1502C device, in which the front panel and a 10-m lead cable are shorted, open, and terminated with a nominal 50 Ω terminating block. The front panel terminated with a 50-Ω terminating block was used for amplitude calibration such that its reflection coefficient at long times is equal to 0.0. In this case, the steady-state reflection coefficient ρ_∞ is 0.995 for the probe open in air, regardless of the cable length. It is not precisely 1.0 due to an imperfect match between the source impedance and the terminating block. This reflection coefficient corresponds to 0.0045 dS m^{-1} for the TDR probe used in this study, a small EC error in the condition of zero EC. The ρ_∞ for the shorted front panel not being –1.0 is attributed to some internal resistance. The ρ_∞ for a shorted cable increases as cable length increases. The amount of increase in ρ_∞ due to cable resistance reduces nonlinearly with increasing ρ_∞ and vanishes at $\rho_\infty = 1$. Applying the calibration Eq. [9], the corrected reflection coefficient $\rho'_\infty(t)$ can be obtained as shown in Fig. 6b. The corrected ρ'_∞ becomes 1.0 under the condition of zero EC. The degree of imperfect match between the source impedance and the terminating block is indicated by $\rho'_\infty = 0.0025$ in Fig. 6b. A TDR device that outputs the reflection coefficient uses the nominal 50 Ω internal cable as the impedance reference and for amplitude calibration. Analogous to Fig. 6, Fig. 7 shows a group of TDR waveforms $\rho(t)$ from the TDR100 device. The mismatch between the reference impedance and source impedance in the TDR100 is more significant, leading to $\rho_\infty = 0.950$ (corresponding to EC = 0.046 dS m^{-1}) for the open front panel and $\rho_\infty = 0.961$ for the probe open in air as shown in Fig. 7a. The

amplitude calibration error in a TDR100 seems to depend on whether the front panel is connected to a cable, a phenomenon that may be related to the fringing field of the open front panel. The apparent error can be corrected by applying the calibration Eq. [9], as shown in Fig. 7b.

Figure 8 shows the results of several TDR EC measurements in the low-EC range using the TDR100 device with 2 and 20 m of RG58 lead cable. The probe constant K_p was fitted as described above. Table 1 lists the fitted K_p using the Castiglione–Shouse method and the series resistors model. The percentage errors between the TDR EC measurements and conductivity meter EC measurements are listed in Table 2. As shown in Fig. 8, the Castiglione–Shouse method inherently corrects the instrument error and provides accurate TDR EC measurements when the probe constants are fitted. But the fitted probe constant K_p varies with cable length, as shown in Table 1. The fitted probe constant decreases as cable resistance increases, as also suggested in Fig. 5.

If the measured reflection coefficient is not corrected for instrument error, the actual reflection coefficient is underestimated, especially in the low-EC range, as shown in Fig. 4a. This will have an effect on the estimated EC using the series resistors model. Depending on the EC data range, the fitted K_p is lower than the actual K_p to some degree. As a consequence, the TDR EC by the series resistors model overestimates at lower EC and underestimates at higher EC, as shown in Fig. 8a and Table 2. This experimental result exactly agrees with the theory illustrated in Fig. 4c. The results of the series resistors model with TDR100 reflection coefficient corrected by Eq. [9] are shown in Fig. 8b and Table 2. The large error percentage for the lowest EC in Table 2 can be attributed to the conductivity meter resolution and TDR quantization resolution. Except for the lowest EC (0.00039 S m^{-1}), both the corrected series resistors model and the Castiglione–Shouse method give TDR EC measurements in precise agreement with that measured by the conventional EC meter. But the fitted probe constant K_p can be considered independent of the cable length only in the case of the series resistors model, as shown in Table 1.

To accurately determine TDR EC, both the instrument error due to imperfect amplitude calibration and cable resistance should be properly addressed. The instrument error results in an underestimation of the reflection coefficient, which linearly decreases with decreasing reflection coefficient and vanishes at reflection coefficient = −1.0. In contrast, the effect of cable resistance leads to overestimation of the reflection coefficient, which nonlinearly decreases with increasing reflection coefficient and vanishes at reflection coefficient = 1.0. The combined effect of instrument error and cable resistance on the steady-state reflection coefficient is nonlinear, so the Castiglione–Shouse method is incorrect, although the error can be compensated by adjusting the probe constant. The series resistors model is theoretically sound and precise if the reflection coefficient is properly calibrated to account for the instrument error.

The instrument error can be calibrated by the steady-state reflection coefficient at the zero-EC condition, while the cable resistance can be determined by the steady-state reflection coefficient when the probe is short-circuited. A calibration equation (Eq. [9]) was derived in this study to correct the measured reflection coefficient for instrument error. The corrected reflection coefficient can then be used in the series resistors model (Eq. [7]) for reduction of electrical conductivity considering the effect of cable resistance. Alternatively, an expression (Eq. [12]) that scales the reflection coefficient according to the cable resistance was derived such that the well-known Giese–Tiemann equation can be used after scaling. To keep the usual practice and simplicity, the effect of instrument error and cable resistance can be addressed in one step by combining Eq. [9] and [12]. An equation replacing the Castiglione–Shouse equation is suggested here:

$$\rho_{\infty,\mathrm{Scale}} = 2\frac{(\rho_{\infty,\mathrm{air}}-\rho_{\infty,\mathrm{SC}})(\rho-\rho_{\infty,\mathrm{air}})}{(1+\rho_{\infty,\mathrm{SC}})(\rho-\rho_{\infty,\mathrm{air}})+(\rho_{\infty,air}-\rho_{\infty,\mathrm{SC}})(1+\rho_{\infty,\mathrm{air}})}+1 \qquad [13]$$

where $\rho_{\infty,\mathrm{Scale}}$ is the scaled reflection coefficient to be used in the usual Giese–Tiemann equation, ρ is the steady-state reflection coefficient of the sample under measurement, $\rho_{\infty,\mathrm{air}}$ is the steady-state reflection coefficient when the probe is open in air, and $\rho_{\infty,\mathrm{SC}}$ is the steady-state reflection coefficient when the probe is short-circuited.

Table 1. Fitted probe constant K_p from laboratory measurements using a Campbell Scientific TDR100.

Cable length	Castiglione–Shouse	Series resistors	
		Uncorrected	Corrected†
m		m^{-1}	
2	8.93	7.58	8.93
20	8.78	7.56	8.92

† Corrected using Eq. [9].

CONCLUSIONS

The imperfect amplitude calibration when transforming the voltage signal into the reflection coefficient is identified as a considerable source of error in addition to the cable resistance for TDR electrical conductivity measurements. The instrument error due to imperfect amplitude calibration results in an overestimation of electrical conductivity while the cable resistance leads to an underestimation. The Castiglione–Shouse scaling method originally proposed to deal with cable resistance in fact inherently corrects the instrument error. The combined effect of instrument error and cable resistance on the steady-state reflection coefficient is nonlinear, however, so the linear Castiglione–Shouse method is incorrect. The deficiency in the Castiglione–Shouse method can be compensated by adjusting the probe constant, resulting in a probe constant dependent on the cable length.

Table 2. Percentage errors between the time domain reflectometry electrical conductivity (EC) measurements and conductivity meter EC measurements (σ_{YSI}).

σ_{YSI}	Error					
	Series resistors				Castiglione-Shouse	
	Uncorrected		Corrected			
	2 m	20 m	2 m	20 m	2 m	20 m
S m^{-1}	%					
0.00039	818.81	849.88	−6.23	68.29	−6.09	68.28
0.00529	46.64	47.07	−1.92	1.01	−1.78	1.01
0.01183	13.41	14.19	−0.80	0.93	−0.66	0.93
0.01525	7.80	7.64	−0.12	0.24	0.03	0.23
0.02014	2.14	2.45	−0.65	0.00	−0.51	0.00
0.03003	−2.55	−2.73	0.11	−0.07	0.25	−0.07
0.04015	−5.22	−5.02	0.18	0.33	0.33	0.33

Unlike what was claimed in Castiglione and Shouse (2003), the series resistors model is theoretically sound. Errors observed when using the series resistors model can be attributed to the instrument error due to imperfect amplitude calibration and insufficient recording time for the steady state. In this study, a countermeasure against the instrument error was proposed to complete the series resistors model in practice. The measurements involved in the Castiglione–Shouse method and the new method presented here are identical. The Castiglione–Shouse method works well if the probe constant is calibrated for each measurement setup, which involves measurements in some electrolytic solutions with known electrical conductivities for all probes even if they are identically manufactured. The probe constant in the corrected series resistors model is independent of the cable resistance. Only one calibration is needed to determine the probe constant of identical probes with varying cable lengths. Finally, we would like to urge that the use of the Castiglione–Shouse scaling method be discontinued. We feel that it is inappropriate to use a theoretically incorrect approach, despite the fact that the results obtained with the incorrect approach are as accurate as the results of the theoretically sound approach derived here.

REFERENCES

Castiglione, P., and P.J. Shouse. 2003. The effect of ohmic cable losses on time-domain reflectometry measurements of electrical conductivity. Soil Sci. Soc. Am. J. 67:414–424.

Giese, K., and R. Tiemann. 1975. Determination of the complex permittivity from thin-sample time domain reflectometry improved analysis of the step waveform. Adv. Mol. Relax. Processes 7:45–59.

Heimovaara, T.J., A.G. Focke, W. Bouten, and J.M. Verstraten. 1995. Assessing temporal variation in soil water composition with time domain reflectometry. Soil Sci. Soc. Am. J. 59:689–698.

Huisman, J.A., and W. Bouten. 1999. Comparison of calibration and direct measurement of cable and probe properties in time domain reflectometry. Soil Sci. Soc. Am. J. 63:1615–1617.

Lin, C.-P. 2003. Analysis of a non-uniform and dispersive time domain reflectometry measurement system with application to dielectric spectroscopy of soils. Water Resour. Res. 39(1):1012, doi:10.1029/2002WR001418.

Lin, C.-P., C.-C. Chung, and S.-H. Tang. 2007. Accurate time domain reflectometry measurement of electrical conductivity accounting for cable resistance and recording time. Soil Sci. Soc. Am. J. 71:1278–1287.

Reece, C.F. 1998. Simple method for determining cable length resistance in time domain reflectometry systems. Soil Sci. Soc. Am. J. 62:314–317.

Robinson, D.A., S.B. Jones, J.M. Wraith, D. Or, and S.P. Friedmane. 2003. A review of advances in dielectric and electrical conductivity measurement in soils using time domain reflectometry. Vadose Zone J. 2:444–475.